NASA/TM-2003-211621/Rev4-Vol.IV

Ocean Optics Protocols For Satellite Ocean Color Sensor Validation, Revision 4, Volume IV:

Inherent Optical Properties: Instruments, Characterizations, Field Measurements and Data Analysis Protocols

James L. Mueller, Giulietta S. Fargion and Charles R. McClain, Editors

Scott Pegau, J.Ronald V. Zaneveld, B. Gregg Mitchell, James L. Mueller, Mati Kahru, John Wieland and Malgorzat Stramska, Authors

National Aeronautical and
Space administration

Goddard Space Flight Space Center
Greenbelt, Maryland 20771

May 2002

NASA/TM-2003-211621/Rev4-Vol.IV

Ocean Optics Protocols For Satellite Ocean Color Sensor Validation, Revision 4, Volume IV:

Inherent Optical Properties: Instruments, Characterizations, Field Measurements and Data Analysis Protocols

J. L. Mueller
CHORS, San Diego State University, San Diego, California
Giulietta S. Fargion
Science ApplicationsInternational Corp., Beltsville, Maryland
Charles R. McClain
NASA Goddard Space Flight Center, Greenbelt, Maryland
Scott Pegau and J. Ronald V. Zaneveld
COAS, Oregon State University, Corvallis
B. Gregg Mitchell, Mati Kahru, John Wieland and Malgorzat Stramska
Scripps Institution of Oceanography, University of California San Diego, California

National Aeronautical and
Space administration

Goddard Space Flight Space Center
Greenbelt, Maryland 20771

May 2003

Preface

This document stipulates protocols for measuring bio-optical and radiometric data for the Sensor Intercomparison and Merger for Biological and Interdisciplinary Oceanic Studies (SIMBIOS) Project activities and algorithm development. The document is organized into 7 separate volumes as:

Ocean Optics Protocols for Satellite Ocean Color Sensor Validation, Revision 4

Volume I: Introduction, Background and Conventions
Volume II: Instrument Specifications, Characterization and Calibration
Volume III: Radiometric Measurements and Data Analysis Methods
Volume IV: Inherent Optical Properties: Instruments, Characterization, Field Measurements and Data Analysis Protocols
Volume V: Biogeochemical and Bio-Optical Measurements and Data Analysis Methods
Volume VI: Special Topics in Ocean Optics Protocols

The earlier version of *Ocean Optics Protocols for Satellite Ocean Color Sensor Validation*, *Revision 3* (Mueller and Fargion 2002, Volumes 1 and 2) is entirely superseded by the seven Volumes of Revision 4 listed above.

The new multi-volume format for publishing the ocean optics protocols is intended to allow timely future revisions to be made reflecting important evolution of instruments and methods in some areas, without reissuing the entire document. Over the years, as existing protocols were revised, or expanded for clarification, and new protocol topics were added, the ocean optics protocol document has grown from 45pp (Mueller and Austin 1992) to 308pp in Revision 3 (Mueller and Fargion 2002). This rate of growth continues in Revision 4. The writing and editorial tasks needed to publish each revised version of the protocol manual as a single document has become progressively more difficult as its size increases. Chapters that change but little, must nevertheless be rewritten for each revision to reflect relatively minor changes in, *e.g.*, cross-referencing and to maintain self-contained consistency in the protocol manual. More critically, as it grows bigger, the book becomes more difficult to use by its intended audience. A massive new protocol manual is difficult for a reader to peruse thoroughly enough to stay current with and apply important new material and revisions it may contain. Many people simply find it too time consuming to keep up with changing protocols presented in this format - which may explain why some relatively recent technical reports and journal articles cite Mueller and Austin (1995), rather than the then current, more correct protocol document. It is hoped that the new format will improve community access to current protocols by stabilizing those volumes and chapters that do not change significantly over periods of several years, and introducing most new major revisions as new chapters to be added to an existing volume without revision of its previous contents.

The relationships between the Revision 4 chapters of each protocol volume and those of Revision 3 (Mueller and Fargion 2002), and the topics new chapters, are briefly summarized below:

Volume I: This volume covers perspectives on ocean color research and validation (Chapter 1), fundamental definitions, terminology, relationships and conventions used throughout the protocol document (Chapter 2), requirements for specific *in situ* observations (Chapter 3), and general protocols for field measurements, metadata, logbooks, sampling strategies, and data archival (Chapter 4). Chapters 1, 2 and 3 of Volume I correspond directly to Chapters 1, 2 and 3 of Revision 3 with no substantive changes. Two new variables, Particulate Organic Carbon (POC) and Particle Size Distribution (PSD) have been added to Tables 3.1 and 3.2 and the related discussion in Section 3.4; protocols covering these measurements will be added in a subsequent revision to Volume V (see below). Chapter 4 of Volume I combines material from Chapter 9 of Revision 3 with a brief summary of SeaBASS policy and archival requirements (detailed SeaBASS information in Chapter 18 and Appendix B of Revision 3 has been separated from the optics protocols).

Volume II: The chapters of this volume review instrument performance characteristics required for *in situ* observations to support validation (Chapter 1), detailed instrument specifications and underlying rationale (Chapter 2) and protocols for instrument calibration and characterization standards and methods (Chapters 3 through 5). Chapters 1 through 5 of Volume II correspond directly to Revision 3 chapters 4 through 8, respectively, with only minor modifications.

Volume III: The chapters of this volume briefly review methods used in the field to make the *in situ* radiometric measurements for ocean color validation, together with methods of analyzing the data (Chapter 1), detailed measurement and data analysis protocols for in-water radiometric profiles (Chapter 2), above water measurements of remote sensing reflectance (Chapter III-3), determinations of exact normalized water-leaving radiance (Chapter 4), and atmospheric radiometric measurements to determine aerosol optical thickness and sky radiance distributions (Chapter 5). Chapter 1 is adapted from relevant portions of Chapter 9 in Revision 3. Chapter 2 of Volume III corresponds to Chapter 10 of Revision 3, and Chapters 3 through 5 to Revision 3 Chapters 12 through 14, respectively. Aside from reorganization, there are no changes in the protocols presented in this volume.

Volume IV: This volume includes a chapter reviewing the scope of inherent optical properties (IOP) measurements (Chapter 1), followed by 4 chapters giving detailed calibration, measurement and analysis protocols for the beam attenuation coefficient (Chapter 2), the volume absorption coefficient measured *in situ* (Chapter 3), laboratory measurements of the volume absorption coefficients from discrete filtered seawater samples (Chapter 4), and *in situ* measurements of the volume scattering function, including determinations of the backscattering coefficient (Chapter 5). Chapter 4 of Volume IV is a slightly revised version of Chapter 15 in Revision 3, while the remaining chapters of this volume are entirely new contributions to the ocean optics protocols. These new chapters may be significantly revised in the future, given the rapidly developing state-of-the-art in IOP measurement instruments and methods.

Volume V: The overview chapter (Chapter 1) briefly reviews biogeochemical and bio-optical measurements, and points to literature covering methods for measuring these variables; some of the material in this overview is drawn from Chapter 9 of Revision 3. Detailed protocols for HPLC measurement of phytoplankton pigment concentrations are given in Chapter 2, which differs from Chapter 16 of Revision 3 only by its specification of a new solvent program. Chapter 3 gives protocols for Fluorometric measurement of chlorophyll *a* concentration, and is not significantly changed from Chapter 17of Revision 3. New chapters covering protocols for measuring, Phycoerythrin concentrations, Particle Size Distribution (PSD) and Particulate Organic Carbon (POC) concentrations are likely future additions to this volume.

Volume VI: This volume gathers chapters covering more specialized topics in the ocean optics protocols. Chapter 1 introduces these special topics in the context of the overall protocols. Chapter 2 is a reformatted, but otherwise unchanged, version of Chapter 11 in Revision 3 describing specialized protocols used for radiometric measurements associated with the Marine Optical Buoy (MOBY) ocean color vicarious calibration observatory. The remaining chapters are new in Revision 4 and cover protocols for radiometric and bio-optical measurements from moored and drifting buoys (Chapter 3), ocean color measurements from aircraft (Chapter 4), and methods and results using LASER sources for stray-light characterization and correction of the MOBY spectrographs (Chapter 5). In the next few years, it is likely that most new additions to the protocols will appear as chapters added to this volume.

Volume VI: also collects appendices of useful information. Appendix A is an updated version of Appendix A in Revision 3 summarizing characteristics of past, present and future satellite ocean color missions. Appendix B is the List of Acronyms used in the report and is an updated version of Appenix C in Revision 3. Similarly, Appendix C, the list of Frequently Used Symbols, is an updated version of Appendix D from Rev. 3. The SeaBASS file format information given in Appendix B of Revision 3 has been removed from the protocols and is promulgated separately by the SIMBIOS Project.

In the Revision 4 multi-volume format of the ocean optics protocols, Volumes I, II and III are unlikely to require significant changes for several years. The chapters of Volume IV may require near term revisions to reflect the rapidly evolving state-of-the-art in measurements of inherent optical properties, particularly concerning instruments and methods for measuring the Volume Scattering Function of seawater. It is anticipated that new chapters will be also be added to Volumes V and VI in Revision 5 (2003).

This technical report is not meant as a substitute for scientific literature. Instead, it will provide a ready and responsive vehicle for the multitude of technical reports issued by an operational Project. The contributions are published as submitted, after only minor editing to correct obvious grammatical or clerical errors.

Table of Contents

Chapter 1

Inherent Optical Property Measurement Concepts: Physical Principles and Instruments

Scott Pegau[1], J. Ronald V. Zaneveld[1] and James L. Mueller[2]

[1]*College of Oceanographic and Atmospheric Sciences, Oregon State University, Corvallis*
[2]*Center for Hydro-Optics and Remote Sensing, San Diego State University, California*

1.1 INTRODUCTION

The Inherent Optical Properties (IOP) of a medium, which describe absorption and scattering interactions that modify a vector light field propagating through it, are defined in Vol. I, Ch. 2, Sect. 2.4 of this protocol document. Geometric conventions and notation underlying definitions of, and relationships between IOP and radiative transfer in the medium are described in Section 2.2 of Vol. I, Ch. 2. The roles of the IOP in radiative transfer descriptions and models of light propagation in the sea are also introduced in Vol. I, Ch. 2, and appear elsewhere in many of the Volumes and Chapters of this protocol document.

The chapters of this volume (Vol. IV) describe the conceptual background, instrument characteristics, and methods of calibration, field measurements and data analysis for determining the IOP of seawater. The scope of this protocol volume is limited to practical methods for using commercially available instruments[1] to determine the IOP identified in Vol. I, Chapter 3 (Table 3.1) of *Ocean Optics Protocols for Satellite Ocean Color Sensor Validation, Rev. 4*. The scope of the present volume does not include applications of measured IOP to aspects of ocean color sensor validation that are described elsewhere in the document. The role of IOP in the determination of *Exact Normalized Water-Leaving Radiance* $L_{\mathrm{WN}}^{\mathrm{ex}}(\lambda)$ as a function of wavelength λ, for example, is discussed in Vol. III, Chapter 4.

In this chapter we extend the IOP definitions and relationships of Vol. I, Ch. 2 to develop the theoretical and mathematical bases for practical instrument concepts and methods for measuring IOP in seawater. Instruments will be described to measure, *in situ* at depth z, the beam attenuation coefficient $c(z,\lambda)$, the volume absorption coefficient $a(z,\lambda)$, and the volume scattering function (VSF) $\beta(z,\lambda,\psi)$ at one or more scattering angles ψ. Spectrophotometric laboratory methods are also described in detail for determining absorption coefficients from filtered, discrete water samples. Methods of data analysis are described to determine, from combinations of these measurements, the volume scattering coefficient $b(z,\lambda)$ and backscattering coefficient $b_{\mathrm{b}}(z,\lambda)$.

We do not consider instrument concepts or methods for measuring either fluorescence, or Raman scattering, in Vol. IV. Even though the Raman and fluorescence cross-sections of water, suspended particles and dissolved materials are also IOP of seawater, ***only elastic scattering processes*** are considered in this volume.

In the remainder of Vol. IV, we will ordinarily omit the explicit notation identifying IOP variables as functions of depth z in the water column. This is partly a desire for simplifying the notation, but the more important motive is to avoid confusing global coordinates (geographic location and vertical depth in the water column) with local coordinates (optical axes and normal planes) used to describe photon-matter interactions and measurement concepts.

[1] Certain commercial equipment, instruments, or materials are identified in this chapter to foster understanding. Such identification does not imply recommendation, or endorsement, by the National Aeronautics and Space Administration, nor does it imply that the materials or equipment identified are necessarily the best available for the purpose.

1.2 ABSORPTION AND SCATTERING PROPERTIES OF WATER, PARTICLES AND DISSOLVED SUBSTANCES

Because the IOP are additive (Vol. I, Ch. 2, Sect. 2.4), the absorption and scattering properties of natural water consists of the sums of these IOP of pure water, suspended particles, dissolved substances and turbulence. It is very difficult to experimentally determine the absorption of pure water in the laboratory, due principally to the difficulty of making and maintaining pure water during the course of an experiment. Nevertheless, there have been several successful experiments (several are cited below), over the past few decades, and the spectral absorption and scattering coefficients of pure water are reasonably well known. Using this information, several types of IOP instruments are calibrated by measuring their responses using pure water as an "optical standard". Thus, the calibrated responses of these instruments in field measurements represent the IOP of particles and dissolved material, independent of water. IOP.

From another perspective, the general characteristics of absorption and scattering properties vary spectrally, and in the case of scattering angularly, between the different optically important constituents of seawater. The contrast in angular distribution characteristics of scattering by water and by particles can be an important element of instrument design concepts.

Absorption by Pure Water

The spectral values recommended in Vol. I, Ch. 2 (Sect. 2.4) for the volume absorption coefficients of pure water, $a_W(\lambda)$ m^{-1}, are those of Sogandares and Fry (1997) for wavelengths between 340 nm and 380 nm, Pope and Fry (1997) for wavelengths between 380 nm and 700 nm, and Smith and Baker (1981) for wavelengths between 700 nm and 800 nm. Here, for wavelengths > 700 nm we recommend values calculated by Van Zee *et al*. (2002) from the imaginary part of the refractive indices for pure water measured by Kou *et al*. (1993). The composite $a_w(\lambda)$ spectrum derived from these sources is listed in Table 1.1, together with the linear temperature dependency $\frac{\partial a_w(\lambda)}{\partial T}$ $\left[m^{-1}°C\right]$ reported by Pegau and Zaneveld (1993) and Pegau *et al*. (1997).

Absorption by Suspended Particulates and Colored Dissolved Organic Material (CDOM)

Variations in the spectral absorption of natural waters result directly from variantions in the concentrations and chemical compositions of material substances distributed within the water volume. These absorbing materials may be present in seawater either in suspended particulates, such as pigment-bearing phytoplankton, or as solutes (*i.e.* CDOM). Fig. 1.1a illustrates qualitative comparisons between the absorption spectrum of pure water, $a_w(\lambda)$ (Table 1.1), a non-dimensional *Chl*-specific absorption spectrum of phytoplankton pigment concentration, $a^*_{chl}(\lambda)$ (Prieur and Sathyendranath 1981), and a typically exponential absorption spectrum of CDOM $a_g(\lambda)$ (Bricaud *et al*. 1981). The amplitude of each absorption spectrum in Fig. 1.1a is arbitrarily scaled to illustrate the characteristic difference in shapes between the constant water background absorption and two varying absorption components associated with *Chl* and CDOM concentrations. The unique shape and magnitude of the specific absorption spectrum for each individual constituent allows measured values of, *e.g.*, *Chl* and CDOM concentrations to be determined from measurements of $a(\lambda)$ at several appropriate wavelengths. The strong inverse depencence of remote sensing reflecance on $a(\lambda)$ (Vol. III, Ch. 4), together with the distinctive shape and magnitude characteristics of the constituents, similarly provides the physical basis for ocean color algorithms for determining their concentrations from satellite measurements of water leaving radiance at several wavelengths.

In Case 1 waters, it is often useful to assume (Gordon and Morel 1983; Morel and Maritorena 2001; Mobley and Sundman 2000) that particle absorption $a_p(\lambda)$ is dominated by phytoplankton pigments and may be expressed as a function of *Chl* concentration [mg m^{-3}] and a Chl-specific absorption spectrum $a^*_{chl}(\lambda)$ (Prieur and Sathyendranath 1981), and that CDOM concentration is correlated with *Chl* so that $a_g(\lambda)$ may also be calculated as

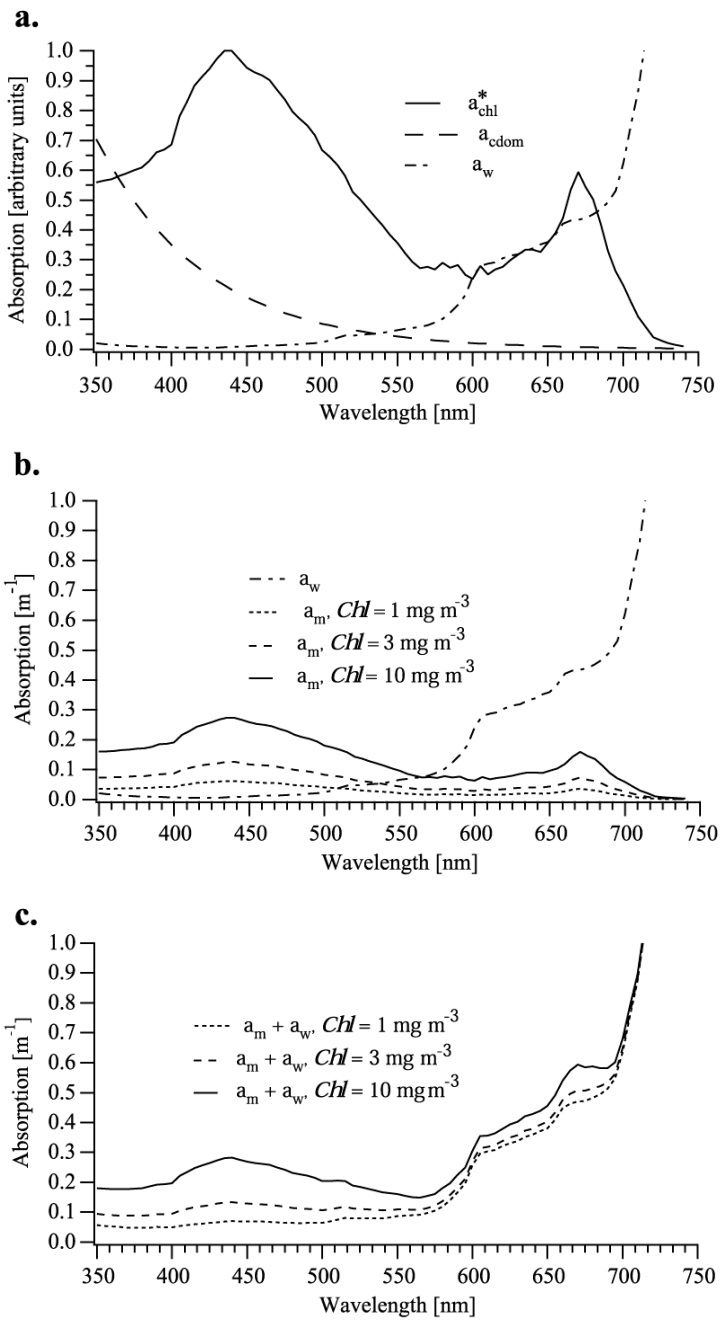

Fig. 1.1: Spectral variations of absorption in seawater. **a:** Qualitative comparison of the shapes of absorption spectra of pure water (Table 1.1), specific absorption by *Chl* (Prieur and Sathyendranath 1981), and CDOM as implemented in the HYDROLIGHT radiative transfer model (Mobley and Sundman 2000) described further by Morel and Maritorena (2001). **b:** Comparisons between $a_w(\lambda)$, the absorption spectrum of pure water, and $a_m(\lambda, Chl)$,the sum of absorption by suspended particles and CDOM for *Chl* concentrations of 1, 3 and 10 mg m^{-3}, following Mobley and Sundman (2000). An absorption meter calibrated relative to pure water would measure $a_m(\lambda; Chl)$. **c:** The sums of pure water and "measured" absorption spectra from panel b.

Table 1.1: Volume absorption and scattering coefficients for pure water, $a_w(\lambda)$ and $b_w(\lambda)$, respectively. Values for $a_w(\lambda)$ are those of Sogandares and Fry (1997) [340 to 390 nm], Pope and Fry (1997) [400 to 700 nm], and Van Zee *et al*. (2002) as derived from Kou *et al*. (1993) [705 to 750 nm]. Alternative values of $b_w(\lambda)$ compared here are denoted (B) (Buitveld, *et al*. 1994) and (M) (Morel 1974). The linear temperature dependence of pure water absorption, $\frac{\partial a_w(\lambda)}{\partial T}$, is due to Pegau and Zaneveld (1993) and Pegau *et al*. (1997).

λ	a_w	$\frac{\partial a_w(\lambda)}{\partial T}$	b_w	b_w	λ	a_w	$\frac{\partial a_w(\lambda)}{\partial T}$	b_w	b_w	λ	a_w	$\frac{\partial a_w(\lambda)}{\partial T}$	b_w	b_w
nm	m^{-1}	$m^{-1}\,{}^oC$	m^{-1} (B)	m^{-1} (M)	nm	m^{-1}	$m^{-1}\,{}^oC$	m^{-1} (B)	m^{-1} (M)	nm	m^{-1}	$m^{-1}\,{}^oC$	m^{-1} (B)	m^{-1} (M)
340	0.0325	0.0000	0.0104	0.0118	500	0.0242	0.0001	0.0021	0.0022	630	0.3184	0.0002	0.0008	0.0009
350	0.0204	0.0000	0.0092	0.0103	505	0.0300	0.0001	0.0020		635	0.3309	0.0000	0.0008	
360	0.0156	0.0000	0.0082	0.0091	510	0.0382	0.0002	0.0019	0.0020	640	0.3382	-0.0001	0.0008	0.0008
370	0.0114	0.0000	0.0073	0.0081	515	0.0462	0.0002	0.0018		645	0.3513	0.0000	0.0007	
380	0.0100	0.0000	0.0065	0.0072	520	0.0474	0.0002	0.0018	0.0019	650	0.3594	0.0001	0.0007	0.0007
390	0.0088	0.0000	0.0059	0.0065	525	0.0485	0.0002	0.0017		655	0.3852	0.0002	0.0007	
400	0.0070	0.0000	0.0053	0.0058	530	0.0505	0.0001	0.0017	0.0017	660	0.4212	0.0002	0.0007	0.0007
405	0.0060	0.0000	0.0050		535	0.0527	0.0001	0.0016		665	0.4311	0.0002	0.0006	
410	0.0056	0.0000	0.0048	0.0052	540	0.0551	0.0001	0.0015	0.0016	670	0.4346	0.0002	0.0006	0.0007
415	0.0052	0.0000	0.0045		545	0.0594	0.0001	0.0015		675	0.4390	0.0001	0.0006	
420	0.0054	0.0000	0.0043	0.0047	550	0.0654	0.0001	0.0014	0.0015	680	0.4524	0.0000	0.0006	0.0006
425	0.0061	0.0000	0.0041		555	0.0690	0.0001	0.0014		685	0.4690	-0.0001	0.0006	
430	0.0064	0.0000	0.0039	0.0042	560	0.0715	0.0001	0.0013	0.0014	690	0.4929	-0.0002	0.0006	0.0006
435	0.0069	0.0000	0.0037		565	0.0743	0.0001	0.0013		695	0.5305	-0.0001	0.0005	
440	0.0083	0.0000	0.0036	0.0038	570	0.0804	0.0001	0.0012	0.0013	700	0.6229	0.0002	0.0005	0.0005
445	0.0095	0.0000	0.0034		575	0.0890	0.0002	0.0012		705	0.7522	0.0007	0.0005	
450	0.0110	0.0000	0.0033	0.0035	580	0.1016	0.0003	0.0011	0.0012	710	0.8655	0.0016	0.0005	0.0005
455	0.0120	0.0000	0.0031		585	0.1235	0.0005	0.0011		715	1.0492	0.0029	0.0005	
460	0.0122	0.0000	0.0030	0.0031	590	0.1487	0.0006	0.0011	0.0011	720	1.2690	0.0045	0.0005	0.0005
465	0.0125	0.0000	0.0028		595	0.1818	0.0008	0.0010		725	1.5253	0.0065	0.0004	
470	0.0130	0.0000	0.0027	0.0029	600	0.2417	0.0010	0.0010	0.0011	730	1.9624	0.0087	0.0004	0.0005
475	0.0143	0.0000	0.0026		605	0.2795	0.0011	0.0010		735	2.5304	0.0108	0.0004	
480	0.0157	0.0000	0.0025	0.0026	610	0.2876	0.0011	0.0009	0.0010	740	2.7680	0.0122	0.0004	0.0004
485	0.0168	0.0000	0.0024		615	0.2916	0.0010	0.0009		745	2.8338	0.0119	0.0004	
490	0.0185	0.0000	0.0023	0.0024	620	0.3047	0.0008	0.0009	0.0009	750	2.8484	0.0106	0.0004	0.0004
495	0.0213	0.0001	0.0022		625	0.3135	0.0005	0.0008						

an exponential function of wavelength (Bricaud *et al*. 1981) scaled as a function of *Chl*. Fig. 1.1b shows the sum $a_{\mathrm{m}}(\lambda;Chl) = a_{\mathrm{p}}(\lambda;Chl) + a_{\mathrm{g}}(\lambda;Chl)$ calculated, for $Chl =$ 1, 3 and 10 mg m^{-3}, using this simple model, as implemented in one of the standard IOP spcification options within the HYDROLIGHT radiative transfer model (Mobley and Sundman 2000). The subscript "m" indicates that the spectra shown in Fig. 1.1b are those that would be measured by an instrument that was calibrated using pure water as a standard reference medium (Chapter 3). The absorption of pure water $a_{\mathrm{w}}(\lambda)$ is compared with $a_{\mathrm{m}}(\lambda;Chl)$ in Fig. 1.1b, and the corresponsding total absorption coefficient spectra $a(\lambda;Chl) = a_{\mathrm{w}}(\lambda) + a_{\mathrm{m}}(\lambda;Chl)$ are illustrated in Fig. 1.1c. The illustrated examples are admittedly an oversimplification, but they are adequate as a basis for considering the nature of IOP components of the signal measured by an absorption meter, or transmissometer, at individual wavelengths.

Scattering by Pure Water

The spectral values of the pure water volume scattering coefficient $b_{\mathrm{w}}(\lambda)$ recommended in Vol. I, Chapter 2 (Sect. 2.4) are those of Morel (1974), as reported by Smith and Baker (1981). Following Van Zee *et al*. (2002), however, we recommend here that preference be given to the $b_{\mathrm{w}}(\lambda)$ scales of Buiteveld, *et al*. (1994). Both scales are listed in Table 1.1 for comparison. The difference between the two scales is ≤ 0.0001 m^{-1} at wavelengths > 475 nm, increases to ≤ 0.0005 m^{-1} as wavelength decreases to 400 nm, and increases further to ≤ 0.0014 m^{-1} at 340 nm. In no instance does the difference closely approach the 0.005 m^{-1} measurement uncertainty of beam attenuation and absorption meters that are commercially available to date.

The angular distribution of the molecular scattering phase function $\tilde{\beta}_{\mathrm{w}}(\psi)$, as approximated with equation (2.29) [Vol. I, Ch. 2] , is illustrated in Fig. 1.2. The magnitude of $\tilde{\beta}_{\mathrm{w}}(\psi)$ represents the probability that a photon scattering interaction with a water molecule will redirect the photon path direction by an angle ψ measured from its original path. The shape of $\tilde{\beta}_{\mathrm{w}}(\psi)$ is sometimes referred to as "isotropic" in the literature, a characterization that is true only in that the function is axially symmetric and the probabilities of forward and backward scattering are equal.

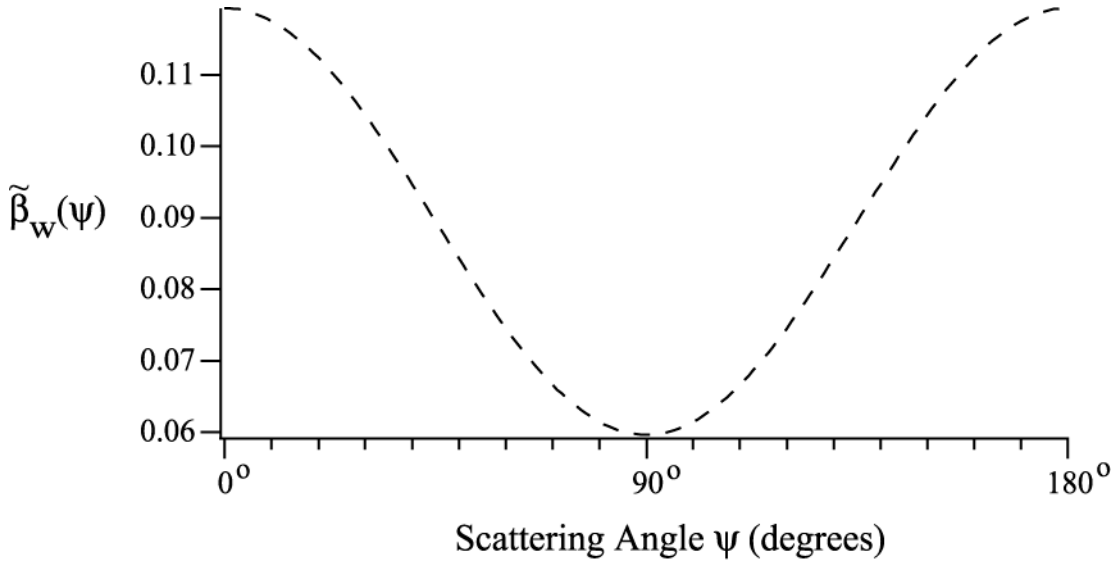

Fig. 1.2: The dashed curve represent the angular distribution of the scattering phase function for pure water, calculated using the approximate Rayleigh scattering model [equation (2.29) of Vol. I, Ch. 2].

Scattering by Particles

In many natural waters, the volume scattering coefficient for particles $b_p(\lambda)$ is comparable to, or larger than, that of pure water. Moreover, the shape of a particle scattering phase function $\tilde{\beta}_w(\lambda,\psi)$, an example of which is illustrated as the solid curve in Fig. 1.3, is strongly peaked - by several orders of magnitude - in the forward direction. The extreme contrast between the angular probability distributions of particulate and molecular scattering (the dashed curve in Fig. 1.3) are important factors that must be considered when designing transmissometers and scattering meters for use in the sea.

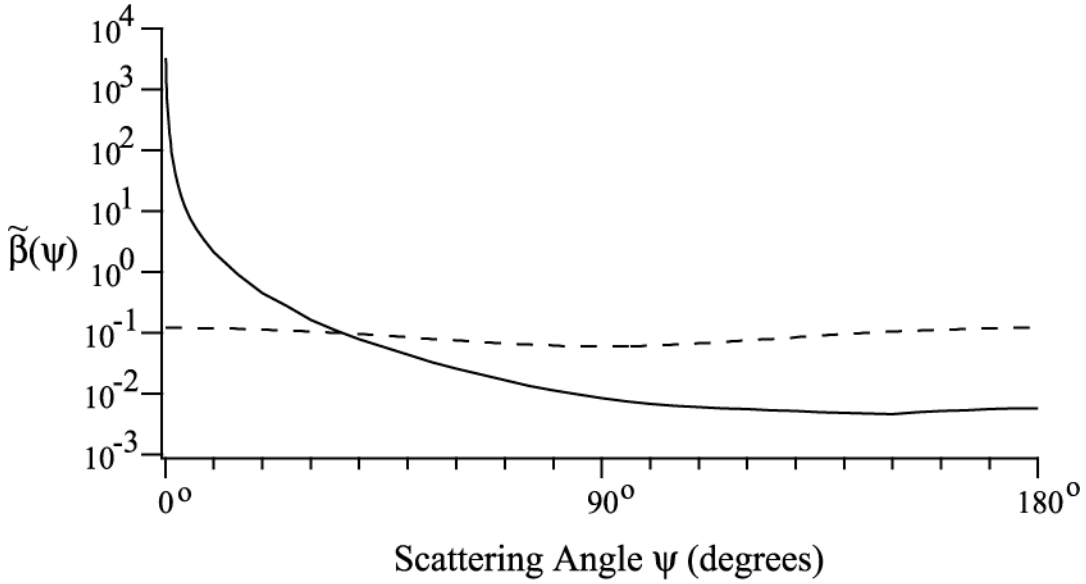

Fig. 1.3: The solid curve is an example of a measured scattering phase function for ocean water dominated by particle scattering (Petzold 1972; San Diego Harbor Stn. 2040). The dashed curve is the pure water phase function from Fig. 1.2, shown here for comparison.

Scattering by Turbulence

Random fluctuations in water density, induced by turbulence, act to steer photons through very small angles in the forward direction, and therefore, scattering by turbulence is also strongly peaked, by orders of magnitude, in the forward direction. Because turbulent fluctuations are completely random in space and time, the variance of photons scattered by turbulence at small angles is much greater than the variance associated with small angle scattering by particles (Bogucki *et al*. 1998)

1.3 RADIANT FLUX TRANSMISSION MEASUREMENT CONCEPTS

Geometry and Nomenclature

In Fig. 1.4 the origin of a local instrument coordinate system is placed at the exit aperture of a source of monochromatic radiant flux $\Phi_o(\lambda,0,0,0)$ $\left[\text{in } \mu\text{W nm}^{-1}\right]$[2] directed as a collimated beam along the positive z_m-axis (see also Fig. 2.2 in Vol. I, Ch. 2). The subscript "m" associated with the coordinate basis vectors $(\hat{\mathbf{x}}_m,\hat{\mathbf{y}}_m,\hat{\mathbf{z}}_m)$ in

[2] The choice of these units, rather than, *e.g.*, W m^{-1}, is customary in ocean color science and is used throughout these protocols.

Fig. 1.4 indicate that the local "measurement" coordinate frame is associated with a particular instrument concept, as distinguished from global coordinates defining positions and directions in the extended medium (*cf* Figs. 2.1 and 2.2 in Vol. I, Ch. 2). The local instrument coordinate framework is related to global coordinates by a translation and rotations that are arbitrary and need not be considered in the present context[3].

The direction associated with an optical path vector intersecting the transmitted beam axis (z_m-axis) is described by the angle pair (ψ,φ), where $0 \le \psi \le \pi$ is measured from the z_m-axis and $0 \le \varphi \le 2\pi$ is measured from the x_m-axis counterclockwise in the $x_m y_m$-plane. The variable r, with various subscripts, will denote geometric distance along any such optical path[4]. Directional radiant flux at distance r from a source, or from a scattering interaction site within the transmitted beam, is denoted $\Phi(\lambda, r, \psi, \varphi)$. In Fig. 1.4 for example, radiometric flux scattered into direction (ψ,φ) at position $\vec{\mathbf{x}}_S$ is denoted as $\Phi_S(\lambda, 0, \psi, \varphi)$, and the scattered flux transmitted in that direction to Detector 2, at position $\vec{\mathbf{x}}_D$, as $\Phi_S(\lambda, r_D, \psi, \varphi)$. Radiometric flux within the beam transmitted to a point on the z_m-axis at distance r from the source is denoted, $\Phi_T(\lambda, r, 0, \bullet)$, where the dot indicates that φ is indeterminate when $\psi = 0$ or $\psi = \pi$. In particular, the flux transmitted from the source to Detector 1 is $\Phi_T(\lambda, r_T, 0, \bullet)$.

Transmittance and Beam Attenuation

The shaded rectangle overlaid on the extended z_m-axis in Fig. 1.4 schematically illustrates a cylinder (of cross sectional area Δs) representing the collimated beam of radiant flux transmitted from the source to Detector 1. The gradient in shading represents the exponential decrease in $\Phi_T(\lambda, r, 0, \bullet)$ with increasing distance r, as photons interact with the medium and are absorbed and scattered out of the beam. During transmission over a path interval from r to $r + \Delta r$, the fraction of radiant flux absorbed in the volume $\Delta s \Delta r$ is ***spectral absorptance***, $A(\lambda)$ and the fraction of flux scattered out of the beam direction in that volume is ***spectral scatterance*** $B(\lambda)$ (see Vol. I, Chapter 2, Sect. 2.4).

One could envision superimposing a lightly shaded "cloud" on Fig. 1.4 to visualize scattered photons escaping from the beam in all directions, but this would not indicate the directional nature of the scattering losses. Instead, the scattering process is schematically illustrated in Fig. 1.4 as a mottled, shaded path of photons scattered in a particular direction (ψ,φ) at a single location $\vec{\mathbf{x}}_S$ in the beam[5]. At this on-axis location, $\vec{\mathbf{x}}_S$, similar beams could be drawn in any other direction to visually indicate scattered flux intensity and its subsequent transmittance and attenuation in the new direction. The same type of graphic could be drawn anywhere along the optical path, and if many were combined we'd generate the aforementioned "photon cloud" masking any indication of the vector nature of the scattered radiant field. Nevertheless, that mental construct is adequate for considering transmission measurement concepts. If the pathlength r_T is short enough that photons initially scattered out of the beam have a negligible chance of undergoing two (or more) additional scattering interactions that could return them to the beam, then it may be assumed that they will not be detected by Detector 1 (Fig. 1.4)[6].

---

[3] When the IOP are used in the context of a radiative transfer model, on the other hand, the translations and rotations relating local coordinates, used to describe scattering interactions (*e.g.* as at position $\vec{\mathbf{x}}_S$ .in Fig. 1.3), to global coordinates, describing locations and directions in the medium as whole, become critically important.

[4] See Footnote 2 in (Vol. 1, Chapter 2) regarding the usage of the variable *z* in Fig. 2.2 and Sect. 2.4 of that chapter. Here we have substituted the symbol *r* for the optical pathlength along the z-axis in Fig. 1.3 (compare with Fig. 2.2 of Vol. 1 Ch. 2).

[5] The transmission of the illustrated beam of scattered photons to Detector 2 will be further considered as a starting point in the discussion of scattering measurement concepts in Sect. 1.5 below.

[6] The question, "What pathlength limit is *'short enough'* to avoid multiply scattered photons from reaching a transmissometer's detector?" is considered in Chapter 2 of this Protocol Volume.

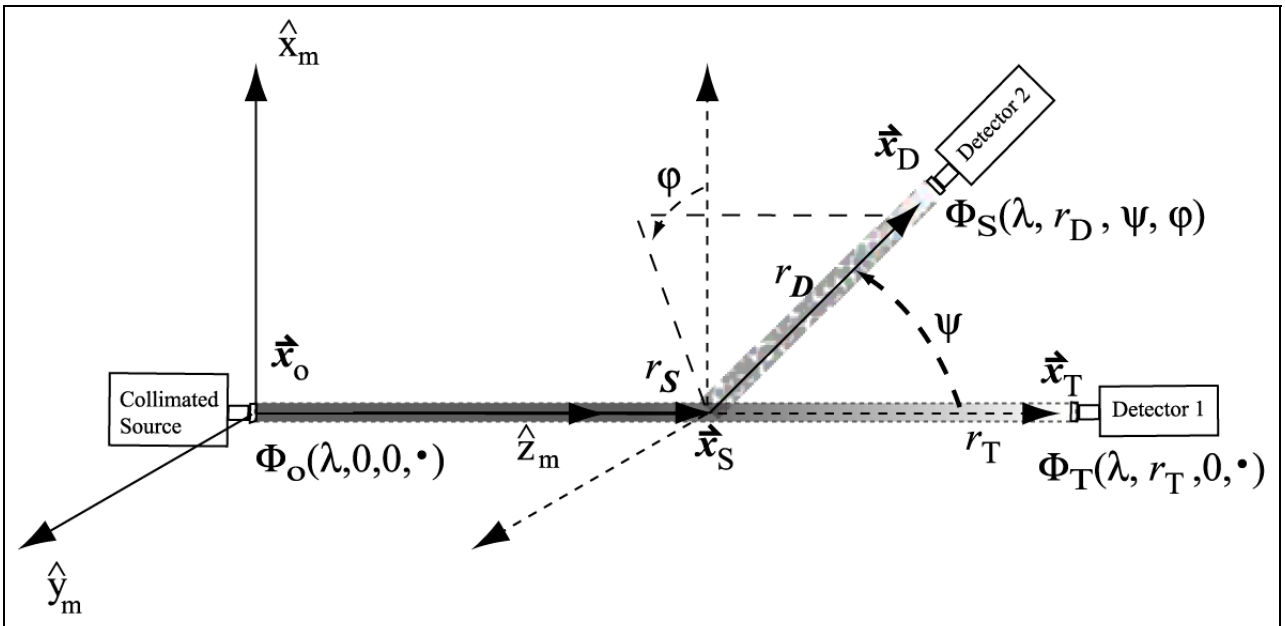

Figure 1.4: The local "Instrument Coordinate" framework describing optical beam transmission and scattering geometry. A collimated beam of radiometric flux $\Phi_o(\lambda,0,0,\bullet)$ is emitted from a source at the origin $\vec{x}_o$. The flux within the collimated beam, shown schematically as a gradient shaded rectangle extending along the z_m-axis to Detector 1, is reduced by scattering and absorption as it is transmitted along the z_m-axis, and a reduced flux $\Phi_T(\lambda,r_T,0,\bullet)$ is measured by Detector 1 at position $\vec{x}_T$. At the intermediate location $\vec{x}_S$, some fraction of the flux $\Phi_T(\lambda,r_S,0,\bullet)$ that reaches that location is scattered out of the beam into direction (ψ,φ). The directionally scattered flux $\Phi_S(\lambda,0,\psi,\varphi)$ is subsequently transmitted a distance r_D in that direction, with further losses due to scattering and absorption, and the reduced scattered flux $\Phi_S(\lambda,r_D,\psi,\varphi)$ is measured by Detector 2 at position $\vec{x}_D$. See text for further explanations.

The ***beam attenuation coefficient*** is defined in equations (2.16) through (2.18) of Vol. I, Chapter 2 (Sect. 2.4) as

$$c(\lambda) = a(\lambda) + b(\lambda),\ \mathrm{m}^{-1}, \tag{1.1}$$

where the ***volume absorption*** and ***scattering coefficients*** $a(\lambda)$ and $b(\lambda)$ are defined in terms of ***absorptance*** $A(\lambda)$ and ***scatterance*** $B(\lambda)$ in the limit of the optical pathlength Δr approaching zero as

$$a(\lambda) = \lim_{\Delta r\to 0}\frac{A(\lambda)}{\Delta r},\ \text{and}\ \ b(\lambda) = \lim_{\Delta r\to 0}\frac{B(\lambda)}{\Delta r},\ \mathrm{m}^{-1}, \tag{1.2}$$

respectively. Equation (2.16) (Vol. I, Chapter 2) may be rearranged as

$$\lim_{\Delta r\to 0}\left\{\frac{\Phi_T(\lambda)-\Phi_i(\lambda)}{\Phi_i(\lambda)\Delta r}\right\} = \lim_{\Delta r\to 0}\left\{-\frac{A(\lambda)+B(\lambda)}{\Delta r}\right\}, \tag{1.3}$$

where Φ_i and Φ_T are incident and transmitted radiant fluxes, respectively. Equation (1.3) may be expressed in differential form as

$$\frac{d\Phi(\lambda)}{\Phi(\lambda,r)} = -c(\lambda)\,dr\,. \tag{1.4}$$

Integrating (1.4) over an optical pathlength r_T as

$$c(\lambda)\int_0^{r_T} dr = -\int_0^{r_T} \frac{d\Phi(\lambda)}{\Phi(\lambda,r)}, \tag{1.5}$$

we obtain the solution for the beam attenuation coefficient

$$c(\lambda) = \frac{\ln \Phi_o(\lambda,0,0,\bullet) - \ln \Phi_T(\lambda,r_T,0,\bullet)}{r_T} = \frac{-\ln T(\lambda,r_T)}{r_T} \text{ m}^{-1}, \tag{1.6}$$

where we adopt the conventions and notations described above and in Fig. 1.4. In (1.6), ***transmittance*** $T(\lambda,r_T) \equiv \frac{\Phi_T(\lambda,r_T,0,\bullet)}{\Phi_o(\lambda,0,0,\bullet)}$ is the fraction of radiant flux transmitted over the path distance r_T. Equation (1.6) is the fundamental equation by which the ***beam attenuation coefficient*** is determined from a measurement made with a ***transmissometer*** (Chapter 2 of this volume).

The attenuation of radiant flux transmitted over a short optical pathlength r_T in seawater may be determined using the *Beer-Lambert-Bouguer Law* [equation (2.41), Vol. I, Ch. 2], which here follows directly from (1.6) as

$$\Phi_T(\lambda,r_T,0,\bullet) = \Phi_o(\lambda,0,0,\bullet)e^{-c(\lambda)r_T}. \tag{1.7}$$

1.4 ABSORPTION MEASUREMENT CONCEPTS

Reflecting Tube Absorption Meters

To determine the volume absorption coefficient $a(\lambda)$ with a source and detector pair arranged on a common axis (*e.g.* the source and Detector 1 in Fig. 1.4), the flux reaching the detector window Φ_K must include the sum of directly transmitted and scattered fluxes, *i.e.* $\Phi_K = \Phi_T + \Phi_B$. If the source and collector are equal in area and the water path between them (the shaded transmission path volume in Fig. 1.4) were enclosed in a perfectly reflecting tube, then all forward scattered photons would be redirected into the beam and reach the detector. For the present, we will postpone consideration of the flux loss due to backscattered photons and treat it as being negligible. Under this construct and assumption, equation (1.3) may be rewritten as

$$\lim_{\Delta r\to 0}\left\{\frac{\Phi_T(\lambda)+\Phi_B(\lambda)-\Phi_i(\lambda)}{\Phi_i(\lambda)\Delta r}\right\} = -\lim_{\Delta r\to 0}\left\{\frac{A(\lambda)}{\Delta r}\right\}, \tag{1.8}$$

expressed in differential form as

$$\frac{d\Phi_K(\lambda,r)}{\Phi(\lambda,r)} = -a(\lambda)dr, \tag{1.9}$$

and integrated over the path from 0 to r_T to obtain

$$a(\lambda) = \frac{\ln \Phi_o(\lambda,0,0,\bullet) - \ln \Phi_K(\lambda,r_T,0,\bullet)}{r_T} = \frac{-\ln T_K(\lambda,r_T)}{r_T} \text{ m}^{-1}. \tag{1.10}$$

The reflecting tube method has been used to measure spectral absorption in the laboratory for many decades (James and Birge 1938). In recent years, this method has been adapted for use in the ocean (Zaneveld *et al*. 1992). Suitable instruments are now commercially available and are coming into general use within the oceanographic community. The best-known, commercially available example of this type of instrument is the "ac-9" manufactured by WET Labs Inc. of Philomath, OR. Protocols for calibrating and using reflecting tube absorption meters, and methods of data analysis are described in Chapter 3 of this volume, and in more specific detail for the ac-9 by Van Zee *et al*. (2002), which is available at (www.wetlabs.com).

Laboratory Methods for Determining Absorption Coefficients

Protocols in Chapter 4, by Mitchell *et al*., describe methods for filtering seawater to capture suspended particles on GF/F filters, and for measuring the absorption spectra of the particle-laden filters with a laboratory spectrophotometer. Methods are also described for extracting phytoplankton pigments from the filters, and measuring the residual absorption spectrum of particulate materials other than phytoplankton pigments. Finally, laboratory methods are also described for measuring the absorption spectrum of CDOM in filtered seawater samples. The material in this chapter derives from the results of recent experimental intercomparison workshops in which the authors participated, as well as from the published literature. Chapter 4 of this volume is a reformatted, but otherwise unchanged, version of Chapter 15 in Revision 3 to the ocean optics protocols (Mueller and Fargion 2002).

Absorption Determinations from Radiometric Measurements of Irradiance Flux Divergence

In situ spectral absorption coefficient profiles can also be measured with spectral radiometers conforming to the performance specifications listed in Vol. II, Chapter 2, if the radiometric package is extended to measure $E_d(z,\lambda)$ and $E_u(z,\lambda)$, as well as scalar irradiances $\overset{o}{E}_d(z,\lambda)$ and $\overset{o}{E}_u(z,\lambda)$. This combination may be approached either using hemispherical collectors to measure upwelling and downwelling hemispherical irradiances (Hojerslev 1975), or by using cosine collectors on one radiometer in tandem with spherical collectors on another radiometer. Given these irradiance components, spectral absorption is then computed using Gershun's equation (Gershun 1939) as

$$a(z,\lambda) = \vec{K}(z,\lambda)\frac{\vec{E}(z,\lambda)}{\overset{o}{E}(z,\lambda)}, \tag{1.11}$$

where $\vec{E}(z,\lambda) = E_d(z,\lambda) - E_u(z,\lambda)$ is vector irradiance, $\vec{K}(z,\lambda)$ is the vertical attenuation coefficient for vector irradiance, and scalar irradiance $\overset{o}{E}(z,\lambda) = \overset{o}{E}_d(z,\lambda) + \overset{o}{E}_u(z,\lambda)$ (see also Vol. I, Chapter 2).

Comparisons between absorption profiles measured using Gershun's equation with $\vec{E}(z,\lambda)$ and $\overset{o}{E}(z,\lambda)$ (scalar irradiance) data, and absorption profiles measured with a reflecting tube instrument, agreed within 8% (Pegau *et al*. 1994). This level of agreement is well within the calibration uncertainties of the particular prototype instruments used for that experiment, which were approximately 10% uncertainties in both the scalar irradiance radiometer and in the reflecting tube instrument. Less than 5% uncertainties in absorption are expected in future experiments, assuming the data are properly averaged to remove near-surface irradiance fluctuations caused by surface waves (Zaneveld *et al*. 2001). In very clear oligotrophic water, moreover, uncertainty in water absorption values may make it impossible to realize this level of relative agreement.

Other Methods of Measuring Absorption

There are several other measurement concepts that may be used to determine the absorption coefficient of seawater, however, none of them are currently useful for making routine measurements during daylight conditions at sea. One possible exception is the determination of absorption by inverting radiance distribution profiles measured using a camera system (Voss 1989), but at present, such camera systems are not commercially available[7]. In a similar method, absorption may be determined by inverting the radiative transfer equation for several measured moments of an axially symmetric radiance distribution in the asymptotic regime (Zaneveld and Pak 1972; Wells 1983) Other examples include the determination $a_w(\lambda)$ using an integrating cavity (Pope and Fry 1997), photothermal methods (Sogandares and Fry 1997), and differential optoacoustic spectroscopy (Voss and Trees 1987). Optoacoustic spectroscopy was also used to measure $a_p(\lambda)$ in phytoplankton cultures (Trees and Voss 1990). Absorption may also be determined from measurements of irradiance divergence from a submerged isotropic

[7] It would be advantageous were this situation to change in the future, as such camera systems are potentially even more useful for determining the Bidirectional Reflectance Distribution Function (BRDF) and Exact Normalized Water-Leaving Radiance (Vol. III, Ch. 4).

source (Maffione *et al*. 1993, and earlier references cited there). The present version of this volume does not address any of these methods.

1.5 SCATTERING MEASUREMENT CONCEPTS

Scattering Coefficient Determinations

There is no practical way to directly measure the volume scattering coefficient $b(\lambda)$. Given measurements of absorption and beam attenuation coefficients, however, the volume scattering coefficient may computed from (1.1) as $b(\lambda) = c(\lambda) - a(\lambda)$, m^{-1}. In practice it's not quite that simple, and several interrelated scattering and absorption corrections must be applied (Chapters 3 and 5 in this Volume). Alternatively, attempts have been made to calculate $b(\lambda)$ by integrating measurements of the VSF, *e.g.*, by Petzold (1972).

Volume Scattering Function Measurements

In Fig. 1.4, the combination of the source at $\vec{\mathbf{x}}_o$, directional scattering at $\vec{\mathbf{x}}_S$, and Detector 2 at location $\vec{\mathbf{x}}_D$ schematically illustrate the conceptual elements of a scattering meter designed to measure the VSF $\beta(\lambda, \psi, \varphi)$. Collimated flux $\Phi_o(\lambda, 0, 0, \bullet)$ is transmitted, in a beam of cross-sectional area A, from the source to $\vec{\mathbf{x}}_S$ as

$$\Phi_T(\lambda, r_S, 0, \bullet) = \Phi_o(\lambda, 0, 0, \bullet) e^{-c(\lambda) r_S}. \tag{1.12}$$

The irradiance incident normal to the optical transmission axis at $\vec{\mathbf{x}}_S$ is

$$E_i = \frac{\Phi_T(\lambda, r_S, 0, \bullet)}{A} = \frac{\Phi_o(\lambda, 0, 0, \bullet) e^{-c(\lambda) r_S}}{A}. \tag{1.13}$$

At position $\vec{\mathbf{x}}_S$, some of the incident radiant flux is scattered in direction (ψ, φ), into the solid angle field-of-view Ω_{FOV} of Detector 1, from the volume $V(\psi)$ defined by the intersection of the beam and detector field of view. The radiant intensity of the scattered flux is

$$I_S(\lambda, \psi, \varphi) = \frac{\Phi_S(\lambda, 0, \psi, \varphi)}{\Omega_{FOV}}, \tag{1.14}$$

and scattered flux reaching the detector is

$$\Phi_S(\lambda, r_D, \psi, \varphi) = \Phi_S(\lambda, 0, \psi, \varphi) e^{-c(\lambda) r_D}. \tag{1.15}$$

From equation (2.30) we may determine the VSF averaged over the working volume and solid angle FOV approximately as

$$\overline{\beta}(\lambda, \psi, \varphi) \cong \frac{I_S(\lambda, 0, \psi, \varphi)}{E_i V(\psi)}, \tag{1.16}$$

or by substituting from (1.12) through (1.13), directly in terms of source and detector fluxes as

$$\overline{\beta}(\lambda, \psi, \varphi) \cong \frac{\Phi_S(\lambda, r_D, \psi, \varphi) A}{\Phi_o(\lambda, 0, 0, \bullet) V(\psi) \Omega_{FOV}} e^{-c(\lambda)(r_S - r_D)}. \tag{1.17}$$

One must know both $c(\lambda)$ and $\Phi_o(\lambda, 0, 0, \bullet)$ to determine the VSF from (1.17). If the same detector were used at positions shown for detectors 1 and 2 in Fig. 1.4, following the method introduced by Kullenberg (1968), and if $r_D = r_T - r_S$, we may substitute from (1.7) and determine the VSF from the two measured detector fluxes as

$$\overline{\beta}(\lambda, \psi, \varphi) \cong \frac{\Phi_S(\lambda, r_D, \psi, \varphi) A}{\Phi_T(\lambda, r_T, 0, \bullet) V(\psi) \Omega_{FOV}}. \tag{1.18}$$

Equation (1.18) could be used to measure the VSF if the source and detector are well collimated, and there were no flux losses, or FOV distortions, associated with an instrument's optical assembly. For most scattering meters, however, the averaged VSF estimate $\overline{\beta}(\lambda,\psi,\varphi)$ is related to the true VSF $\beta(\lambda,\psi,\varphi)$ by a weighted integral

$$\overline{\beta}(\lambda,\psi,\varphi)=\int_0^{2\pi}\int_0^{\pi}\beta(\lambda,\psi,\varphi)W(\lambda,\psi,\varphi;c)\sin\psi d\psi d\varphi\,. \tag{1.19}$$

where the weighting function $W(\lambda,\psi,\varphi;c)$ accounts for instrumental factors including the divergence and uniformity of the source beam and detector angular response function, the working volume geometry, variations in attenuation of flux scattered to the detector from different volume elements, and optical reflection and absorption losses in the system. Practical methods for determining $W(\lambda,\psi,\varphi;c)$ are described in Chapter 5.

The VSF of ocean water is usually considered to be azimuthally symmetric about the transmission axis. Therefore, the VSF is usually reported as $\beta(\lambda,\psi)$, which is a function of the polar "scattering angle" alone. In terms of the VSF measurements as represented in (1.19), we have that

$$\overline{\beta}(\lambda,\psi)=\int_0^{2\pi}\overline{\beta}(\lambda,\psi,\varphi)d\varphi=2\pi\overline{\beta}(\lambda,\psi,\varphi)\,. \tag{1.20}$$

Backscattering Coefficient Determination

The backscattering coefficient $b_b(\lambda)$ [Vol. I, Ch. 2, equation (2.23)] is an important factor in the physical relationship between the IOP and remote sensing reflectance (Vol. III, Ch. 4, Sect. 4.3 and references cited therein). As is the case for the volume scattering coefficient $b(\lambda)$, there is no practical way to directly measure $b_b(\lambda)$ in the sea. If that is true, then how can $b_b(\lambda)$ be determined using the so-called "backscattering meters" in common use within the community? These instruments actually measure the VSF $\overline{\beta}(\lambda,\psi)$ at one angle ψ^*, or several angles ψ_i^*, $i=1,2,\ldots,N$, in the backward direction. For single angle VSF instruments, such as the HOBILABS HydroScat-series and WET Labs ECO-BB series , one uses the fact that most observed phase functions and modeled VSFs show a common crossover angle ψ^* at which $\overline{\beta}(\lambda,\psi^*)\propto b_b(\lambda)$. An empirical linear equation is used to calculate $b_b(\lambda)$ from $\overline{\beta}(\lambda,\psi^*)$; where the angle ψ^* is selected to minimize the uncertainty in $b_b(\lambda)$ associated with a simulated uncertainty in $\tilde{\beta}_P(\lambda,\psi)$ (Oishi 1990; Maffione and Dana; Boss and Pegau 2001). The approach used to determine $b_b(\lambda)$ from measurements of $\overline{\beta}(\lambda,\psi_i,\varphi);\ i=1,2,\ldots,N$ angles, *e.g.* using a WET Labs VSF-3, is to fit a polynomial to the N+1 values $2\pi\overline{\beta}(\lambda,\psi_i,\varphi)\sin\psi_i$ derived from the N measurements and the endpoint $2\pi\beta(\lambda,\pi,\bullet)\sin\pi\equiv 0$ and integrate it from $\frac{\pi}{2}$ to π (following Beardsley and Zaneveld 1969).

REFERENCES

Beardsley, G.F. and J.R.V. Zaneveld, 1969: Theoretical dependence of the near-asymptotic apparent optical properties of sea water. *J. Opt. Soc. Amer*. 59: 373-377.

Boss, E. and W.S. Pegau, 2001: Relationship of light scattering at an angle in the backward direction to the backscattering coefficient. *Appl. Opt.,* **40:** 5503-5507.

Bogucki, D.J., J.A. Domaradzki, D. Stramski and J.R.V. Zaneveld, 1998. Comparison of near-forward light scattering on oceanic turbulence and particles. *Appl. Opt.*, **37(21):** 4669-4677.

Bricaud, A., A. Morel and L. Prieur, 1981. Absorption by dissolved organic matter of the sea (yellow substance) in the UV and visible domains. *Limnol Oceanogr,* **26(1):** 43-53.

Buiteveld, H., J.H.M. Hakvoort and M. Donze, 1994: The optical properties of pure water. *Ocean Optics XII*, SPIE Vol. 2258: 174-183.

Gordon, H.R. and A. Morel, 1983: *Remote Assessment of Ocean Color for Interpretation of Satellite Visible Imagery, a Review; Lecture Notes on Coastal and Estuarine Studies, Vol. 4*, Springer Verlag, New York, 114pp.

Gershun, A., 1939: The light field. *J. Math. Phys*. **18**: 51-151.

Hojerslev, N.K., 1975: A spectral light absorption meter for measurements in the sea. *Limnol. Oceanogr*., **20**: 1024-1034.

James, H.R., and E.A. Birge, 1938: A laboratory study of the absorption of light by lake waters. *Trans. Wis. Acad. Sci*., **31**: 1--154.

Kou, L., D. Labrie and P. Chylek, 1993: Refractive indices of water and ice in the 0.65 to 2.5 μm spectral range, *Appl. Opt.*, **32:** 3531-3540.

Kullenberg, G., 1968: Scattering of light by Sargasso Sea water, *Deep-Sea Res.*, **15:** 423-432.

Maffione, R.A. and D.R. Dana, 1997: Instruments and methods for measuring the backward-scattering coefficient of ocean waters. *Appl. Opt*. **36**: 6057-6067.

Maffione, R.A., K.J. Voss and R.C. Honey, 1993. Measurement of the spectral absorption coefficient in the ocean with an isotropic source. *Appl. Opt.*, **32(18):** 3273-3279.

Morel, A., 1974: Optical properties of pure water and pure sea water. In: *Optical Aspects of Oceanography*, N.G. Jerlov and E.S. Nielson, Eds., pp1-23.

Morel, A. and S. Maritorena, 2001. Bio-opical properties of oceanic waters: A reappraisal, *J. Geophys. Res.*, **106(C4):** 7163-7180.

Mueller, J.L. and G.S. Fargion,[Eds.], 2002: Ocean Optics Protocols for Satellite Ocean Color Sensor Validation, Revision 3. *NASA Tech. Memo. 2002-210004*, NASA Goddard Space Flight Center, Greenbelt, Maryland, 308pp.

Oishi, T., 1990. Significant relation between the backward scattering coefficient of sea water and the scatterance at 120 degrees. *Appl. Opt.*, **29(31):** 4658-4665.

Pegau, W.S. and J.R.V. Zaneveld, 1993: Temperature dependent absorption of water in the red and near infrared portions of the spectrum. *Limnol. Oceanogr*., **38**(1): 188-192.

Pegau, W.S., J.S. Cleveland, W. Doss, C.D. Kennedy, R.A. Maffione, J.L. Mueller, R. Stone, C.C. Trees, A.D. Weidemann, W.H. Wells, and J.R.V. Zaneveld, 1995: A comparison of methods for the measurement of the absorption coefficient in natural waters. *J. Geophys. Res.*, **100**(C7): 13,201-13,220.

Pegau, W.S., D. Gray and J.R.V. Zaneveld, 1997: Absorption and attenuation of visible and near-infrared light in water: dependence on temperature and salinity. Appl. Opt., **36**(24): 6035-6046.

Petzold, T.J., 1972. Volume scattering functions for selected ocean waters. Contract No. N62269-71-C-0676, UCSD, SIO Ref. 72-78.

Pope, R.M. and E.S. Fry. 1997: Absorption spectrum (380-700 nm) of pure water. II. Integrating cavity measurements. *Appl. Opt*. **36**: 8710-8723.

Prieur, L. and S. Sathyendranath, 1981. An optical classification of coastal and oceanic waters based on the specific spectral absorption curves of phytoplankton pigments, dissolved organic matter, and other particulate materials. *Limnol. Oceanogr.*, **26(4):** 671-689.

Smith, R.C. and K.S. Baker, 1981. Optical properties of the clearest natural waters (200-800 nm), *Appl Opt*. **20 (2):** 177-184.

Sogandares, F.M. and E.S. Fry, 1997. Absorption spectrum (340-640 nm) of pure water. I. Photothermal measurements. *Appl. Opt.*, **36(33):** 8699-8709.

Trees, C.C. and K.J. Voss, 1990. Optoacoustic spectroscopy and its application to molecular and particle absorption. *OCEAN OPTICS X*, SPIE **1302:** 149-156.

Voss, K.J., 1989: Use of the radiance distribution to measure the optical absorption coefficient in the ocean, *Limnol. Oceanogr.*, **34:** 1614-1622.

Van Zee, H., D. Hankins, and C. deLespinasse, 2002: *ac-9 Protocol Document (Revision F)*. WET Labs Inc., Philomath, OR, 41pp.

Wells, W.H., 1983: Techniques for measuring radiance in sea and air. *Appl. Opt.*, **22:** 2313-2321.

Zaneveld, J.R.V., E. Boss and A. Barnard, 2001. Influence of surface waves on measured and modeled irradiance profiles. Appl. Opt., **40**(9): 1442-1449.

Zaneveld, J.R.V., J.C. Kitchen, A. Bricaud, and C. Moore, 1992: Analysis of *in situ* spectral absorption meter data. *Ocean Optics XI,* G.D. Gilbert, Ed., SPIE, 1750, 187--200.

Zaneveld, J.R.V., and H. Pak, 1972. Some aspects of the axially symmetric submarine daylight field. *J. Geophys. Res*., **77(15):** 2677-2680.

Chapter 2

Beam Transmission and Attenuation Coefficients: Instruments, Characterization, Field Measurements and Data Analysis Protocols

Scott Pegau[1], J. Ronald V. Zaneveld[1] and James L. Mueller[2]

[1]*College of Oceanographic and Atmospheric Sciences, Oregon State University, Corvallis*
[2]*Center for Hydro-Optics and Remote Sensing, San Diego State University, California*

2.1 INTRODUCTION

Beam transmittance $T(\lambda, r_T)$ over an optical path of length r_T m, and the beam attenuation coefficient $c(\lambda)$ $\left[\mathrm{m}^{-1}\right]$, are introduced in Chapter 1 (Sect. 1.3). The two variables are related by equation (1.6). A ***beam transmissometer*** is an instrument that combines a source of collimated spectral radiant flux $\Phi_o(\lambda, 0, 0, \bullet)$ and a co-aligned detector, to measure the flux $\Phi_T(\lambda, r_T, 0, \bullet)$ transmitted over distance r_T, to measure $T(\lambda, r_T)$ (Fig. 1.4 and related text in Sect. 1.3, Ch. 1). A beam transmissometer is also frequently called a ***beam attenuation meter***, or a ***c-meter***.

2.2 TRANSMISSOMETER DESIGN CHARACTERISTICS

In concept, a beam transmissometer is a relatively simple instrument to build, and the derived beam attenuation coefficient is needed in many optical studies of the sea. Therefore, instruments of this type have been in use for many years. While a great number of different transmissometer designs have appeared, most follow one of the two basic designs illustrated in Fig. 2.1.

Direct and Folded Path Transmissometers

Probably the most common transmissometer design uses a collimated light beam[8], with a source in one housing and a detector facing the source (Fig. 2.1, top panel). In such an ideal ***direct-path transmissometer***, either a white light, or a light emitting diode (LED), source is combined with a pinhole to provide a point source. A lens is inserted into the path to collimate the light beam, an interference filter is inserted to select the waveband of the measurement, and the light is passed into the water through a window. At the other end of the optical path, the light enters the detector assembly through another window and is focused by a lens. An aperture at the focal point removes off-axis scattered light, and the transmitted light falls on the detector. Although this instrument is conceptually simple, it is difficult to build. The alignment of components is critical, and something as simple as the filament in the source sagging as the instrument is moved can create significant apparent changes in the derived beam attenuation coefficient. Several commercial transmissometers[9] including, some laboratory

[8] Cylindrically limited beam, as opposed to collimated beam, transmissometers will be discussed later in this section.

[9] Certain commercial equipment, instruments, or materials are identified in this chapter to foster understanding. Such identification does not imply recommendation, or endorsement, by the National Aeronautics and Space Administration, nor does it imply that the materials or equipment identified are necessarily the best available for the purpose.

spectrophotometers, and the (former) SeaTech and WET Labs field instruments use this basic design. Design variations include the addition of a reference detector and placing the wavelength filter in the detector housing.

The folded pathlength design (Fig. 2.1, bottom panel) uses one or more reflectors to create a longer pathlength. The basic idea for this design can be attributed to Petterson (1934). Initial designs used plane mirrors to expand the pathlength (Wattenberg, 1938; Timofeeva, 1960). The introduction of prisms to separate the incident and reflected beam (Nikolayev and Zhil'tsov 1968; Petzold and Austin 1968) and of concave mirrors as the reflectors, have led to improved versions of this general design. An optical pathlength of 10 m was achieved by Jerlov (1957) by using multiple reflections between three concave mirrors. A currently available commercial instrument with a folded path is the HOBILabs c meter.

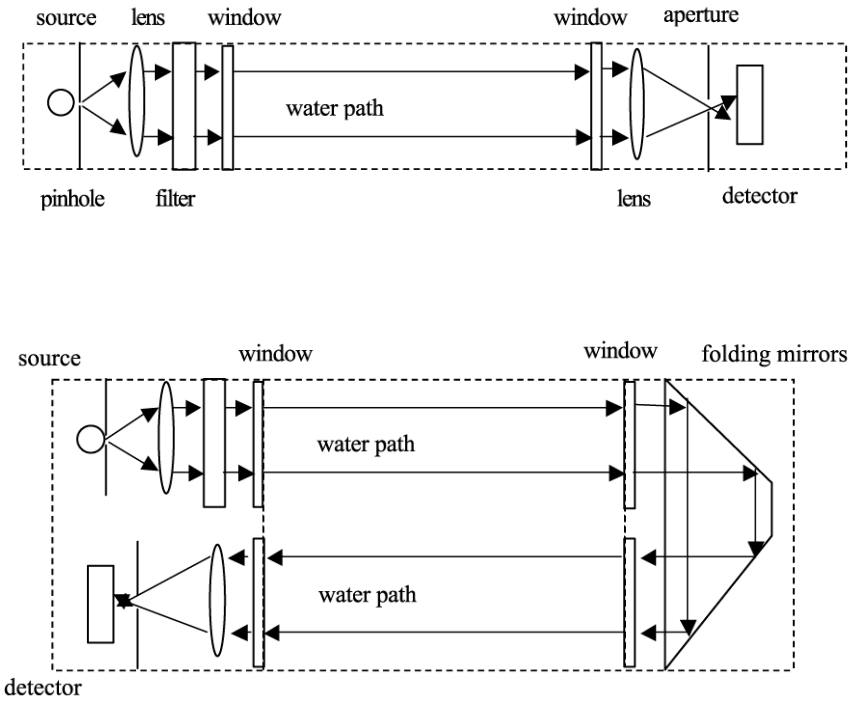

Fig. 2.1 Schematic illustrations of direct path (top panel) and folded path (bottom panel) beam transmissometers designs.

Other Types of Transmissometers

A ***variable pathlength transmissometer*** is probably the most desirable, and elusive, c-meter design concept. One desirable factor would be such an instrument's ability to adjust the pathlength to make it optimal for the measuring conditions (see *Pathlength Considerations*, below). More importantly, the variable pathlength instrument is self-calibrating. To understand this property of such an instrument, examine the basic equation (1.6) for transmissometer measurements. For any transmissometer measurement over pathlength r_i, the dark-corrected detector output $V_T(\lambda, r_i)$ is proportional to the flux reaching the detector window $\Phi_T(\lambda, r_i, 0, \bullet)$. If two transmissometer measurements are made using different path lengths, r_1 and r_2, the transmittance over the pathlength difference between the two measurements is simply

$$T(\lambda, r_2 - r_1) \equiv \frac{\Phi_T(\lambda, r_2, 0, \bullet)}{\Phi_T(\lambda, r_1, 0, \bullet)} = \frac{V_T(\lambda, r_2)}{V_T(\lambda, r_2)}, \tag{2.1}$$

and $c(\lambda)$ may be calculated from (1.6) with $r_T = r_2 - r_1$. The assumptions implicit in this calculation are that the beam attenuation coefficient is constant over the time and space extents of the measurements, and that the optical alignment and electronic properties of the instrument also are constant over time.

Barth *et al*. (1997) describe the design and application of a variable pathlength instrument for use in coastal waters. However, they also note that the errors in alignment made their instrument unsuitable for clear water applications. The requirement to exactly repeat the optical alignment at two distances is the most difficult aspect of building a variable pathlength instrument. Small changes in the alignment of the reference detector, or reflector will introduce large errors in the beam attenuation coefficient by causing the focal point of the beam to wander relative to the aperture in front of the detector. If biofouling exists, the spatial gradients in the fouling will cause $V_T(\lambda, r_i)$ to vary if the alignment is not perfect. Additionally, if the beam is not truly collimated, but instead has a slight divergence, the beam divergence will cause a different area of the detector window to be illuminated in each measurement, and any spatial gradients in the optical properties of the window will translate into errors in $c(\lambda)$.

Many laboratory ***benchtop spectrophotometers*** have a design very similar to a collimated beam transmissometer. A complication that arises when using laboratory spectrophotometers to measure beam attenuation is that much of the scattered light is kept in the sample by the total-internal-reflection at the glass-air interface. This makes it more likely that multiply scattered light will be received at the detector. This problem can be reduced by the addition of light baffles within the sample cuvette.

Source and Detector Characteristics

The transmittance ratio $\frac{\Phi_T(\lambda, r_T, 0, \bullet)}{\Phi_o(\lambda, 0, 0, \bullet)}$, *i.e.* the ratio of the flux transmitted to the detector window divided by the flux entering the water at the source window, must be known to compute $c(\lambda)$ from (1.6). A transmissometer does not actually measure either of these quantities. A transmissometer's detector output signal $V_D(\lambda)$ represents its response in the presence of flux $\Phi_D(\lambda)$, the part of $\Phi_T(\lambda, r_T, 0, \bullet)$ that arrives at the detector after passing through the instrument's detector assembly window and other optical elements (Fig. 2.1). Because of reflections and absorption during transmission through windows and other optical components, $\Phi_T(\lambda, r_T, 0, \bullet) > \Phi_D(\lambda)$, but assuming the optical throughput is linear, $\Phi_T(\lambda, r_T, 0, \bullet) \propto \Phi_D(\lambda)$. The detector's "dark" response $V_D^{dark}(\lambda)$ is any signal output that is present when the source is off and $\Phi_T(\lambda, r_i, 0, \bullet) = 0$. If the detector's electrical response is linear, $\Phi_D(\lambda) \propto \left[V_D(\lambda) - V_D^{dark}(\lambda)\right]$ and we may write

$$\Phi_T(\lambda, r_T, 0, \bullet) = C_D\left[V_D(\lambda) - V_D^{dark}(\lambda)\right], \text{ W nm}^{-1}, \tag{2.2}$$

where C_D is a constant, with units of $\left[\text{W nm}^{-1}\text{V}^{-1}\right]$, accounting for the combined effects of optical losses and the detector's flux responsivity.

A measure of the flux $\Phi_o(\lambda, 0_i, 0, \bullet)$ is still required if the transmission is to be determined. A beam splitter before the source window can be used to shunt a proportion of the source light to a reference detector to provide a measure of the flux being sent into the water. Because of losses associated with the source windows and beam splitter, the reference detector receives, and responds to, a flux proportional to $\Phi_o(\lambda, 0_i, 0, \bullet)$ and we have that

$$\Phi_o(\lambda, 0, 0, \bullet) = C_R\left[V_R(\lambda) - V_R^{dark}(\lambda)\right], \text{ W nm}^{-1}, \tag{2.3}$$

where $V_R(\lambda)$ and $V_R^{dark}(\lambda)$ are the reference detector response and ambient (dark) signals, respectively, and C_R is a second system response constant.

The transmittance may now be written as the ratio of (2.2) and (2.3)

$$T(\lambda, r_T) = \frac{\Phi_T(\lambda, r_T, 0, \bullet)}{\Phi_o(\lambda, 0, 0, \bullet)} = C_T \frac{\left[V_D(\lambda) - V_D^{dark}(\lambda)\right]}{\left[V_R(\lambda) - V_R^{dark}(\lambda)\right]}, \quad (2.4)$$

where $C_T = \frac{C_D}{C_R}$.

If the source output is constant, the constant $\left[V_R(\lambda) - V_R^{dark}(\lambda)\right]$ may be absorbed in C_T and (2.4) reduces to

$$T(\lambda, r_T) = \frac{\Phi_T(\lambda, r_T, 0, \bullet)}{\Phi_o(\lambda, 0, 0, \bullet)} = C_T\left[V_D(\lambda) - V_D^{dark}(\lambda)\right], \quad (2.5)$$

and there is no need to use a reference detector[10] output to calculate transmittance.

Depending on a transmissometer's design, we must determine the coefficient C_T in either (2.4) or (2.5). It is not practical to determine the system response constants based on first principles, because they are dependent on the optical component throughputs, the combined response(s) of the detector(s), and electronic circuits. Instead , a system's calibration constant C_T [dimensionless in (2.4), or in V^{-1} in (2.5)] is typically determined by measuring the instrument's output in a "standard" medium having a known beam attenuation coefficient $c_{STD}(\lambda)$. For oceanographic transmissometers, the "standard" medium is highly purified water (Sect. 2.3 below), and $c_{STD}(\lambda) = c_w(\lambda)$ (Ch. 1, Sect. 1.2).

Transmissometer Response Temperature Dependence

The source output, responsivity of the detector, and performance of other electronic components tend to be temperature dependent. This causes the calibration constants to be temperature dependent. Two approaches are used to remove the temperature dependence, 1) add compensating electronics that allow the voltage output to remain constant over a temperature range, or 2) measure the temperature of the instrument and determine the how the constants change with temperature. The first technique is used in many single-wavelength transmissometers, such as the Sea Tech and WET Labs transmissometers. The second approach is used in the WET Labs ac-9 spectral absorption and beam attenuation meter.

Spectral Characteristics

Many areas of research in ocean optics require knowledge of the spectral beam attenuation coefficient $c(\lambda)$ at more than one wavelength λ. Several c-meters have been built to provide this spectral information. Matlack (1974) used an instrument with a grating monochromator to measure $c(\lambda)$ in the wavelength range from 385 nm to 565 nm. Using a pair of circular wedge interference filters, Lundgren (1975) was able to measure the beam attenuation coefficient at wavelengths between 340 nm and 730 nm. More recent transmissometers that use a monochromator as the detector include the one described by Barth *et al*. (1997), and the WET Labs Histar. Another design for obtaining the spectral beam attenuation coefficient utilizes several interference filters mounted in a wheel that rotates them through the beam. Examples of filter-wheel c-meter designs include the VLST (Petzold and Austin 1968) and the WET Labs ac-9 (Moore *et al*. 1992; Van Zee *et al*. 2002).

Beam Geometry, Detector Acceptance Angle and Scattered Light

Real transmissometers do not have perfectly collimated sources or detectors. Unlike the idealized detector concept of Fig. 1.4 (Ch. 1, Sect. 1.3), a detector with a finite acceptance angle, or Field of View (FOV) ψ_{FOV}, detects photons that are singly scattered in the range $0 < \psi \le \psi_{FOV}$. Therefore, the flux $\Phi_T^M(\lambda, r_T, 0, \bullet)$ arriving at a

[10] A reference detector may be used in a feedback circuit to stabilize an LED source. However, the reference detector signal is not usually included in the instrument's data output stream in constant source output designs of this type.

transmissometer's detector assembly window and subsequently measured (see above) exceeds the true flux directly transmitted along the path direction $\psi \equiv 0$ according to

$$\Phi_T^M(\lambda, r_T, 0, \bullet) = \Phi_T(\lambda, r_T, 0, \bullet) + 2\pi \int_0^{\psi_{FOV}} \beta(\lambda, \psi, \varphi) \sin\psi d\psi \,, \tag{2.6}$$

where $\beta(\lambda, \psi, \varphi)$ is the volume scattering function (VSF) (Ch. 1, Sect. 1.5). In other words, because a transmissometer measures a portion of the forward scattered light, its measurement overestimates the transmittance $T(\lambda, r_T)$ and underestimates the beam attenuation coefficient calculated with equation (1.6). The acceptance angle, and thus the scattering error, is dependent on the optical elements of the instrument. There is no standard specified for transmissometer acceptance angle, and each manufacturer may use a different one for each particular instrument design. Therefore, were the transmittance of a homogeneous water volume to be measured a number of perfectly calibrated beam attenuation meters from HOBILabs, WET Labs, or Sea Tech, for example, each instrument model would yield a slightly different $c(\lambda)$, because of its different acceptance angle. These differences also depend on the shape of VSF.

These considerations lead to two questions. What is the best detector acceptance angle choice for a transmissometer design? What method should be used to correct the beam attenuation measurements for scattered light acceptance?

The first question appears to have a simple answer. The above discussion and equation (2.8) would seem to imply that the smaller the acceptance angle, the better the measurement. That may not be correct. One must further consider what is being measured when choosing the acceptance angle (Pegau *et al*. 1995), and particularly at very small angles, in the presence of near-forward scattering. Density fluctuations due to natural, or instrument related, turbulence steer the beam into random fluctuations and increase the apparent beam attenuation coefficient (Bogucki *et al*. 1998) independently from ordinary molecular and particle scattering processes (Ch. 1, Sect. 1.5). How might this phenomenon affect a particular application of the measurement? Were a person interested in inverting the spectral beam attenuation coefficient to determine particle properties, they wouldn't want a beam attenuation meter that is very sensitive to scattering by turbulence. For active LIDAR imaging systems, on the other hand, it may be important to know the transmittance effects due to very near forward scattering independent of the sources that may dominate the scattering process. From another perspective, the angular resolution of radiative transfer models tends to be larger than one degree, so fine angular resolution of the volume scattering coefficient and related beam attenuation coefficient is not needed for accurate model calculations (Mobley *et al*, 1993). For many such calculations it is preferable to smooth the highly forward peaked phase function (Fig. 1.3, Ch. 2) and decrease the beam attenuation coefficient accordingly. Gordon (1993) indicates that for irradiance level radiative transfer it is possible to completely disregard scattering in the first 15°, an angle much larger than the acceptance angles of transmissometers. Finally, from an engineering perspective, it is more difficult to build a stable transmissometer with a very small acceptance angle. Based on these considerations, most transmissometers are designed with an acceptance angle $\lesssim 1°$.

The second question has been addressed by several investigators over the years (Gumprecht and Sliepcevich, 1953; Jones and Wills, 1956; Jerlov, 1957; Duntley, 1963; Voss and Austin, 1993). Voss and Austin (1993) examined the scattering error for both collimated beam and cylindrically limited instruments designs. They found that the percent error increases with increasing acceptance angle and with increasing $c(\lambda)$. The average error for a 670 nm transmissometer with a 1.0° acceptance angle is approximately 19%. However, accurate correction of an apparent $c_M(\lambda)$ measured by that instrument would require knowing both the VSF $\beta(\lambda, \psi, \varphi)$ over the range $0 < \psi \le \psi_{FOV}$, and the single scattering albedo $\omega_o(\lambda) = \dfrac{b(\lambda)}{c(\lambda)}$ (Vol. I, Ch. 2, Sect. 2.4). To date, very few reliable measurements have been made of $\beta(\lambda, \psi, \varphi)$ at angles less than 1°. Given the extreme rate of increase in the magnitude of the VSF for particles $\beta_p(\lambda, \psi, \varphi)$, and for turbulence, as $\psi \to 0$ (Ch. 1, Fig. 1.3), any estimate of its integrated value over the range $0 < \psi \le 1°$ would be highly uncertain. That uncertainty would transmit directly into any $c(\lambda)$ correction algorithm attempting to account for the effects of the near-forward VSF.

The best approach to dealing with the effects of scattered light in measured beam attenuation coefficients may be that proposed by both Voss and Austin (1993) and Pegau *et al*. (1995). That is, do not try to apply any scattering corrections to the measured determination of $c(\lambda)$. Simply report the acceptance angle characteristics of the transmissometer used to make the measurements, and leave all considerations of how to handle scattering artifacts to the user of the data. Internal consistency of IOP is obtained by including light scattered up to a certain acceptance angle ψ_{FOV} in the beam attenuation coefficient, and not including it in the VSF. We may rerwrite (1.1), $c(\lambda) = a(\lambda) + b(\lambda)$, as

$$c(\lambda) = a(\lambda) + 2\pi \int_{\psi_{FOV}}^{\pi} \beta(\lambda,\psi)\sin\psi d\psi + 2\pi \int_{0}^{\psi_{FOV}} \beta(\lambda,\psi)\sin\psi d\psi ,$$

or,

$$c_m(\lambda) = c(\lambda) - 2\pi \int_{0}^{\psi_{FOV}} \beta(\lambda,\psi)\sin\psi d\psi = a(\lambda) + 2\pi \int_{\psi_{FOV}}^{\pi} \beta(\lambda,\psi)\sin\psi d\psi = a(\lambda) + b_m(\lambda)$$

where $c_m(\lambda)$ and $b_m(\lambda)$ are the measured beam attenuation and volume scattering coefficients, respectively.

In another design variant, the beam is cylindrically limited, rather than collimated. In the cylindrically limited light arrangement, the pinhole at the source is imaged on the receiver lens, and the receiver aperture is focused on the source lens. This design illuminates a large volume of water and uses more of the source light. No currently available commercial instruments use the cylindrically limited design, although at one point in history, transmissometers of this type were manufactured by Martek. The Visibility Laboratory Spectral Transmissometer (VLST) was a laboratory-built instrument using a cylindrically limited beam in a folded path configuration (Petzold and Austin 1968). Several copies of the VLST, built in the late 1970's, continued in use to measure $c(\lambda)$ until *circa* 1990.

Pathlength Considerations

One issue that must be addressed when designing a transmissometer is what the in-water pathlength should be. Scientifically, it is important to keep the pathlength long enough that the sample volume presents a statistical average of the surrounding water, and short enough that multiply scattered light is not incorporated into the beam. In most ocean waters, multiply scattered light is not in general a problem for the commercially available transmissometers. If scattered light leaves the beam then it will take two additional scattering events to get the light back into the beam and redirected towards the detector. The addition of baffles along the light path can nearly eliminate any possibility of multiply scattered light being detected in ordinary circumstance. In extremely turbid waters, however, the single scattering albedo is very large, and the volume scattering phase function $\tilde{\beta}(\lambda,\psi,\varphi)$ is extremely biased in the near forward direction (Fig. 1.3, Ch. 1). Under such conditions, if $r_T > 3c(\lambda)^{-1}$ m , there is a significant probability that some fraction of scattered photons will undergo 3 or more successive small angle scattering events, re-enter the transmission path, and join the flux reaching the detector. The apparent beam attenuation coefficient will be artificially reduced if this occurs.

There are also engineering concerns associated with the optical pathlength. The path must be short enough that light reaches the detector; it would do no good to have an instrument with a pathlength $r_T \approx 10c(\lambda)^{-1}$ m , because the transmitted signal would not be detectable. On the other hand, the pathlength must be long enough for attenuation to reduce the transmitted flux enough that the difference in incident and transmitted fluxes are large enough to be measurable. Longer pathlengths also reduce the relative uncertainty in the measurement of the pathlength r_T .

A pathlength in the range $c(\lambda)^{-1} \le r_T \le 3c(\lambda)^{-1}$ is generally considered close to optimal. As electronics and sources have improved, however, instruments with pathlengths $r_T < c(\lambda)^{-1}$ m have been shown to work well over a wide range of oceanic conditions.

Ambient Light Rejection in Open and Enclosed Path Transmissometers

The basic transmissometer designs (Fig. 2.1) do not physically reject all ambient sunlight, which could add to the measured flux. Enclosed path designs that place the optical path within a cell through which the water is pumped, such as the ac-9, have more physical blocking of ambient light, but are not totally immune to its effects. Some scheme must be developed to remove ambient light artifacts. A simple approach is to measure the signal with the source on and with the source off. The ambient signal with the source off is used as the dark reference for relating output signal to transmitted flux. The current generation of instruments use a more sophisticated, but similar, approach. The light source is rapidly modulated (chopped) and the detector output is phase locked to the modulation frequency, so that the transmitted flux is proportional to the amplitude of the alternating component of detector output. The key underlying assumption is that the natural light field varies slowly and is not part of the alternating signal. This approach may have difficulties when the ambient light also varies rapidly, such as with indoor lights that have a 60 Hz fluctuation, or near the ocean surface where waves may rapidly modulate the light field. Even with good electronic rejection of ambient light, it is wise to reduce the possible influence of ambient light by using baffles and careful positioning of the instrument.

2.3 CHARACTERIZATION and CALIBRATION OF BEAM TRANSMISSOMETERS

Calibration With Pure Water

As explained above, the calibration constant C_T for a transmissometer is determined by measuring its response to a "standard" medium having a known value of $c_{\mathrm{STD}}(\lambda)$. The optical "standard" medium commonly used to calibrate oceanographic transmissometers and absorption meters (Ch. 3) is pure water, so that $c_{\mathrm{STD}}(\lambda) = c_{\mathrm{w}}(\lambda) = a_{\mathrm{w}}(\lambda) + b_{\mathrm{w}}(\lambda)$. The recommended values of $a_{\mathrm{w}}(\lambda)$ and $b_{\mathrm{w}}(\lambda)$ are taken from Table 1.2, as explained in Ch. 1, Sect. 1.2.

Pure water of optical calibration grade is freshly prepared by methods described in Chapter 3. This difficult step is critical, because residual traces of particles and/or dissolved organic material introduce serious calibration offsets and relative uncertainties between calibrations. The pure water standard is introduced into the optical path by one of two methods:

1. An open path transmissometer must be thoroughly cleaned and rinsed in purified water, and then immersed in a test tank containing the pure water standard. Care must be taken to prevent bubbles from collecting on the instrument's optical windows. It is ordinarily not practical to carry out this calibration procedure at sea.
2. To calibrate an enclosed path instrument, a volume of the pure water standard is pumped through the flow-through measurement cell, as described in detail in Chapter 3 for the ac-9, as an example. Procedures to assure bubbles do not form within, or be introduced into, the flow-through measurement cell (Ch. 3) must be followed carefully. This pure-water calibration procedure can be carried out at sea, and it is recommended to do so daily, whenever possible.

In either case, after allowing suitable time for the instrument to warm up, the instrument signal outputs in response to flux transmitted in the pure water standard and dark (ambient) background, $V_{\mathrm{D,w}}(\lambda)$ and $V_{\mathrm{D,w}}^{\mathrm{dark}}(\lambda)$ [and if appropriate, also $V_{\mathrm{R,w}}(\lambda)$ and $V_{\mathrm{R,w}}^{\mathrm{dark}}(\lambda)$], are recorded over a several minute sampling period and averaged.

For pure water, the forward scattering is sufficiently small that the acceptance angle has little effect on the calibration. From equation (1.7) (Ch. 1), the transmittance of the pure water standard is $T_{\mathrm{w}}(\lambda, r_{\mathrm{T}}) = e^{-c_{\mathrm{w}}(\lambda) r_{\mathrm{T}}}$. For an instrument with a source reference detector we substitute from (2.4) to write

$$\mathrm{C_T}(\lambda) = T_{\mathrm{W}}(\lambda, r_{\mathrm{T}}) \frac{\left[V_{\mathrm{R,w}}(\lambda) - V_{\mathrm{R,w}}^{\mathrm{dark}}(\lambda)\right]}{\left[V_{\mathrm{D,w}}(\lambda) - V_{\mathrm{D,w}}^{\mathrm{dark}}(\lambda)\right]}, \tag{2.7}$$

or for an instrument with a constant source output we substitute from (2.5) to write

$$\mathrm{C_T}(\lambda) = \frac{T_\mathrm{W}(\lambda, r_\mathrm{T})}{\left[V_\mathrm{D,w}(\lambda) - V_\mathrm{D,w}^\mathrm{dark}(\lambda)\right]}, \tag{2.8}$$

as appropriate.

By straightforward combinations of (1.6), (2.4) and (2.7) it is easy to show that for a transmissometer with a source reference detector,

$$\begin{aligned} T(\lambda, r_\mathrm{T}) &= T_\mathrm{W}(\lambda, r_\mathrm{T}) \frac{\left[V_\mathrm{R,w}(\lambda) - V_\mathrm{R,w}^\mathrm{dark}(\lambda)\right]}{\left[V_\mathrm{D,w}(\lambda) - V_\mathrm{D,w}^\mathrm{dark}(\lambda)\right]} \frac{\left[V_\mathrm{D}(\lambda) - V_\mathrm{D}^\mathrm{dark}(\lambda)\right]}{\left[V_\mathrm{R}(\lambda) - V_\mathrm{R}^\mathrm{dark}(\lambda)\right]}, \text{ and} \\ c(\lambda) - c_\mathrm{w}(\lambda) &= \frac{1}{r_\mathrm{T}} \ln\left\{ \frac{\left[V_\mathrm{R,w}(\lambda) - V_\mathrm{R,w}^\mathrm{dark}(\lambda)\right]}{\left[V_\mathrm{D,w}(\lambda) - V_\mathrm{D,w}^\mathrm{dark}(\lambda)\right]} \frac{\left[V_\mathrm{D}(\lambda) - V_\mathrm{D}^\mathrm{dark}(\lambda)\right]}{\left[V_\mathrm{R}(\lambda) - V_\mathrm{R}^\mathrm{dark}(\lambda)\right]} \right\} \end{aligned}, \tag{2.9}$$

or combining (1.6), 2.(5) and (2.8) for a transmissometer with a constant source output

$$\begin{aligned} T(\lambda, r_\mathrm{T}) &= T_\mathrm{W}(\lambda, r_\mathrm{T}) \frac{\left[V_\mathrm{D}(\lambda) - V_\mathrm{D}^\mathrm{dark}(\lambda)\right]}{\left[V_\mathrm{D,w}(\lambda) - V_\mathrm{D,w}^\mathrm{dark}(\lambda)\right]}, \text{ and} \\ c(\lambda) - c_\mathrm{w}(\lambda) &= \frac{-1}{r_\mathrm{T}} \ln\left\{ \frac{\left[V_\mathrm{D}(\lambda) - V_\mathrm{D}^\mathrm{dark}(\lambda)\right]}{\left[V_\mathrm{D,w}(\lambda) - V_\mathrm{D,w}^\mathrm{dark}(\lambda)\right]} \right\}. \end{aligned} \tag{2.10}$$

The essential calibration factors to be reported, therefore, are the detector response and ambient (dark) offset in pure water $V_\mathrm{D,w}(\lambda)$ and $V_\mathrm{D,w}^\mathrm{dark}(\lambda)$, and if a source reference detector is used also its response and ambient offset $V_\mathrm{R,w}(\lambda)$ and $V_\mathrm{R,w}^\mathrm{dark}(\lambda)$. The total beam attenuation coefficient $c(\lambda)$ may be easily determined by adding $c_\mathrm{w}(\lambda)$ from Table 1.1 (Ch. 1) to the difference calculated with equation (2.9) or (2.10).

An alternative approach to determining the total beam attenuation coefficient directly from the measured voltage response is to determine, from the pure water calibration, a calculated offset reference voltage $V_\mathrm{ref}(\lambda)$ and dark offset $V_\mathrm{dark}(\lambda)$ such that the total transmittance may be calculated directly as

$$T(\lambda, r_\mathrm{T}) = \frac{\left[V_\mathrm{D}(\lambda) - V_\mathrm{D,w}^\mathrm{dark}(\lambda)\right]}{\left[V_\mathrm{ref}(\lambda) - V_\mathrm{D,w}^\mathrm{dark}(\lambda)\right]}, \tag{2.11}$$

where it is assumed that $V_\mathrm{D}^\mathrm{dark}(\lambda) = V_\mathrm{D,w}^\mathrm{dark}(\lambda)$ varies very slowly over time and may be treated as an instrument constant. This approach is only used with transmissometers assumed to have a constant source output, examples of which include the former SeaTech red transmissometers. The value of $V_\mathrm{ref}(\lambda)$ is calculated by combining (2.11) with the transmittance relationship (2.10) as

$$T(\lambda, r_\mathrm{T}) = T_\mathrm{W}(\lambda, r_\mathrm{T}) \frac{\left[V_\mathrm{D}(\lambda) - V_\mathrm{D}^\mathrm{dark}(\lambda)\right]}{\left[V_\mathrm{D,w}(\lambda) - V_\mathrm{D,w}^\mathrm{dark}(\lambda)\right]} = \frac{\left[V_\mathrm{D}(\lambda) - V_\mathrm{D,w}^\mathrm{dark}(\lambda)\right]}{\left[V_\mathrm{ref}(\lambda) - V_\mathrm{D,w}^\mathrm{dark}(\lambda)\right]},$$

from which it easily follows that

$$V_\mathrm{ref}(\lambda) = \frac{V_\mathrm{D,w}(\lambda) - V_\mathrm{D,w}^\mathrm{dark}(\lambda)}{T_\mathrm{W}(\lambda, r_\mathrm{T})} + V_\mathrm{D,w}^\mathrm{dark}(\lambda), \text{ V}. \tag{2.12}$$

The Sea Tech transmissometers were calibrated to read $c_\mathrm{w}(650) = 0.364$ m^{-1} in pure water. This representation and approach perhaps simplifies the determination of $c(\lambda)$ for the inexperienced user, but at the same time obscures the value of $c_\mathrm{w}(\lambda)$ used to determine the offset reference voltage.

Air "Calibrations"

The sensors output signal response $V_{\mathrm{D,air}}^{\mathrm{f}}$ and dark offset $V_{\mathrm{D,air}}^{\mathrm{dark,f}}$ are recorded in air by the manufacturer at the time of each factory water calibration. These values are typically reported with the calibration records, as "factory" air calibration and dark values (and thus the superscript "f"), to allow the user to periodically record "air calibration", or "air tracking" data as a check on instrument stability. Air tracking is primarily intended to be used to monitor offsets in the instrument's output due to changes in the optical system caused by shipping or mounting of the instrument to a cage or other deployment package. Air tracking can also be used to monitor instrument drift over extended periods of time. Historically, before the advent of pure water field calibrations, the air calibration was the only stability tracking method available.

Air tracking data is best obtained in the laboratory, where the environment is consistently clean and dry, preferably before and after each transmissometer deployment. Although air calibrations can be performed while in the field, it is at best, difficult to do them on a ship due to the moist environment. Readings in air may be significantly offset by small amounts of moisture either condensed on, or adsorbed in the windows.

Detailed protocols for carrying out air calibrations are provided for particular instruments by the manufacturer. In general terms, the protocols include instructions and methods for careful cleaning of optical surfaces, allowing time for exposed optical surfaces to dehydrate in a dry environment, and procedures to avoid or compensate for temperature increases when the instrument is operated in air.

User air calibration values can be used to adjust the pure water calibration and responses to correct for instrument drift as

$$V_{\mathrm{D,w}}^{\mathrm{adjusted}} = \frac{V_{\mathrm{D,air}} - V_{\mathrm{D,air}}^{\mathrm{dark}}}{V_{\mathrm{D,air}}^{\mathrm{f}} - V_{\mathrm{D,air}}^{\mathrm{dark,f}}}\left[V_{\mathrm{D,w}}^{\mathrm{f}} - V_{\mathrm{D,w}}^{\mathrm{dark,f}}\right], \tag{2.13}$$

and the adjusted pure water-response and dark values are substituted into (2.10) to calibrate field measurements. If the manufacturer instead provides a factory reference voltage for calibrating the instrument using equation (2.11), the adjusted pure water and dark values should be substituted in (2.12) to determine $V_{\mathrm{ref}}^{\mathrm{adjusted}}$. Air calibration adjustments of this type are usually recommended only for instruments with "constant" LED source output, such as the WET Labs C-Star, older SeaTech red transmissometers, and other similar instruments by different manufacturers. Field water calibrations are the recommended basis for correcting drifts in closed path, flow-through cell instrument, such as the ac-9.

Instrument Temperature Dependence

The change in a transmissometer's response and dark values are usually determined by measuring response variations, with the optical path in air, or in a dry, inert gas such as Nitrogen or Argon, as the instrument temperature is varied. The response and dark values at each internal instrument temperature (an ancillary measurement and data output needed for temperature corrections) are recorded, and reported either as a lookup table of correction factor and temperature pairs, or as the coefficients of a polynomial function of temperature that has been fit to the correction factors. Instruments that have a closed, flow-through optical cell are usually characterized in a water bath, the temperature of which is cycled over a range typically from 5 $^{\mathrm{o}}$C to 30 $^{\mathrm{o}}$C over the course of the experiment; to avoid condensation, the flow-through cell is usually filled with a dry, inert gas and sealed. The internal instrument temperatures are somewhat higher than the ambient temperature, due to heating by the electronic circuits and source. If this experiment is done with air in the optical path of an open-path transmissometer, *i.e.* in a temperature controlled chamber, some method must be used and documented to avoid artifacts due to condensation on the windows.

2.4 FIELD MEASUREMENT METHODS

The procedures for measuring *in situ* profiles, over depth *z*, of $c(z,\lambda)$ using constant output LED source transmissometers are straightforward. The instrument is connected into a data acquisition system and mounted on a profiling cage following the manufacturer's instructions. If the instrument has an analog output, the user must

ensure that the external analog-to-digital converter used to digitize the readings is calibrated in absolute units of V, since that is the basis on which the instrument has been calibrated.

The windows on the beam transmissometer must be cleaned with lens cleaner, or a mild detergent solution, and a soft cloth, or tissue, rinsed with distilled water, then rinsed with isopropyl alcohol and wiped dry. An approximate air calibration reading should be made before every cast to verify that the windows are clean. A transmissometer dark voltage should also be measured at this time. These on-deck air calibrations should be logged and compared to the more careful air calibrations done under dry laboratory conditions before and after each cruise (Section 2.3). If pre- and post-cruise air calibrations are significantly different, the time history should indicate whether the change occurred suddenly (*e.g.* a scratch in the window), or as a drift over time.

Each time an open-path transmissometer is placed into the water, care must be taken to assure that bubbles do not collect on the windows, particularly if the instrument is mounted in a vertical orientation.

Protocols covering methods for making field measurements with the ac-9 instrument are described in detail in Zee *et al*. (2002). Some critical aspects of these protocols are briefly reviewed in Chapter 3 to emphasize their importance.

2.5 DATA ANALYSIS METHODS

There are several generic steps needed to process and analyze a vertical profile of measured transmissometer data:

1. ***Merge the transmissometer data*** with externally measured ***depth*** and ***temperature data***. Assuming that the transmissometer does not have an internal, high-quality depth transducer, it is usually mounted together with a CTD to provide the depth and water temperature fields. If the transmissometer output data record does not include the internal instrument temperature measured by a built-in thermistor, external water temperature provides the basis for any temperature compensation adjustments that may be required.
2. Apply ***lag corrections*** to account for the time interval between when water enters the intake port and when it enters the beam-attenuation measurement optical path in a flow-through transmissometer.
3. Subtract the ***depth offset*** between the pressure transducer used to measure package depth and either

a. the intake port of a flow-through transmissometer, or

b. the midpoint of the optical path in an open path transmissometer.

4. ***Field calibration adjustments*** should be applied by the methods specified by the manufacturer of a particular instrument. In many cases this will involve entering the changes in an instrument calibration file used by the computer software that implements and applies (2.9) or (2.10) to calibrate the data.

    a. Pure water calibration results are the preferred source of these adjustments for flow-through instruments.

    b. Air calibration for tracking drift corrections should be applied using only data from calibrations carried out under dry laboratory conditions and showing insignificant variations between replicated calibrations. When the manufacturer represents the calibration coefficients in terms of a reference signal to be applied using (2.11), the corrected air calibration factor is computed using (2.13).

5. ***Instrument Internal Temperature Compensation*** factors should be applied in the manner specified by the manufacturer of a particular instrument.
6. *Compute transmittances* $T(\lambda, r_T)$, ***and beam attenuation coefficients*** $c(\lambda) - c_w(\lambda)$ offsets, ***relative to pure water*** using the appropriate combination of equations (2.9), (2.10), or (2.11) with (1.6) for the instrument type and output data.
7. ***Add pure water*** $c_w(\lambda)$, determined from Table 1.1, to $c(\lambda) - c_w(\lambda)$ to obtain the ***total beam attenuation coefficient*** $c(\lambda)$.

Detailed procedures required to carry out each of the above steps for particular instrument are typically provided by the manufacturer. WET Labs Inc., for example, provides both a User's Manual for it's *ac-9* absorption and beam attenuation coefficient meter, and a detailed ac-9 Protocol Manual (Van Zee *et al*. 2002); additional information from the latter document, regarding absorption and beam attenuation measurements, is outlined in Chapter 3.

Many of the steps listed above apply also when a transmissometer is installed and operated on a ship as a component of an along-track measurement system. The lengthy plumbing path in such a system introduces intake-to-measurement lags of up to several minutes, while a research vessel typically advances approximately one Km in 3 min. Therefore, accurate temporal and spatial co-registration of, *e.g.*, surface water temperature, chlorophyll a fluorescence, and $c(\lambda)$ requires accurate determination of the flow rate and lag time between a water volume's intake (usually in a ship's sea chest), passage through some debubbler apparatus, and its arrival in the measurement cell of each instrument.

REFERENCES

Barth, H., K. Grisard, K. Holtsch, R. Reuter, and U. Stute, 1997. Polycromatic transmissometer for *in situ* measurements of suspended particles and gelbstoff in water. *Appl. Opt.*, **36(30):** 7919-7928.

Bogucki, D.J., J.A. Domaradzki, D. Stramski and J.R.V. Zaneveld, 1998. Comparison of near-forward light scattering on oceanic turbulence and particles. *Appl. Opt.*, **37(21):** 4669-4677.

Duntley, S.Q., 1963. Light in the sea. J. Opt. Soc. Amer., 53(2): 214-233.

Gordon, H.R., 1993. Sensitivity of radiative transfer to small-angle scattering in the ocean: Quantitative assessment. *Appl. Opt*., **32(36):** 7505-7511.

Gumprecht, R.O. and C.M. Sliepcevich, 1953: scattering of light by large spherical particles, *J. Opt. Soc. Am.*, **57:** 90-94.

Jerlov, N.G., 1957: A transparency-meter for ocean water, *Tellus*, 9: 229-233.

Jones, D. and M.S. Wills, 1956: The attenuation of light in sea and estuarine waters in relation to the concentration of suspended solid matter, *J Mar. Biol. Assoc. U.K*., **35:** 431-444.

Kitchen, J.C., J.R.V. Zaneveld and H. Pak, 1982: Effect of particle size distribution and chlorophyll content on beam attenuation spectra. Applied Optics. **21**: 3913-3918.

Lundgren, B., 1975: Measurements in the Baltic with a spectral transmittance meter, *Univ. Copenhagen, Inst. Phys. Oceanogr. Rep.*, **30:** 28pp.

Matlack, D.E., 1974: Deep ocean optical measurements (DOM) report on North Atlantic, Caribbean, and Mediterranean cruises, *Tech. Rep. Naval Ordnance Lab.*, pp 1-103.

Moore, C., J.R.V. Zaneveld and J.C. Kitchen, 1992: Preliminary results from an *in situ* spectral absorption meter, *Ocean Optics XI*, *Proc. SPIE* **1750:** 330-337.

Mobley, C.D., and OTHERS, 1993. Comparison of numerical models for computing underwater light fields. *Appl. Opt.*, **32(36):** 7484-7504

Nikolayev, V.P. and A.A. Zhil'tsov, 1968: Simple photoelectric transparency meter, *Oceanology (U.S.S.R.)*, **8:** 428-432.

Pegau, W. S., J. R. V. Zaneveld, and K. J. Voss, 1995: Toward closure of the inherent optical properties of natural waters, *J. Geophys. Res.*, **100:** 13,193-13.

Pettersson, H., 1934: A transparency-meter for sea-water, Medd. Oceanogr. Inst. Gothenberg, Ser. B **4**.

Petzold, T. and R.W. Austin, 19686: An underwater transmissometer for ocean survey work, In: *Underwater Photo-optical Instrument Applications*, Proc. SPIE 12: 133-137.

Timofeeva, V.A., 1960: Instrument for determining the attenuation coefficient of directed light in the sea, *Sov. Oceanogr. 1962 Ser.*, **4:** 79-83.

Van Zee, H., D. Hankins, and C. deLespinasse, 2002: *ac-9 Protocol Document (Revision F)*. WET Labs Inc., Philomath, OR, 41pp.

Voss, K.J. and R.W. Austin, 1993. Beam-attenuation measurement error due to small-angle scattering acceptance. *J. Atmos. and Oceanic Tech*., **19(1):** 113-121

Wattenberg, H., 1938: Untersuchungen uber Durchsichtigkeit und Farbe des Seewassers, I. *Kieler Meeresforsch*., **2**.

Chapter 3

Volume Absorption Coefficients: Instruments, Characterization, Field Measurements and Data Analysis Protocols

Scott Pegau[1], J. Ronald V. Zaneveld[1] and James L. Mueller[2]

College of Oceanographic and Atmospheric Sciences, Oregon State University, Corvallis
[2]Center for Hydro-Optics and Remote Sensing, San Diego State University, California

3.1 INTRODUCTION

Concepts and methods for measuring the absorption coefficient $a(\lambda)$ of seawater are briefly reviewed in Chapter 1 (Sect. 1.4) of this Volume. Chapter 4 of this Volume is devoted to laboratory spectrophotometric methods of measuring absorption of particles and dissolved materials in filtered water samples. The present chapter focuses on commercially available instruments[11] that may be used from ships and moored platforms to practically measure $a(\lambda)$ in support of satellite validation activities. This first version of absorption protocols is particularly focused on instruments that fall under the "reflective tube" design concept briefly introduced in Sect. 1.4. However, the conceptual basis for determining absorption by measuring flux reflected from a diffuse target is also described later in this section. Expanded reviews of protocols using instruments based on other design concepts are deferred for possible consideration in future revisions to this volume.

Reflective Tube Absorption Meter Concepts

In Sect. 1.4 it was observed that to determine the absorption coefficient associated with transmission over an optical pathlength r_T (Fig. 1.4), it would be necessary to measure the sum of transmitted and scattered flux at the detector, $\Phi_K(r_T) = \Phi_T(r_T) + \Phi_B(r_T)$. Neglecting backscattering, it was suggested that perhaps one might redirect all forward scattered flux to the detector using an *ideal reflective tube*, and determine the absorption coefficient as

$$a = \frac{-1}{r_T} \ln\left(\frac{\Phi_T(r_T) + \Phi_B(r_T)}{\Phi_o(0)}\right). \tag{3.1}$$

Of course a perfectly reflecting tube cannot be realized in a real instrument. Nevertheless, because the scattering phase function of suspended particles in natural waters is strongly peaked in the forward direction (Fig. 1.3), it is possible to use this approach to retain more than approximately 85% of scattered photons in the beam reaching the detector of such an instrument. James and Birge (1938) built a laboratory version of such an instrument to measure absorption spectra of lake waters, and Zaneveld *et al*. (1992) introduced an instrument of this type for *in situ* absorption measurements. In essence, such an instrument is simply a poor transmissometer (Chapter 2) that fails to exclude all of the singly scattered photons from its beam transmittance measurement, and therefore, in its ideal realization would measure only losses due by absorption as per equations (1.9) and (1.10).

The transmittance, absorption, scattering and reflection interaction processes that occur in a real reflective tube absorption meter are illustrated schematically in Fig. 3.1. A source emits collimated flux with a cross sectional area slightly less that that of the reflective tube, and flux reaching the other end of the tube is measured by a detector that covers its entire cross-sectional area. Ray paths extending directly from the source to the detector indicate direct transmittance of flux. Ray paths that terminate within the water volume enclosed by the tube indicate absorbed flux.

[11] Certain commercial equipment, instruments, or materials are identified in this chapter to foster understanding. Such identification does not imply recommendation, or endorsement, by the National Aeronautics and Space Administration, nor does it imply that the materials or equipment identified are necessarily the best available for the purpose.

In natural waters a large fraction of scattered photons are only slightly deflected in the near forward direction (Fig. 1.3) and proceed directly to the large-area detector without encountering the tube walls. Ray paths with scattering angles large enough to encounter the water-quartz interface, where refraction and reflection take place; the refracted portion is transmitted to the outer quartz-air interface, where another refraction and reflection interaction occurs. For simplicity in this conceptual discussion, we do not consider multiple reflection and refractive transmittance interactions within the thin quartz layer. Ray paths containing a scattering angle less than the critical angle ψ_c associated with total internal reflection at the outer quartz-air interface, are totally reflected on each encounter with the tube wall and are transmitted to the detector over a slightly elongated path; for a quartz reflective tube, $\psi_c \cong 42°$, and thus the total internal reflectance represents a very large fraction of all flux scattered by particles (Fig. 1.3). Flux transmitted along ray paths with a scattering angle in the range $\psi_c < \psi < \frac{\pi}{2}$ undergoes partial transmittance losses $[1-\rho_g(\psi)]$ at each encounter with the reflectance tube, with the reflected portion continuing over a zig-zag path until either reaching the detector or disappearing due to attenuation by absorption and transmission losses in multiple encounters with the tube wall. Flux along ray paths containing a scattering angle $\psi \geq \frac{\pi}{2}$, *i.e.* backscattered flux, is lost from the forward transmittance altogether. Backscattering accounts for only a few percent of scattering by marine particulates (Fig. 1.3).

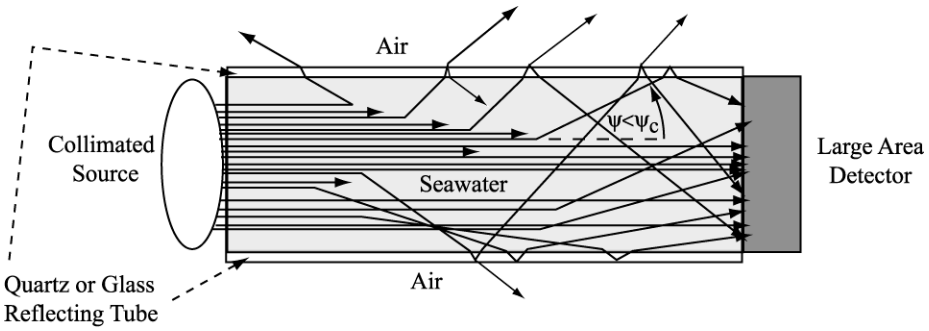

Figure 3.1: Schematic illustration of light interactions and transmission in a reflective tube absorption meter. Ray paths ending in the water represent absorption, and those extending directly from the source to detector represent beam transmittance. Other ray paths indicate scattering interactions: 1) backward scattered paths do not reach the detector, 2) paths with forward scattering at an angle less than the critical angle, *i.e.* $\psi \leq \psi_c$, experience total internal reflection by the tube and reach the detector over an elongated optical path, and 3) forward scattered ray paths at angles in the range $\psi_c < \psi < \frac{\pi}{2}$ experience partial losses from the tube at the quartz-air interface, and may or may not reach the detector depending on whether the internally reflected path survives the absorption process.

In the single scattering approximation, the flux measured by the detector of a reflective tube absorption meter may be written

$$\Phi_m(r_T) = \Phi_T(r_T) + 2\pi\Phi_o(0)\int_0^{r_T}\int_0^{\psi_c}\beta(\psi)e^{-cr}e^{-a\frac{r_T-r}{\cos\psi}}\sin\psi\, d\psi\, dr + 2\pi\Phi_o(0)\int_0^{r_T}\int_0^{\psi_c}\beta(\psi)e^{-cr}e^{-a\frac{r_T-r}{\cos\psi}}\left[\rho_g(\psi)\right]^{N(r_T-r)}\sin\psi\, d\psi\, dr, \quad (3.2)$$

where $\rho_g(\psi)$ is net reflectance of the quartz tube beyond the critical angle, and the exponent $N(r_T - r;\psi)$ is the average number of wall reflections required for a ray path to reach the detector following a scattering event at

distance r and angle ψ. The first integral on the right-hand-side of (3.2) represents flux scattered at angles less than the critical over the optical path, and the second integral represents flux reaching the detector following scattering by angles greater than the critical angle. In either case, the pathlength to the detector from a scattering interaction at distance *r* is $\frac{r_T - r}{\cos\psi}$, and both types of scattered-reflected paths are attenuated by absorption over this elongated path. The second term also is reduced by incomplete reflectance in $N(r_T - r;\psi) \geq 1$ interactions with the reflective tube.

The measured absorption coefficient is therefore greater than the true absorption coefficient since

$$a_m = \frac{-1}{r_T}\ln\left(\frac{\Phi_m(r_T)}{\Phi_o(0)}\right) > a = \frac{-1}{r_T}\ln\left(\frac{\Phi_T(r_T)+\Phi_B(r_T)}{\Phi_o(0)}\right),$$

and the two may be related as

$$a_m = a + 2\pi\int_0^\pi W(\psi)\beta(\psi)\sin\psi d\psi, \tag{3.3}$$

where the weighting coefficients $W(\psi)$ account for the absorption and wall reflection losses in the two integral terms of (3.2) and for the exclusion of backscattering in the measured flux. In other words, the weighting coefficient $W(\psi)$ may be interpreted as the fraction of light that is scattered at angle ψ that does not reach the absorption detector; it may take values from 0, indicating all light scattered at that angle reaches the detector, to 1, indicating that none of the light reaches the detector. The uncertainty of absorption coefficients determined from measurements with a reflective tube instrument is largely determined by the uncertainty of the methods used to correct for the integrated scattering error (Zaneveld *et al*. 1994), which will be briefly summarized below in Sect. 3.4. The remaining sections of this chapter summarize protocols related to characterization, measurement and data analysis using the ac-9 reflective tube absorption meter.

Determination of Absorption by Measuring Flux Reflected from a Diffuse Reflectance Surface

Figure 3.2 illustrates an alternative proposed instrument concept for use in combination with a backscattering meter (Chapter 5) to determine $a(\lambda)$ *in situ*. A divergent source illuminates a diffusely reflecting target oriented parallel to the instrument's window at a fixed distance d_ρ. An instrument of this type, called the "**α-βeta**", is commercially available through HOBILABS, Inc.

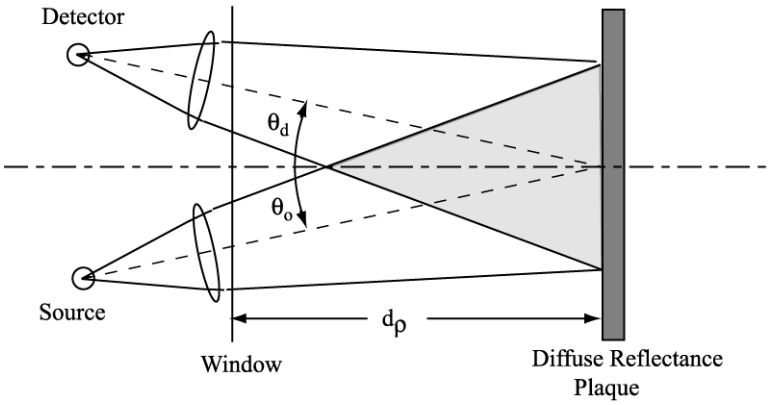

Figure 3.2: Conceptual schematic illustration of an instrument designed to determine the volume absorption coefficient by measuring diffuse reflectance from a plaque. The VSF at one or more angles must be independently and concurrently measured in this approach. See also Figure 5.1, and the related discussion of calibrating a VSF meter using a diffuse reflecting plaque in Section 5.3, in Chapter 5 of this Volume.

For simplicity in this conceptual discussion, we will assume: 1) that the source beam and detector FOV geometries are identical, 2) that the central viewing angles of each are equal, *i.e.* $\theta_o = \theta_d$ (Fig. 3.2), and 3) that the plaque's Bidirectional Reflectance Distribution Function (BRDF) is a constant $\frac{\rho}{\pi}$. The flux reaching the plaque from the source, including flux scattered in the near forward direction (up to ~15° or so) as well as direct transmission, may be expressed as

$$\Phi_r = k_o \Phi_o \exp\left[-(a + \breve{b}_o)\bar{z}\right], \tag{3.4}$$

where k_o is a constant representing the optical characteristics (reflection and transmission losses, effective detector area, etc.) of the source, $\bar{z}$ is the mean effective pathlength for flux transmitted from the source window to the plaque, $\breve{b}_o = b - 2\pi \int_0^{\psi_f} \beta(\psi) \sin\psi d\psi$ is flux scattered beyond a forward scattering angle $\psi_f \lesssim 15°$ comparable to the beam geometric width. For typical particle phase functions, a very large fraction of singly scattered flux is confined within the forward 15° cone. By similar reasoning, the flux reflected diffusely from the plaque and reaching the detector may be written as

$$\Phi_d = k_d \frac{\rho}{\pi} \Phi_r \exp\left[-(a + \breve{b}_d)\bar{z}\right] = k_d \frac{\rho}{\pi} k_o \Phi_o \exp\left[-(2a + \breve{b}_o + \breve{b}_d)\bar{z}\right], \tag{3.5}$$

where k_d is a constant accounting for the optical characteristics of the detector assembly, and $\breve{b}_d$ represents scattering losses at angles too large to be detected in a single scattering approximation, *i.e.* the counterpart for $\breve{b}_o$ for a diffuse source and the detector FOV. Equation (3.5) assumes further that the flux backscattered from the intersection volume of the source beam and detector FOV, the shaded conical region in Fig. 3.2, is negligibly small compared to the flux reflected from the plaque. At this point it may be appropriate for the reader to compare the similarities between the instrument concept illustrated Fig. 2.2 (Chapter 2) and the calibration geometry for determining the weighting function of a VSF, as illustrated in Fig. 5.1, and as described for a plaque reflectance measurement geometry at a fixed distance *z* as part of the VSF calibration described in Sect. 5.2 (Chapter 5 of this volume) and in Maffione and Dana (1997).

Following the approach used to determine the backscattering coefficient from a measurement $\beta(\psi^*)$ of the VSF at a single angle ψ^* in the backward direction (Chapter 5, Sect. 5.4), Dana, Maffione and Coenen (HOBILabs, Inc., personal comm., *circa* 2000) originally assumed that

$$\breve{b}_o + \breve{b}_d \cong \chi \beta(\psi^*), \tag{3.6}$$

where χ is an unknown constant. The "α-βeta" instrument designed and manufactured by HOBILabs combines a VSF meter (Chapter 5) to measure $\beta(140°)$ with a device conceptually similar to that illustrated in Fig. 3.2, mounted at opposite ends of a small cylinder.

If the source is regulated to emit constant flux, the system constants of the diffuse reflectance device may be collected as

$$k = F_d k_d \frac{\rho}{\pi} k_o \Phi_o, \tag{3.7}$$

where F_d is the detector assembly's signal responsivity to flux received at the instrument window in water, *i.e.* $F_d = \frac{V_d - V_d^{dark}}{\Phi_d}$. V_d and V_d^{dark} are the detector flux response and dark response signals, respectively.

Substituting (3.6) and (3.7) allows (3.5) to be rewritten in terms of the dark-corrected detector response $V_d - V_d^{dark}$ as

$$V_{\mathrm{d}} - V_{\mathrm{d}}^{\mathrm{dark}} = \mathrm{F_d}\Phi_{\mathrm{d}} = \mathrm{k}\exp\left\{-\left[2a + \chi\beta(\psi^*)\right]\bar{\mathrm{z}}\right\},$$

and taking the natural logarithm of both sides and rearranging yields

$$a = \frac{1}{2\bar{\mathrm{z}}}\left[\ln(\mathrm{k}) - \ln\left(V_{\mathrm{d}} - V_{\mathrm{d}}^{\mathrm{dark}}\right)\right] - \chi\beta\left(\psi^*\right). \tag{3.8}$$

Equation (3.7) contains one unknown variable, a, two measured variables $\left(V_{\mathrm{d}} - V_{\mathrm{d}}^{\mathrm{dark}}\right)$ and $\beta\left(\psi^*\right)$, and three unknown coefficients $\bar{\mathrm{z}}$ (the mean effective pathlength between the source, or detector, and reflectance target), k (an overall system optical characteristics constant), and χ (the scaling factor relating the VSF at one angle to the combined sum of backscattering plus forward scattering beyond ψ_{f} for the two optical paths).

The constant coefficients in (3.8) may be determined by placing the "α-βeta", or a similar instrument in pure water, and sequentially adding scattering and absorbing materials to increase a, b and $\beta(\psi)$ in $n = 1, 2, \ldots, \mathrm{N}$ increments spanning a suitable range of each variable. At each $n^{\underline{\mathrm{th}}}$ incremental step, the reflectance detector response $V_{\mathrm{d}n}$ and VSF measurement $\beta_n\left(\psi^*\right)$ are recorded, together with the absorption coefficient $a_n(\lambda)$ measured using a WET Labs ac-9. It is convenient to define two new constants $\gamma = \dfrac{\ln(\mathrm{k})}{2\bar{\mathrm{z}}}$ and $\vartheta = \dfrac{1}{2\bar{\mathrm{z}}}$, and express (3.8) in matrix form for the N sets of measurements as

$$\vec{\mathbf{a}} = \mathbf{X}\vec{\boldsymbol{\gamma}}, \tag{3.9}$$

where

$$\vec{\mathbf{a}} = \begin{bmatrix} a_1 \\ a_2 \\ \vdots \\ a_{\mathrm{N}} \end{bmatrix}, \quad \mathbf{X} = \begin{bmatrix} 1 & \ln(V_{\mathrm{d1}} - V_{\mathrm{d}}^{\mathrm{dark}}) & \beta_1\left(\psi^*\right) \\ 1 & \ln(V_{\mathrm{d2}} - V_{\mathrm{d}}^{\mathrm{dark}}) & \beta_2\left(\psi^*\right) \\ \vdots & \vdots & \vdots \\ 1 & \ln(V_{\mathrm{dN}} - V_{\mathrm{d}}^{\mathrm{dark}}) & \beta_{\mathrm{N}}\left(\psi^*\right) \end{bmatrix}, \text{ and } \vec{\boldsymbol{\gamma}} = \begin{bmatrix} \gamma \\ \vartheta \\ \chi \end{bmatrix}.$$

Multiplying both sides of (3.9) by $\mathbf{X^T}$, the transpose of the matrix **X**, we obtain

$$\mathbf{X^T}\vec{\mathbf{a}} = \left[\mathbf{X^T}\mathbf{X}\right]\vec{\boldsymbol{\gamma}},$$

leading to the normalized least squares solution for the three coefficients as

$$\vec{\boldsymbol{\gamma}} = \left[\mathbf{X^T}\mathbf{X}\right]^{-1}\mathbf{X^T}\vec{\mathbf{a}}, \tag{3.10}$$

where $\left[\mathbf{X^T}\mathbf{X}\right]^{-1}$ is the inverse of the 3 x 3 matrix $\left[\mathbf{X^T}\mathbf{X}\right]$.

Having thus described the conceptual basis for determining the absorption coefficient from measurements with a HOBILabs "a-beta" instrument, or a similar instrument, time constraints on the publication schedule for this document preclude exploring more detailed protocols for its calibration and use, or the uncertainty budgets associated with this approach. These considerations must be deferred to a possible future revision to this protocol volume.

3.2 CHARACTERIZATION and CALIBRATION OF REFLECTIVE TUBE SPECTRAL ABSORPTION METERS

Perhaps the best-known version of a reflective tube absorption meter is the ac-9 manufactured by WET Labs, Inc. This instrument measures both the spectral beam attenuation coefficient $c(\lambda)$ in an enclosed flow-through non-reflective optical path, and the spectral volume absorption coefficient $a(\lambda)$ using parallel enclosed flow-through reflective tube optical paths, one of which (the absorption side) is a reflective tube (Fig. 3.1). Many aspects of the characterization, calibration, field measurements and data analysis protocols relating to this type of instrument were introduced in Chapter 2 and will not be repeated here. Moreover the manufacturer provides extremely detailed

protocols for calibrating and using this instrument, and for analyzing its data, both in the ac-9 User Manual, and in a detailed protocol manual (Van Zee *et al*. 2002), both of which are available online (www.wetlabs.com). Additional background information related to characterization, calibration and data analysis methods for this instrument may be found in Moore *et al*. (1992), Zaneveld *et al*. (1992) and Twardowski *et al*. (1999). Here we will briefly highlight critical aspects of the protocols that must be carefully followed to obtain accurate $a(\lambda)$ measurements using this, or a similar, instrument in the field. Many of these topics, as they relate to the beam transmissometer side of the instrument, have been discussed in Chapter 2 of this volume.

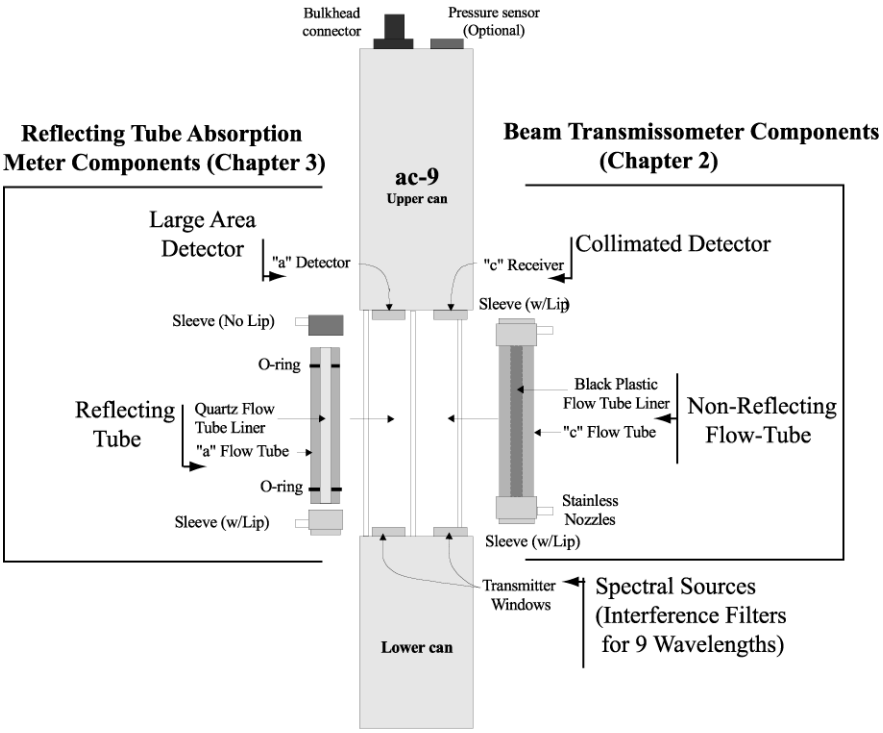

Fig. 3.3 Schematic illustration of the ac-9 beam attenuation and absorption meter (courtesy of WET Labs , Inc).

Pure Water Calibration

The procedure for using pure water to calibrate the reflective tube absorption meter side of an ac-9 is identical to that described in Chapter 2 (Sect. 2.4) for its flow-through beam-transmissometer side. The calibration equation for measured absorption a_{m} relative to pure water, corresponding to equation (2.9) for c, is

$$a_{\mathrm{m}}(\lambda) - a_{\mathrm{w}}(\lambda) = \frac{1}{r_{\mathrm{T}}} \ln \left\{ \frac{\left[V_{\mathrm{R,w}}(\lambda) - V_{\mathrm{R,w}}^{\mathrm{dark}}(\lambda)\right]\left[V_{\mathrm{D}}(\lambda) - V_{\mathrm{D}}^{\mathrm{dark}}(\lambda)\right]}{\left[V_{\mathrm{D,w}}(\lambda) - V_{\mathrm{D,w}}^{\mathrm{dark}}(\lambda)\right]\left[V_{\mathrm{R}}(\lambda) - V_{\mathrm{R}}^{\mathrm{dark}}(\lambda)\right]} \right\}, \tag{3.11}$$

where the signal notations on the right-hand-side are the same as those defined in Chapter 2, and pure water absorption values are listed in Table 1.1 of Chapter 1.

Pure Water Preparation

The methods for preparation of optical calibration grade pure water were not addressed in Chapter 2, and are included here.

To prepare pure water for instrument calibrations, the manufacture uses a commercial de-ionization system and filtration system. After primary de-ionization, the water is processed using a Barnstead, or equivalent, purification unit and stored in a large holding tank. To maintain purity, water in the holding tank should be re-circulated through a ultra-violet chamber and additional purification filters. Water for calibration is drawn through a 0.01-micron ultra-filter at the point of delivery. The circulating holding tank allows the highly reactive de-ionized water to equilibrate with the ambient conditions and the ultra-violet chamber prevents any biological contamination from entering the reservoir.

For field calibrations, one approach is to either purchase HPLC grade pure water, or produce it in the lab, and transport it to the ship, especially for short cruises. On some research vessels, a water deionization and purification system is permanently installed to support the scientific party. If so, care must be taken to insure that the filters are fresh and do not produce Colored Dissolved Organic Matter (CDOM) from decaying particles trapped in the filter. Alternatively, a portable system consisting of a commercial filtration unit, such as the Barnstead E-Pure or the Milli-Q Q-Pak treatment systems may be set up temporarily on the ship. The input water should be pre-filtered using a 1.5 μm commercial filter cartridge and an activated charcoal filter to increase the lifetime of the primary unit. Pure water should be produced in advance of the calibration and stored in a clean 20-liter polycarbonate carboy and be allowed to stand for approximately 12 hours to equilibrate with the ambient temperature and to remove bubbles.

To calibrate an ac-9, the carboy may be equipped with a cap having barb fittings to connect tubing to a pressurization unit that pushes water to the instrument (Fig. 3.4). The carboy is pressurized to approximately 10 psi using an oil free air pump, or a tank of dry nitrogen gas. The air supply tube inside the carboy should be kept above the water level to prevent the creation of bubbles when pressurizing the carboy, and the outlet tube should extend nearly to the bottom of the carboy. To connect the carboy to the ac-9, Teflon tubing is recommended, rather than Tygon tubing, which may contain plasticizers that can contaminate the water. The tubing from the carboy is connected to the bottom nozzle on the ac-9 flow tube. The tubing near the ac-9 inlet and outlet should be covered with black tape to avoid ambient light leaks into the optical path. A short piece of tubing with a valve is connected to the top nozzle on the flow tube, both to control water flow through the system, and to provide backpressure, which helps to keep gases in solution and prevents the formation of micro-bubbles. An optional 0.2-micron filter may be placed at the point of delivery.

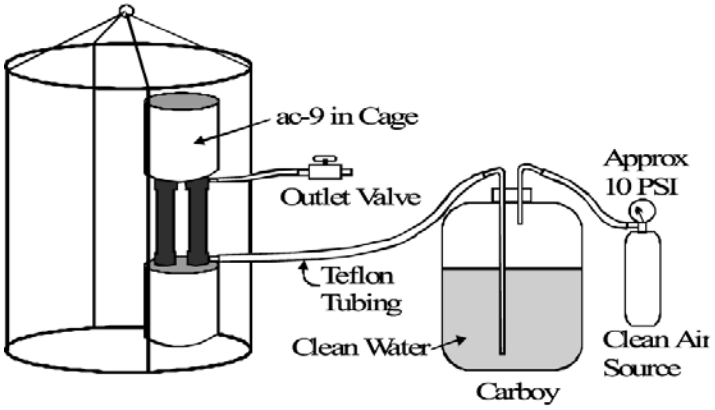

Fig. 3.4. Schematic illustration of a pure-water supply system for field calibrations of an ac-9.

Air "Calibrations"

This procedure is discussed adequately in Chapter 2.

3.3 MEASURING SPECTRAL ABSORPTION COEFFICIENTS WITH REFLECTIVE TUBE METERS

The ac-9 should be mounted in a profiling instrument cage following directions provided by the manufacturer (Van Zee *et al*. 2002). It is strongly recommended to mount a CTD data the same profiling package as an ac-9, and to develop a method for accurately merging the measurements from both instruments; combining the data streams from the two instruments in real time as part of the data acquisition system is the preferred approach, with a second choice being to time-tag both data records and merge the data on that basis. The basis of these recommendations is that water temperature and salinity data are essential for the corrections described below in Sect. 3.4.

To begin a cast, place the instrument package in the water before they are powered up. Then hold the package underwater near the surface allow approximately 5 min for the instruments to warm up, stabilize the electronics, and reduce the possibility that thermal shock may adversely affect the measurements. Monitor the instrument outputs and wait to begin profiling until the instrument stabilizes at the surface. If an absorption meter will not stabilize its readings after 5-10 minutes under these conditions, it is recommended that it be returned to the manufacturer for characterization of the problem and necessary repairs.

If possible place the instrument 10 to 20 meters below the surface to help purge bubbles. Purging bubbles is more difficult when making filtered measurements (see below). If you are not making filtered measurements the instruments will generally purge at the surface, but purging them below 10 m is still a good idea.

The reader is referred to Van Zee *et al*. (2002) for detailed recommendations concerning rates of descent during profiles using an ac-9.

After the instruments are brought on deck following a cast, they should be immediately rinsed, and the flow tubes flushed, with fresh water to mitigate corrosion. If the instrument will be on deck for more than 30 min between casts, the optics and flow tubes should be cleaned with Nannopure water and dried. At least once per day, while at sea, the optics and flow tubes should be cleaned with methanol, cleaned again using a mild detergent dissolved in Nannopure water, rinsed with Nannopure water, cleaned again with methanol, and finally dried. Use soft tissues, such as KimWipes, to gently clean and dry the optical surface, and be extremely careful to wipe them in a constant direction and to not scrub the optical surfaces.

When the instrument package is be stored on deck for a prolonged period between casts, cover it with a tarpaulin to protect the absorption meter from direct exposure to the sun. Excessive solar heating of the instrument may exceed the practical limits (5 ^{o}C to 30 ^{o}C) of internal temperature corrections for an ac-9, and thus invalidate its measurements until it has cooled sufficiently to restore normal operations.

Filtering the Water Intake Port of an ac-9 for Measurements of Absorption by CDOM and Particles

The absorption coefficient of dissolved material may be measured by attaching a 0.2 μm pore-size filter to the intake of an ac-9. The recommended practice is to locate the intake filter below the instrument at the bottom of the cage. Measurements in the filtered intake configuration are also very useful for testing the operational performance of ac-9; quality control procedures using dissolved measurements are discussed in Sect. 3.5.

Examples of suitable filters are the Gelman Suporcap 100 and Gelman Maxi-cap (0.2 μm) filters. These filters have high flow rates at low differential pressure and don't adsorb or leach materials. The outer housings of these commercial filter cartridges may be cut off to allow some flushing of the filter and increase the flow-rate. Make sure you don't handle the filter material, or lay a filter on the deck, where it can be exposed to oil and grease. Hose clamp the filter to the tubing and make sure any vents on the filter are closed. Before use, a filter should be either flushed for several minutes with DI water, or soaked several hours in DI water, to remove air pockets in the filter membrane. As a note of caution, never flush a filter in the reverse direction!

There are alternative ways to plumb the filters into the ac-9 instrument. The preferred arrangement is to filter the *a* and *c* sides separately using two filters and two pumps, so that each side is plumbed independently. This approach is expensive, however, and is not necessary for measuring the absorption by the dissolved component. For measurement of the absorption by dissolved materials, only one side needs to be filtered, because scattering by particles less than 0.2 μm in size is not detectable by an ac-9, and hence the filtered *a* and *c* measurements are equal. On the other hand, measurements with filters on intakes of both sides are useful for quality control tests (Sect. 3.5).

If possible replace the filter daily. If you choose to replace a filter less frequently, soak it in DI water during long breaks between profile measurements during a deployment. Record the date of each filter change in the cruise log.

Mixing of water within the filter cartridge will smear measurements of a vertical gradient in the absorption by dissolved materials, and an unfiltered instrument will detect a gradient in total absorption with better vertical resolution. In addition, the reduced flow rate through the filter will increase the time lag to approximately 4 to 6 sec, compared to 1.2 to 1.8 sec for unfiltered measurements. Moreover, the lag rate will gradually increase as a filter accumulates particles during its use. The preferred means of determining flow rate and lag corrections is to attach a flow-meter in-line into the supply or exhaust tubing. An indirect technique for estimating flow-rate related lag times is to match depths of changes in the $a(715)$ channel with depths of strong changes in water temperature; these changes are linked because absorption by water is temperature dependent in the near infrared (Sect. 3.4), and the time lag between matched changes can be derived from the depth separation and the profiler's rate of descent.

A combination of unfiltered and filtered ac-9 measurements can be used to derive particle absorption and attenuation coefficients, as well as absorption by CDOM. There are several combinations that can be used:

- From measurements using a single ac-9 with the *c* side filtered and the *a* side unfiltered, particle absorption can be obtained as $a_p(\lambda) = a(\lambda) - a_w(\lambda) - \left[c_g(\lambda) - c_w(\lambda)\right]$, where the measurements have been corrected using the methods described in 3.6 below. The subscript "g" is associated with CDOM, based on historical use of the term "gelbstoffe", or yellow-matter, as a pseudonym of CDOM.
- From measurements with two ac-9's, one filtered and one unfiltered, $a_g(\lambda)$ is derived directly from the filtered measurements, after the corrections of Sect. 3.6, and $a_p(\lambda) = a(\lambda) - a_g(\lambda)$, where $a(\lambda)$ is derived from the unfiltered instrument and the pure water terms cancel. This approach may also be used with a single instrument by making successive casts, one with the filter attached and the second with the filter removed.
- Another alternative approach is to make successive casts with one instrument, filtering the a intake on one cast, and the c intake on the other. The filtered and unfiltered measurements from the two casts are combined as above.

The approach yielding the lowest instrumental uncertainty of the particulate absorption is to derive it from filtered and unfiltered measurements with the same instrument on successive casts. Calibration offsets, whether known or not, are identical in the filtered and unfiltered measurements on each side, and therefore, the offsets cancel when particle absorption is determined as the difference between the two measurements. On the other hand, potentially larger uncertainty may result from possible changes in the IOP profiles between casts, due to horizontal advection and/or vertical displacement of IOP features by internal waves.

3.6 DATA ANALYSIS METHODS

The initial steps in processing absorption measurements using an ac-9 reflective tube absorption meter are identical to those presented for processing beam transmissometer measurements in Chapter 2, Sect. 2.5 [substituting equation (3.11) for (2.9) in Step 4). This information will not be repeated here. Two additional analysis steps are necessary to obtain accurate absorption coefficients from combined ac-9, or similar instrument, measurements of $a_m(\lambda)$ and $c_m(\lambda)$: 1) corrections for water temperature and salinity induced offsets in water absorption and attenuation, and 2) corrections for scattering errors [equation (3.3)] in $a_m(\lambda)$.

Temperature and Salinity Corrections

The absorption of pure water is dependent on water temperature T [^{o}C] (Pegau and Zaneveld 1993) and the absorption coefficient of seawater is also dependent on its salinity S [PSU] (Pegau *et al*. 1997). These variations affect the measured coefficients of absorption $a_m(\lambda)$ and attenuation $c_m(\lambda)$ in the following ways:

1. The difference $(T - T_r)$ between the water temperature T during a measurement at sea and the temperature T_r of the pure water reference standard at the time the instrument was calibrated changes the water absorption "baseline" value $a_w(\lambda)$. This change affects $a_m(\lambda)$ and $c_m(\lambda)$ equally, because scattering by pure water is not significantly temperature dependent.
2. The absorption of seawater varies with salinity S, and of course $S = 0$ PSU for the pure water reference standard used to calibrate the ac-9. This additional shift in the water-absorption "baseline" also affects $a_m(\lambda)$ and $c_m(\lambda)$ equally.
3. The salinity dependent variations in the refractive index of seawater affect the transmission of the optical windows, and the effects are different for the windows of the absorption and beam transmission sides of the instrument. This effect may also vary slightly between instruments (Van Zee *et al*. 2002).
4. Therefore, separate coefficients $\frac{\partial a(\lambda)}{\partial S}$ and $\frac{\partial c(\lambda)}{\partial S}$ combine salinity dependent instrument characteristics and water-absorption variations (Pegau *et al*. 1997; Van Zee *et al*. 2002), and must be applied separately to correct to $a_m(\lambda)$ and $c_m(\lambda)$

The temperature and salinity corrections are applied to measured absorption as

$$a_m^{TS}(\lambda) = a_m(\lambda) - \frac{\partial a_w(\lambda)}{\partial T}(T - T_r) - \frac{\partial a(\lambda)}{\partial S} S \,, \tag{3.12}$$

and to measured beam attenuation as

$$c_m^{TS}(\lambda) = c_m(\lambda) - \frac{\partial a_w(\lambda)}{\partial T}(T - T_r) - \frac{\partial c(\lambda)}{\partial S} S \,. \tag{3.13}$$

The temperature dependence coefficients are listed in Table 1.1 (Pegau and Zaneveld 1993; Pegau *et al* 1997), and the salinity dependence coefficients are provided by the manufacturer (Van Zee *et al*. 2002). Temperature and salinity must be measured, using a CTD, concurrently with an ac-9 profile to apply these corrections using (3.12) and (3.13). Therefore, it is strongly recommended that the ac-9 be mounted on the same profiling package as an accurate CTD, and from this perspective, the priority of CTD measurements is higher than is implied in Table 3.1 (Vol. I, Chapter 3).

These corrections become directly significant only at red and near-infrared wavelengths (see Table 1.1). However, the methods of the next section depend on accurate values of $a_m^{TS}(\lambda_{NIR})$ and $c_m^{TS}(\lambda_{NIR})$ at a near-infrared reference wavelength $\lambda_{NIR} \approx 715$ nm to determine *scattering corrections* at all wavelengths. Moreover, the temperature correction in (3.12) must also be applied to laboratory spectrophotometric measurements of absorption by CDOM (Chapter 4), if the temperatures of the pure-water reference blank and filtered seawater sample differ significantly.

Scattering Corrections

The systematic scattering offsets between true absorption and absorption measured with a reflective tube instrument, as described in equations (3.2) and (3.3) and related text in Sect. 3.1, were evaluated by Zaneveld *et al*. (1994). They recommended a hierarchy of three alternative methods for correcting the scattering offsets to the temperature and salinity corrected measured absorption $a_m^{TS}(\lambda)$:

1. Subtract the measured absorption at a near infrared reference wavelength, *e.g.* $\lambda_{NIR} \approx 715$ nm for an ac-9, or $\lambda_{NIR} \approx 750$ nm for measurements with a laboratory spectrophotometer (Chapter 4). After first applying the *temperature and salinity* corrections using (3.12) and (3.13), assume that the $a(\lambda_{NIR}) - a_w(\lambda_{NIR}) \approx 0$ and that the entire measured signal at the reference wavelength is due to wavelength independent scattering errors, so that

$$a(\lambda) - a_w(\lambda) = a_m^{TS}(\lambda) - a_m^{TS}(\lambda_{NIR}). \tag{3.14}$$

The value of $a_{\mathrm{m}}^{TS}(\lambda_{\mathrm{NIR}})$ should be reported with the corrected absorption values when this method is used.

2. Assuming a wavelength-independent scattering phase function appropriate for the type of particulates in a given water mass, and a weighting function $W(\psi)$ based on instrument characteristics [see equation (3.3) and the preceding discussion in Sect. 1.1 above], estimate the scattering error as a fraction ε of the measured scattering coefficient, and subtract it from the measured absorption at each wavelength, *i.e.*

$$a(\lambda) - a_{\mathrm{w}}(\lambda) = a_{\mathrm{m}}^{TS}(\lambda) - \varepsilon\left[c_{\mathrm{m}}^{TS}(\lambda) - a_{\mathrm{m}}^{TS}(\lambda)\right]. \tag{3.15}$$

Based on analyses of field measurements, laboratory experiments using an ac-9, and theoretical calculations (Kirk 1992), the fraction ε varies from approximately 0.14 for predominately biological particles in the open ocean (Case 1 waters) and increases to approximately 0.18 in waters were scattering is dominated by suspended sediments (Case 2 waters). Note that although the scattering correction using (3.15) is not sensitive to temperature and salinity corrections at wavelengths < 650 nm, it is nevertheless strongly recommended that the temperature and salinity corrected values be used here as well - if for no other reason than facilitating quality control comparisons between corrections made by different methods.

3. Combine methods 1 and 2, and the assumptions underlying both methods, to use the ac-9 measurements at the reference wavelength to determine ε, so that (3.15) becomes

$$a(\lambda) - a_{\mathrm{w}}(\lambda) = a_{\mathrm{m}}^{TS}(\lambda) - \left[\frac{a_{\mathrm{m}}^{TS}(\lambda_{\mathrm{NIR}})}{c_{\mathrm{m}}^{TS}(\lambda_{\mathrm{NIR}}) - a_{\mathrm{m}}^{TS}(\lambda_{\mathrm{NIR}})}\right]\left[c_{\mathrm{m}}^{TS}(\lambda) - a_{\mathrm{m}}^{TS}(\lambda)\right]. \tag{3.16}$$

The ac-9 instrument design constrains the scattering error fraction to $\varepsilon \geq 0.07$ (Kirk 1992), and although it is theoretically possible for ε to reach values exceeding 0.5, the authors have not encountered values greater than 0.35.

The choice of which method should be used to correct scattering errors in ac-9 absorption measurements depends largely on the combination of measured variables, the uncertainty of each measurements, and a judgment of how likely the assumption that $a(\lambda_{\mathrm{NIR}}) - a_{\mathrm{w}}(\lambda_{\mathrm{NIR}}) \approx 0$ is true in a given water mass.

1. It is strongly recommended to use Method 3 to apply the scattering correction, if all variables in (3.16) have been measured with acceptable uncertainty, and there is no reason to suspect that particle absorption is significant at the near-infrared reference wavelength λ_{NIR}.

2. Method 2 is recommended if both $a_{\mathrm{m}}^{TS}(\lambda)$ and $c_{\mathrm{m}}^{TS}(\lambda)$ are available at one or more visible wavelengths, but $a_{\mathrm{m}}^{TS}(\lambda_{\mathrm{NIR}})$ and $c_{\mathrm{m}}^{TS}(\lambda_{\mathrm{NIR}})$ either were not measured with acceptable uncertainties, or there is reason to suspect that $a(\lambda_{\mathrm{NIR}}) - a_{\mathrm{w}}(\lambda_{\mathrm{NIR}}) > 0$.

3. Method 1 must be used if only $a_{\mathrm{m}}^{TS}(\lambda)$ and $a_{\mathrm{m}}^{TS}(\lambda_{\mathrm{NIR}})$ are measured, as for example, when a laboratory benchtop spectrophotometer is used to measure $a_{\mathrm{g}}(\lambda)$ in filtered water samples (Chapter 4). This situation might also occur if the *c* side data of an ac-9 were lost due to an electronic failure, or blockage of its flow-tube, and one wished to salvage the absorption profile measured with that instrument.

3.7 QUALITY CONTROL PROCEDURES

There are several quality assurance tests that can be made to check how well an ac-9 is operating.

When using intake filters for quality control measurements in tests of instrument performance, it is best to filter both sides of an ac-9. This can be done by filtering one side at a time, and doing multiple profiles, or by connecting a single filter and pump to both sides of the ac-9. When connecting to both sides using a single filter you are reducing an already low flow, which makes it more difficult to remove bubbles from the system, but it requires fewer casts to complete an instrument test. A degassing Y may be used on the outflow side of the combined plumbing arrangement to facilitate bubble removal.

The noise level in the measurements should be >0.005 m^{-1} at all channels. Measurements with noise exceeding this criterion indicate instruments with large measurement noise, a rough check of quality of the calibration, and pressure or temperature dependencies that may exist.

Assuming that there is no measurable scattering by particles that pass through the filter then the filtered a and c measurements should be equal, and departures >0.005 m^{-1} are symptoms of drift in pure water calibration offsets, or calibration errors due to optical impurity of the reference water.

Comparisons of profiles between successive down and up casts may help in separating suspected temperature effects from pressure dependencies. Evidence of hysteresis in different up and down profile responses to gradient features is symptomatic of a problem with an instrument's internal temperature compensation Care must be taken in this interpretation, however, because the upcast water intake is taken in the wake of the rising package and turbulence may also cause apparent hysteresis symptoms to appear in the measurements. Pressure effects should not have hysteresis.

If more than one ac-9 is available, it is useful to plumb both instruments in identical configurations (both with, or without an intake filter) on the same instrument and measure a quick sequence of comparative profiles to intercalibrate the instruments. The profile data from the two instruments should be compared only after each has been fully processed and corrected for temperature, salinity and scattering errors (Sect. 3.4). Discrepancies in this type of comparison cannot indicate which instrument is incorrect, but does provide a clear indication that the calibration of one, or both, is not correct.

REFERENCES

James, H.R., and E.A. Birge, 1938: A laboratory study of the absorption of light by lake waters. *Trans. Wis. Acad. Sci*., **31**: 1--154.

Kirk, J.T.O., 1992. Monte Carlo modeling of the performance of a reflective tube absorption meter. *Appl. Opt.* **31(30):** 6463-6468.

Moore, C., J.R.V. Zaneveld and J.C. Kitchen, 1992: Preliminary results from an *in situ* spectral absorption meter, *Ocean Optics XI*, *Proc. SPIE* **1750:** 330-337.

Maffione, R.A. and D.R. Dana, 1997: Instruments and methods for measuring the backward-scattering coefficient of ocean waters. *Appl. Opt.* **36:** 6057-6067.

Pegau, W.S. and J.R.V. Zaneveld, 1993: Temperature dependent absorption of water in the red and near infrared portions of the spectrum. *Limnol. Oceanogr*., **38**(1): 188-192.

Pegau, W.S., D. Gray and J.R.V. Zaneveld, 1997: Absorption and attenuation of visible and near-infrared light in water: dependence on temperature and salinity. Appl. Opt., **36**(24): 6035-6046.

Twardowski, M.S., J.M. Sullivan, P.L. Donaghay and J.R.V. Zaneveld. 1999: Microscale quantification of the absorption by dissolved and particulate material in coastal waters with an ac-9. *J. Atmos. Oceanic Tech.* **16**: 691-707.

Van Zee, H., D. Hankins, and C. deLespinasse, 2002: *ac-9 Protocol Document (Revision F)*. WET Labs Inc., Philomath, OR, 41pp.

Zaneveld, J.R.V., J.C. Kitchen, A. Bricaud, and C. Moore, 1992: Analysis of *in situ* spectral absorption meter data. *Ocean Optics XI,* G.D. Gilbert, Ed., SPIE, 1750, 187--200.

Zaneveld, J.R.V., J.C. Kitchen, and C. Moore, 1994: The scattering error correction of reflecting-tube absorption meters. *Ocean Optics XII, Proc. SPIE*, **2258**: 44-55.

Chapter 4

Determination of spectral absorption coefficients of particles, dissolved material and phytoplankton for discrete water samples

B. Greg Mitchell, Mati Kahru, John Wieland and Malgorzata Stramska
Scripps Institution of Oceanography, University of California San Diego, California

4.1 INTRODUCTION

The spectral absorption coefficient is one of the inherent optical properties that influence the reflectance of aquatic systems. The absorption coefficient $a(\lambda)$, in m^{-1}, at any point within a natural water body can be described in terms of the additive contribution of its components as

$$a(\lambda) = a_w(\lambda) + a_p(\lambda) + a_g(\lambda),\ m^{-1}, \tag{4.1}$$

where $a_w(\lambda)$, $a_p(\lambda)$ and $a_g(\lambda)$ are the spectral absorption coefficients of water, particles, and soluble components, respectively. The spectral absorption coefficients of pure water adopted for the protocols are given in Table 1.1 (Ch. 1), and combine the results of Pope and Fry (1997), Sogandares and Fry (1997), Fry (2000) and Kou *et al*. (1993). The depth (z) dependence of the absorption coefficients is omitted for brevity. The particle absorption coefficient may be further decomposed as

$$a_p(\lambda) = a_\varphi(\lambda) + a_d(\lambda),\ m^{-1}, \tag{4.2}$$

where $a_\varphi(\lambda)$ and $a_d(\lambda)$ are the spectral absorption coefficients of phytoplankton, and de-pigmented particles, respectively. Laboratory methods are described for determining operational estimates of these fractions. It is conceptually possible to further separate $a_d(\lambda)$ into absorption fractions due to de-pigmented organic and inorganic particles, but at present, there are no well established protocols for separately determining the absorption coefficient for inorganic particles.

To interpret aquatic spectral reflectance and better understand photochemical and photobiological processes in natural waters, it is essential to quantify the contributions of the individual constituents to the total absorption coefficients in the ultraviolet (UV) and visible region of the spectrum. The protocols presented here are based on the evolution, starting with articles by Kalle (1938) and Yentsch (1962), of methods for analyzing the absorption by soluble and particulate material in natural waters. Laboratory measurements and data analysis protocols are described for separating the total spectral absorption coefficient, $a(\lambda)$, into its components by spectrophotometric measurements of samples prepared from filtration of discrete water samples.

The spectral absorbance of the filters and filtrate from these samples, as measured in a spectrophotometer, are expressed in units of Optical Density (OD), defined as $OD(\lambda) = \mathrm{Log}_{10}[V_o(\lambda)] - \mathrm{Log}_{10}[V_t(\lambda)]$. $V_o(\lambda)$ is the spectrometer response for spectral flux transmitted through the reference material and $V_t(\lambda)$ is the response for spectral flux transmitted through the sample. For the methods presented here the reference is either a properly hydrated GF/F blank filter for particle absorption, or a clean quartz glass optical cuvette filled directly from a

purified water source for soluble material absorption. Note that OD is a dimensionless quantity. The use of base-10 logarithms in this context is a carryover from common practice in chemical spectroscopy and is the typical output of commercial spectrophotometers routinely used for these methods. Therefore, it is necessary to convert the OD measurements described in this chapter to the base-e representation of absorbance, *i.e.* to multiply OD by 2.303, to conform to the convention used throughout the ocean optics protocols. In general, these protocols are written assuming that the instrument that is used directly computes the optical density of the sample relative to the appropriate reference sample.

There has been considerable research to develop robust protocols that provide the most accurate estimates of absorption for various material fractions in natural waters. NASA-sponsored workshops were held at Scripps Institution of Oceanography and Bigelow Laboratory for Ocean Sciences to review absorption protocols, evaluate instrumentation, and define areas of consensus as well as areas of uncertainty that warrant further research (Mitchell *et al.* 2000).

The most widely used approach for estimating absorption by particulate matter in water samples involves analysis of the particles concentrated on filters (Yentsch, 1957). Absorption of phytoplankton suspensions determined using procedures that capture most of the forward scattered light (Shibata, 1958) can be related to the absorption measured on the filters to make quantitative corrections for the pathlength amplification effect (β) caused by the highly scattering filter medium (Duntley, 1942; Butler, 1962). The pathlength amplification parameter was symbolized as β by Kiefer and SooHoo (1982) following the nomenclature of Butler (1962). This symbol should not to be confused with the volume scattering coefficient $\beta(\lambda,\Psi)$ used in other chapters of this Technical Memorandum.

Kiefer and SooHoo (1982) reported a constant to scale the red peak of chlorophyll absorption for natural particles retained on GF/C filters to the diffuse absorption coefficients determined on suspensions by Kiefer *et al*. (1979). The diffuse absorption coefficient is double the value of the volume absorption coefficient of interest here (Preisendorfer, 1976). Mitchell and Kiefer (1984, 1988a) made direct estimates of volume absorption coefficients for phytoplankton suspensions and absorbance on glass fiber filters with the same particles to develop empirical equations that relate the amplification factor to the glass fiber sample optical density. This procedure is the basis of most laboratory methods for determining particle absorption in water samples.

Field applications of these quantitative estimates of $a_{\mathrm{p}}(\lambda)$ were reported by Mitchell and Kiefer (1984, 1988b) and Bricaud and Stramski (1990). More detailed empirical results to correct for pathlength amplification were reported by Mitchell (1990) for various filter types and diverse cultures coccoid cyanobacteria, nanochlorophytes, diatoms, chrysophytes and dinoflagellates with sizes ranging from 2 μm to 20 μm. Cleveland and Weidemann (1993) and Tassan and Ferrari (1995) found that the empirical relationships of Mitchell (1990) were consistent with similar types of phytoplankton, but Moore *et al.* (1995) reported large differences in the amplification factor for *Synechococcus sp*. (WH8103) and *Prochlorococcus marinus* that were about half the size of the smallest cells studied by Mitchell (1990). Similar results were obtained by Allali *et al*. (1997) for natural populations of the Equatorial Pacific dominated by picoplankton. For samples with substantial turbidity and scattering due to inorganic matter (coastal, shelf, coccolithophore blooms), methods to correct for resulting artifacts have been described by Tassan and Ferrari (1995a, 1995b). Table 4.1 provides a summary of various published results for pathlength amplification factors.

Separation of the particle fraction into phytoplankton and other components is of considerable ecological and biogeochemical interest. Early efforts to separate absorbing components for natural particles included treatment with organic solvents, UV radiation, and potassium permanganate (references can be found in Shifrin, 1988, and Bricaud and Stramski, 1990). The most widely used chemical method is based on methanol extraction (Kishino *et al.* 1985, 1986). A recent method consists of bleaching the phytoplankton pigments by sodium hypochlorite (Tassan and Ferrari, 1995a; Ferrari and Tassan, 1999). Spectral fluorescence methods to estimate the fraction of photosynthetically active absorption, if separate total particulate absorption has been determined, have been reported by Sosik and Mitchell, (1995).

Soluble absorption observations were described by Bricaud *et al*. (1981) for diverse ocean environments, including oligotrophic and eutrophic regions. Other field reports can be found in the references listed in more recent articles (Carder *et al.*, 1989a, 1989b; Blough *et al.*, 1993; Vodacek *et al.*, 1996; Hoge *et al.*, 1993; Nelson *et al.*, 1998; D'Sa *et al*., 1999). Spectrophotometric measurement of absorption by dissolved materials is straightforward,

but has limits due to the very small signal for short pathlengths routinely employed (usually 10 cm), and to difficulties in maintaining quality control of purified water used as a reference.

This chapter defines protocols for the operational determinations of absorption coefficients for particulate and soluble matter in water samples. Methods are specified for separating particulate and soluble material by filtration, partitioning total particulate absorption into contributions by phytoplankton and de-pigmented particles (detritus), and corrections for pathlength amplification due to semi-diffuse transmittance of the filters. Recommendations are made based on widely accepted methods and processing procedures. NASA-sponsored workshops have confirmed various aspects of previously reported methods (Mitchell *et al*. 2000).

4.2 SAMPLE ACQUISITION

Water samples should be taken using Niskin (or similar) bottles at the site of, and simultaneously with, the surface in-water optical measurements, and at depth increments sufficient to resolve variability within at least the top optical depth. When possible, samples should be acquired at several depths distributed throughout the upper 300m of the water column (or in turbid water, up to seven diffuse attenuation depths for PAR irradiance, $\ln(E(0)/E(z))=7$), to provide a basis for relating the spectroscopic measurements of absorption to *in situ* profile measurements. Samples should be drawn immediately from the *in situ* sampling bottles into clean sampling bottles using clean silicon rubber or Tygon tubing or by directly filling the sample bottles from the Niskin bottle spigot. If Niskin bottles will not be sampled immediately, precautions must be taken to ensure large particles that settle are re-suspended. This can be done by transferring all water from the Niskin to a bottle or carboy larger than the total volume of the Niskin so that the entire water sample can be mixed (invert bottle numerous times to mix by turbulence), or by draining a small amount of water from the Niskin and manually inverting the entire Niskin prior to sub-sampling. Sample bottles should be kept cool (ideally near *in situ* temperatures), and dark prior to sample preparations. Preparations should be completed as soon as possible after sampling, but no later than several hours after the sample was acquired.

4.3 SPECTROPHOTOMETER CHARACTERISTICS AND CALIBRATION

A spectrophotometer used for absorption measurements following the protocols presented in this chapter must meet the following minimum performance specifications:

1. The unit's monochromator, or spectrograph, must yield a Full-Width at Half-Maximum (FWHM) bandwidth ≤ 4 nm. A larger FWHM bandwidth will not adequately resolve the red chlorophyll *a* absorption band.
2. The instrument's baseline spectrum characteristics, specified below, must be maintained over the range from 300 nm to 850 nm for measuring absorption by particles concentrated on filters, and from 250 nm to 850 nm for measuring absorption by dissolved materials.
3. For measuring absorption by particles concentrated on filters, baseline noise must be <0.01 *OD*, and noise <0.005 *OD* is strongly recommended.
4. For measuring absorption by dissolved materials, baseline noise must be <0.001 *OD* units, and noise <0.0005 *OD* is strongly recommended.
5. The instrument's baseline spectrum must be relatively flat over the wavelength range of interest and its shape and magnitude must be stable over time. Any tendencies for the spectral shape and magnitude of an instrument's baseline to drift must be well-behaved and slow enough that the rate of baseline drift may be characterized with an uncertainty less than the noise levels specified above. It is recommended to check the instrument baseline at intervals of 1 hr to 2 hr during an extended series of measurements.

Other desirable, but not absolutely essential, spectrophotometer features are variable slit width (to allow reducing the FWHM spectral resolution, when desired), automatic baseline corrections (the adequacy of which must nevertheless be verified), and automatic spectral calibration during instrument warm-up (using mercury emission lines supplied by an internal lamp source).

The spectral accuracy of the spectrometer should be verified by scanning a holmium oxide filter, with reference to an air-to-air baseline. This spectral calibration should be repeated each time the instrument is turned on, and at

the conclusion of a series of measurements. Alternatively, a spectrophotometer's spectral characteristics may be calibrated using an internal line source (*e.g.* a mercury lamp), if the instrument is so equipped, but independent checks with the holmium oxide filter are also strongly advised. A set of absorbance reference filter standards, of known OD, must be used to calibrate a spectrophotometer's responses over the range of OD associated with the samples to be measured. This calibration, together with instrument baseline spectrum determinations, should be repeated at intervals necessary to characterize (within the noise tolerances given above) any measurable drifts in the instrument baseline and/or OD response. Unless the investigator can confirm the stability of the instrument that is used, these calibration procedures should be repeated each time the spectrophotometer is turned on. As a minimum they should be performed at any time there is a change of lamp source, blocking filter, or other instrument setup characteristic that affects the optical response and on a regular basis during routine work.

The present version of these protocols is written assuming the use of a commercial dual-beam spectrophotometer, with the sample and reference targets illuminated by the collimated output of a grating monochromator. The protocols also apply, with minimal modifications, to measurements using a single-beam monochromator or otherwise similar optical configuration. Mitchell *et al*. (2000) report comparisons between OD measurements of a common set of GF/F filtered particle samples using several spectrophotometers of these types, as well as spectrophotometers based on very different optical configurations. For a diatom culture measured during the Scripps workshop, several commercial dual beam spectrophotometers estimated sample filter OD spectra consistently within 5 % (Figure 4.1). Some of the differently configured instruments were within 10 % of the selected reference dual-beam instrument but in some cases had limited spectral range either in the UV or the near-infrared, or both (data not shown). The largest divergence was found for a grating spectrograph instrument that illuminates the filter with diffuse white light (Figure 4.1). This unit yielded OD values that were significantly higher than, albeit linearly related to (with a slope of approximately 0.7), the OD measurements made with conventional dual beam spectrophotometers (Mitchell *et al*. 2000). This result indicates that the pathlength amplification (β factor) associated with this instrument is significantly different from previously published values (Table 4.1), which were derived using conventional dual beam spectrophotometers. An investigator using this type of spectrophotometer, or another design with yet a different optical configuration, must either compare filter OD spectra measurements to reference measurements on the same filters with a "conventional" spectrophotometer to derive an OD scaling function, or otherwise determine pathlength amplification factors for the instrument configuration, using methods discussed in Mitchell *et al*. (2000) and references cited therein.

4.4 PARTICLE ABSORPTION: SAMPLE FILTER PREPARATION AND ANALYSIS

The procedures described in this section are recommended for determining the spectral absorption coefficients of particles in discrete samples of natural waters. These laboratory measurements are complementary to methods for measuring *in situ* profiles of absorption, as described in Chapter 3 of this volume, and provide additional information on the partition of particle absorption by phytoplankton and other particles. Water samples are filtered and absorbance spectra of the filter, $OD_{\mathrm{fp}}(\lambda)$, are estimated for the retained particles using a laboratory spectrophotometer. After measurement, the sample filters are soaked in chemical solvents to extract, or bleach, phytoplankton pigments (Kishino *et al*., 1985; Tassan and Ferrari 1995a) then rinsed to remove the chemicals and pigments from the material retained on the filter. The $OD_{\mathrm{fd}}(\lambda)$ spectrum of the filter is then determined in the spectrophotometer to obtain the absorption component of the de-pigmented particles, which are sometimes referred to as detritus or tripton. Depending on the method used to de-pigment the samples, this fraction also includes bleached cells and phycobilipigments that are not extractable in methanol and also inorganic minerals that may be important absorbers in some water samples. The raw $OD_{\mathrm{fp}}(\lambda)$ and $OD_{\mathrm{fd}}(\lambda)$ data are used to calculate total particulate and de-pigmented absorption coefficients $a_{\mathrm{p}}(\lambda)$ and $a_{\mathrm{d}}(\lambda)$, respectively. The absorption coefficient of phytoplankton, $a_{\phi}(\lambda)$, is then calculated as the difference $a_{\mathrm{p}}(\lambda) - a_{\mathrm{d}}(\lambda)$.

Filtration

The Whatman GF/F™ filter (which is binder-free and combustible, with a nominal pore size of 0.7 μm) is recommended for particle absorption sampling. This type of filter is also recommended by (JGOFS 1991) for

various particulate and pigment analyses. Some authors have reported that particulate material less than 0.7 μm in size will not be retained by the GF/F filter, and that this fraction may contain up to 10 % or 15 % of the phytoplankton biomass as measured by chlorophyll concentration. Chavez *et al*. (1995), however, found no statistical difference between GF/F and 0.2 μm filters for chlorophyll and productivity measurements. The absorption of particles having diameters between 0.22 μm and 0.7 μm may be selectively determined by filtering the GF/F filtrate again through a 0.22 μm Millipore cellulose acetate membrane filter, and measuring its absorbance with a spectrophotometer (Ferrari and Tassan, 1996). Note that Mitchell (1990) reported pathlength amplification factors for cellulose acetate filters that are substantially different than those for GF/F filters and also described the relative difficulty of keeping cellulose acetate filters properly hydrated.

The optical transparency of the GF/F filter relative to air decreases significantly below 380 nm but many spectrophotometers can still make optical density determinations to 300 nm with these filters. The transparency of the filter also increases with hydration; so all samples must be fully - but not excessively - hydrated for proper performance of analytical procedures and accurate optical corrections. Pre-soaking GF/F filters 1 to 2 hrs before use can lead to less variability between individual filters (Bricaud and Stramski 1990). For oceanic water samples, seawater filtered through a 0.2 μm filter should be used to hydrate the filters. Freshly filtered seawater should be used since water that is left standing in clear containers may grow considerable amounts of algae over relatively short periods of time if there are any nutrients in the filtered seawater. For fresh inland water samples, purified fresh water may be used.

Glass fiber, cellulose acetate, and other strongly diffusing filters have large scattering coefficients, which increase the optical path length of photons in the measurement beam. Filtration volume V_f should be adjusted so that the optical densities of the filter samples, relative to the blank filter satisfy the criteria that $0.05 < OD_{fp}(675) \le 0.25$ and $OD_{fp}(440) \le 0.4 \;\; OD$ (Mitchell 1990). Optical density spectra of the sample filters should be measured as soon as possible following filtration, because pigment decomposition may occur (Stramski 1990). If filters must be stored, immediately place the unfolded filters into flat tissue containers designed for liquid nitrogen storage. Liquid nitrogen storage is recommended because alternative freezing methods were shown to have more artifacts in comparison tests (Sosik, 1999).

a. Sample Filter Preparation

- Collect water samples, and maintain them in the dark at, or near, *in situ* water temperature.
- Prepare 0.2 μm filtered seawater (FSW) in sufficient volume for hydrating sample and blank filters.
- Set up and maintain the filter apparatus in dim light to minimize photodegradation of the samples.
- For each sample, place a GF/F filter onto the filtration rig. Also prepare two blank GF/F filters by soaking them in ~25 ml of 0.2 μm filtered water while mounted on the filtration funnel (with valves closed) during the sample filtration.
- Filter the samples on GF/F filters under low vacuum (~125 mm Hg).
- Filter a sufficient volume of water V_f to yield sample optical density relative to the blank filter in the range specified above. For field samples collected in the upper 100-150 m and filtered onto 25 mm GF/F filters, V_f is typically in the range 0.5 L to 5 L, depending on the *in situ* density concentration of particles.
- Do not let the preparations run dry during filtration. Turn off the vacuum to each sample as it completes filtering. Immediately place samples on a drop of 0.2 μm FSW in the appropriate container, depending on how they will be stored.
- Record the filter and filtration funnel type, the diameter D_f of the area on the filter that contains the concentrated particles, and the volume of water filtered V_f.
- Measure the absorption spectra in a spectrophotometer, or store the filters in liquid nitrogen, as soon as possible.

b. Sample Filter Storage

- If the filter samples will be analyzed immediately, store each filter in a labeled petri dish (*e.g.* Gelman™ snap-top dishes). Ensure proper hydration of the sample by placing the GF/F filter on a small drop of 0.2 μm FSW. Store each filter sample in the dark and refrigerate it (~4 deg. C) until it is to be measured in the spectrophotometer.
- If the spectrophotometric measurements will be delayed more than 24 hours following sample filtration, the filter samples should be prepared for liquid nitrogen storage. Samples should be stored in containers that allow the filter to remain flat, and which are specifically designed for immersion in liquid nitrogen (*e.g.* Fisher Histoprep™ tissue capsules). One pair of blank filters should also be prepared each day for use as the reference blank for samples collected that day. Samples may be stored in liquid nitrogen for extended periods, but it is strongly recommended to analyze them as soon as possible.
- Non-pressurized liquid nitrogen dewars generally retain liquid nitrogen for 2-4 weeks. Pressurized liquid nitrogen dewars can be rented at low cost for extended cruises (4-5 weeks) so that the sample dewars may be replenished and kept full. Care must be taken at sea, and in return shipping, to ensure that the samples are properly frozen. Samples should be shipped in liquid nitrogen dry shippers, which will maintain proper temperatures for 2 to 3 weeks, if they are properly charged and in good condition.
- Air transport of liquid nitrogen dry shippers is approved under International Air Transportation Agreement (IATA 41st Edition Section A800; US Federal Aviation Administration Dangerous Good Bulletin DGAB-98-03; August 25, 1998). That approval notwithstanding, many investigators have experienced difficulties in clearing customs, and in transport of liquid nitrogen dry shippers via commercial airfreight, or as checked baggage. The investigator should contact the carriers in advance and provide the IATA approval and FAA bulletins pertaining to liquid nitrogen dry shipper transport. If the dry shipper is to be transported as checked baggage, advanced coordination with the airline is strongly recommended to avoid confiscation of samples and delays in return shipment. When samples are shipped as checked baggage or freight, the IATA memo, DOT memo, and manufacturer's certificate should be affixed to the dry shipper to minimize potential delays.
- Temporary storage of filter samples on dry ice can be considered during transport. But maximum duration of dry ice in insulated shipping boxes is several days, so the use of liquid nitrogen dry shippers is strongly recommended.

Determination of spectral optical density of sample filters

After preparation, the optical density spectrum of each sample filter is measured using a laboratory spectrophotometer. The performance characteristics and calibration requirements of the spectrophotometer used for these measurements are described above in Section 4.3.

a. Reference Blank Spectra

With a dual beam spectrophotometer, two reference filter blanks saturated with FSW are used to measure the reference spectrum, and one is left in the reference beam during sample measurements. For typical single beam instruments, generally the reference is scanned, and then samples are placed into the beam and scanned. Most modern spectrophotometers, whether single or double beam, automatically store the instrument's reference spectrum and recorded sample spectra are automatically corrected to yield $OD_{\mathrm{fp}}(\lambda)$ relative to the reference blank filter. A new instrument reference baseline scan should be measured each time the spectrophotometer is powered up, and whenever its configuration has been changed. The baseline should also be checked regularly (every 1 hr to 2 hr) during extended periods of analysis. Frequency of baseline verification will depend on the performance and stability of each instrument and should be determined by the investigator prior to executing routine work. Uncorrected baseline drift, and changes in sorting filters or lamp source can cause systematic measurement anomalies. Wavelength accuracy and measurement precision should also be checked during the analyses (Sect. 4.3 above).

b. Spectrophotometric Measurement Procedure

- Warm up the spectrophotometer for 30 minutes.
- Measure the initial instrument baseline and wavelength calibration.
- If using frozen samples, remove the filters from the storage container and place them in petri dishes on FSW to ensure hydration. Allow the samples to thaw for approximately 5 min and then refrigerate them in the dark until each filter is ready for analysis.
- An instrument-specific sample-mounting device is recommended to hold filters against a quartz glass mounting plate. These mounts should be secure when placed in the sample compartment and hold the sample perpendicular to the illumination beam so only the filter and the quartz plate are in the beam. Usually, these mounts must be custom fabricated specifically for each different instrument.
- Clean the quartz faceplates of the mounting device with purified water and detergent if needed. Rinse them with purified water and ethanol, and dry them thoroughly using lint-free laboratory tissues.
- Set the appropriate instrument parameters according to the manufacturer's instructions.
- Mount two pre-soaked and water saturated blank filters (one for the sample beam, and one for the reference beam).
- To test for proper filter hydration, confirm that there is a drop of FSW left on the mounting plate when the filter is lifted. With the filter on the mounting plate there should be a slight sheen on the top surface of the filter, and a very narrow (~1 mm) border of water around the edges of the filter. Be careful not to use too much water, or the sample may wash away.
- Examine the back of the filter on the mounting plate to be sure that no bubbles are trapped between the filter and the quartz glass plate on the sample holder. There should be a uniform layer of water between the filter and quartz glass mounting plate. If bubbles are present, which will be obvious, pick up the filter with forceps, and replace it on the plate with a slight dragging motion across a drop of filtered seawater. Re-inspect the back of the filter and repeat the foregoing procedure until no bubbles are present. Adjust the amount of FSW as necessary to ensure proper hydration.
- Alternative mounts that expose both sides of the filter to air may be used to avoid bubbles altogether. Sample hydration is more difficult to maintain when using this type of filter mount so the investigator must develop a satisfactory procedure to ensure proper hydration of sample and reference.
- Run the instrument baseline correction using the two blanks. For most commercial units, this baseline will be automatically used as the reference to calculate $OD_{\mathrm{fp}}(\lambda)$. Immediately after the baseline correction is finished, and without touching the blank filters, run the two blanks as a sample scan to confirm that baseline performance is within acceptable tolerance over the spectral range of determination (Sect. 4.3 above). This spectrum should be flat spectrally. Baseline noise less than $\pm\ 0.005\,OD$ is recommended. Save this scan for confirmation of instrument performance. If a spectrally flat baseline cannot be achieved over the spectral range of interest, the stored baseline must be subtracted from subsequent measurements of sample filter $OD_{\mathrm{fp}}(\lambda)$.
- If using a single beam instrument, or instruments run in the single beam mode the blank is not kept in the instrument so one does not need to rehydrate the blank reference filter regularly. Most modern single beam spectrophotometers will also automatically use the blank reference stored in memory for estimates of $OD_{\mathrm{fp}}(\lambda)$.
- Remove the blank filter from the quartz glass sample mount in the measurement beam, and replace it with a sample filter, ensuring proper hydration of the sample (see above). Measure the sample $OD_{\mathrm{fp}}(\lambda)$ spectrum, save it in a digital file, and record all relevant information.

- The blank reference filter will dry out over time, and must be hydrated regularly. If absorption signal deviates significantly from zero (more than 0.02 OD) in the infrared (750-800 nm), this often indicates a dry reference or sample filter. If using a quartz plate, check the reference filter after every 5-6 scans, and hydrate as needed. If the filters are mounted in air, hydrate the blank before every scan.

Sample Filter Preparation for De-pigmented Particle Absorption

After preparing an $a_{\mathrm{p}}(\lambda)$ filter sample and determining its $OD_{\mathrm{fp}}(\lambda)$ spectrum on the spectrophotometer, the sample should be processed to remove its pigments and determine $a_{\mathrm{d}}(\lambda)$. The shape of the $a_{\mathrm{d}}(\lambda)$ spectrum usually decreases monotonically with wavelength, following exponential form that is flatter than the shape of the soluble absorption spectrum. Since the goal is generally to get an estimate of phytoplankton absorption, if there is a residual chlorophyll *a* absorption peak in the red near 675 nm, the extraction process should be repeated to remove it. Variations of this method include use of hot or boiling methanol and varying extraction times. Use of hot methanol has risks due to flammability, and volatility. If this process is used, extra precautions must be taken.

Bleaching of the organic pigments can also be accomplished for situations with difficult to extract pigments including phycobilins or other chemically polar pigments that do not extract well in methanol. Pigment extraction in a chemical solvent, such as methanol, is a fundamentally different chemical process than bleaching the pigments using sodium hypochlorite (NaClO). Bleaching involves placing a small amount of 0.1 % active chlorine solution onto the filter, then rinsing it off with FSW. The NaClO oxidizes the pigment molecules, making their light absorption negligible. FSW rinses then remove the excess NaClO, which absorbs negligibly at wavelengths >400 nm, but absorbs strongly at shorter wavelengths. The bleaching method of pigment removal has been shown to be effective *in situ*ations where methanol cannot be used, as on cellulose membranes such as the 0.22 μm Millipore filter, or when phycobilins are present (Tassan and Ferrari 1995a; Mitchell *et al*. 2000). This procedure can also be adapted for use with particulate suspensions.

Neither methanol extraction, nor NaClO oxidation, provides an ideal means of separating particulate absorption into 'algal' and 'detrital' components. In each case, the action of the chemical agent is not well understood, and in many situations the two methods will yield very different results. The decision to apply either the bleaching, or methanol extraction, method will depend on the situation. For example, in inland waters where either cyanobacteria, or chlorophytes, are dominant, the bleaching technique is preferred, because of the presence of phycobilins and of extraction resistant algae (*e.g.* Porra 1990). In coastal oceanic waters, on the other hand, the methanol technique is preferred, because the results will be comparable to previously published results and there is no particular advantage to using bleach. In open-ocean samples (*e.g.* the Sargasso Sea), however, absorption by phycobilins is small, but present in some particulate absorption samples and in methanol-extracted filters (N.B. Nelson unpublished data). The methanol technique will provide results which are comparable to earlier studies, but with errors due to incomplete extraction and wavelength shifts in the phycobilin absorption bands.

a. Methanol Extraction method

- Replace the sample and blank filters on the filtration system. Treat blank filters exactly as if they were sample filters.
- Add 5 mL to 10 mL of 100 % methanol to each filter by gently pouring it down the sides of the filter funnel to minimize resuspension of the sample particles, and let stand for 1 min.
- Filter the methanol through the sample, turn off the vacuum, close the valves and add 10 - 15 mL of methanol.
- Allow the sample to stand in methanol for approximately 1 hr. Do not allow the filter to go dry during the extraction period. Time of extraction will vary depending on the filter load and phytoplankton species composition. Place aluminum foil over the filtration cups to minimize contamination during extraction.
- After extraction is complete, turn on the vacuum and draw the methanol and dissolved pigments through the filter. Rinse the sides of the filter tower twice with small amounts of methanol. Finally, rinse the sides of the filter tower three times with ~20 mL of 0.2 μm FSW. Also rinse the blanks with FSW after methanol extraction to minimize filter dehydration during spectrophotometric analysis.

- Pigment extraction is complete when the 675 nm chlorophyll *a* absorption peak is not present in the $OD_{\mathrm{fd}}(\lambda)$ spectrum.
- Successive, short extractions of 10 minutes can sometimes improve the pigment extraction.
- Phycobilins, and some eukaryotic pigments, will not be extracted efficiently by methanol.

b. Sodium Hypochlorite oxidation method

- Prepare NaClO solution:
- For freshwater samples: 0.1 % active chlorine in purified water (*e.g.* Milli-Q water).
- For marine samples: 0.1 % active chlorine in purified water containing 60 gl^{-1} Na_2SO_4, to match osmotic pressure of sample cells.
- The volume of 0.1% active chlorine solution needed to bleach pigments from a filter sample has been empirically shown to be approximately $3OD_{\mathrm{fp}}(440)$ mL .
- Place the sample, particle side up, on the filtration system (closed valves).
- Gently pour the solution down the sides of the filter funnel.
- Let the solution act for 5 min to 10 min, adding solution as necessary to compensate for loss through the filter.
- Cover the filtration cup with aluminum foil to prevent contamination during bleaching.
- Rinse the sample by gentle filtration of 50 mL of water (either fresh water or FSW, depending on sample source).
- Complete bleaching of the pigments is indicated by the absence of a 675 nm peak, together with a concave shape near 440 nm, in the $OD_{\mathrm{fd}}(\lambda)$ spectrum of the bleached filter. If evidence of residual pigment absorption persists, repeat the NaClO oxidation treatment, as indicated above.

Spectrophotometric Measurement of De-pigmented Optical Density Spectra

- The $OD_{\mathrm{fd}}(\lambda)$ spectrum of the de-pigmented samples should be measured in the spectrophotometer, as described above for $OD_{\mathrm{fp}}(\lambda)$.
- Note that methanol-extracted sample and blank filters will tend to dry out quickly if the methanol is not thoroughly rinsed from the filters prior to spectrophotometric measurements.
- NaClO oxidized sample and reference filters must be thoroughly rinsed with FSW (or fresh water for inland water samples) to extend the spectral range below 400 nm.

4.5 SOLUBLE ABSORPTION SAMPLE PREPARATION AND ANALYSIS

The measurement methods described in this section are used to determine $a_{\mathrm{g}}(\lambda)$, the spectral absorption coefficient spectrum of gelbstoff, often referred to as dissolved organic matter (CDOM). Water samples are collected and particulate material is removed by filtration. The absorption of the filtrate is measured, relative to purified water, using a spectrophotometer. All equipment utilized to prepare soluble absorption samples must minimize contamination by organic, or otherwise colored, material. Samples must be protected from photo-degradation during preparation and measurements. Plastic or glass filtration apparatus may be used, provided that the units are equipped with mesh filter supports made either of stainless steel or plastic, and not with ground glass frits. Glass frits tend to become clogged over time, and may cause uneven distribution on the filter, reduce the rate of filtration and may contaminate the sample filtrate.

Membrane filters with 0.2 μm pore size (*e.g*., Nuclepore™ polycarbonate filters) are recommended for this procedure. The membrane filters should be pre-soaked in 10% HCl, rinsed with 75-100 mL of freshly purified water, and rinsed again with a 75 – 100 mL of the sample before it is used. Tests with purified water have shown that all filters leach contamination that resembles soluble absorption (data not shown). Using polycarbonate membrane filters, an acid soak, pure water rinse and sample rinse minimizes this contamination. Still, we have found the sample preparation procedure increases the apparent absorption spectra of purified water that is prepared as though it were a sample when referenced to purified water drawn directly into the measuring cuvette from the pure water system. Therefore correction for this sample preparation blank is recommended.

Glass fiber filters should be avoided if possible because they have been shown to cause rather severe contamination of the filtrate in tests using purified water. For samples collected from very turbid waters, glass fiber filters have routinely been used as a pre-filter to minimize clogging of the final filtration with a membrane filter (Kowalczuk, 1999). In such cases the investigator must develop a procedure to rinse the glass fiber filter to ensure that the contamination from this method is minimized. Since situations requiring pre-filtration often coincide with large soluble absorption coefficients, the effects may be easily corrected but it is the responsibility of the investigator to demonstrate this. Careful assessment of the contamination of any method, and proper corrections must be carried out and reported.

Previously we recommended the use of amber-colored borosilicate glass bottles (*e.g*. Qorpak™ bottles), that screen ambient light, for sample preparation and to store laboratory prepared standard water. However, recent work (details not shown) indicate that the amber bottles may leach some colored material into the purified standard water that is prepared before cruises and used to assess the quality of purified water prepared at sea. Therefore we now recommend use of clear borosilicate Qorpak™ bottles (or equivalent) for sample preparations and for the preparation of the standard reference water. Prior to each experiment, all filtration apparatus and storage bottles should be thoroughly cleaned.

Purified water for soluble absorption measurements

Purified water freshly drawn from a water purification system, such as the Millipore Milli-Q, Millipore Alpha-Q, and Barnstead Nanopure units, or their equivalent, is strongly recommended for use at sea in preparing pure water for absorption reference, blanks and for equipment rinses specified in these protocols. Mitchell *et al*. (2000) compared the water-to-air baseline reference of purified water prepared with these three water purification systems. All three systems provided similar results in baseline tests relative to air at wavelengths between 300 nm and 900 nm, while small differences were found below 300 nm. It is also recommended to prepare a set of standard purified water samples prior to a field deployment as a reference to check daily for pure-water system degradation, *e.g*. due to poor quality feed water. Even though bottled purified water standards have been found to deteriorate slightly over time, especially from 250 nm to 325 nm, they provide invaluable quality control and an alternative source of reference water *in situ*ations when the purification system performance degrades dramatically.

Pre-cruise preparations

- Sample bottles (clear borosilicate Qorpak™ with polyethylene lined caps) used to collect sample filtrate or to store standard reference water need to be thoroughly cleaned in advance to remove any potential organic contaminants. Sequential soaks and rinses in dilute detergent, purified water, and 10 % HCl, followed by a final copious rinse in purified water, are recommended.
- Rinse plastic caps with 10 % HCl, twice with freshly prepared purified water (*e.g.* using a Millipore Alpha-Q system), and dry them at 70^{o} C for 4 hr to 6 hr.
- Combust bottles with aluminum foil covers at 450^{o} C for 4 hr to 6 hr.
- Fill clean, combusted bottles with fresh purified water drawn directly from the purification unit.
- Assemble the combusted bottles and clean caps. Store in the dark.
- These standards are used daily during cruises to evaluate the quality of purified water freshly prepared at sea.

- This carefully prepared standard water sometimes must be used as the reference material for actual sample analysis. If this is planned, the investigator should determine the optical density of the standard water preparations before and after a cruise relative to fresh purified water drawn directly into the quartz cuvettes. An assessment of the change in this water over time may indicate a need to use a time-dependent reference water correction.
- As a precaution, even if the investigator intends to have high quality purified water at sea, it is wise to determine the standard water optical density relative to freshly purified water before a cruise, and as a time-series to understand the quality of the purified water system used for reference.

Soluble Absorption Sample Preparation, Storage and Analysis

- Wash hands with soap and water to avoid contaminating the samples.
- Use 0.2 μm polycarbonate filters (*e.g.* Nuclepore or equivalent). Do not use irgalan black stained (low fluorescence background) polycarbonate filters for this preparation. Other membrane filters, or Sterivex cartridges, may also be used, but the investigator must then test for any contamination by the filter and ensure that no artifacts are introduced.
- The filtration system used should be equipped with control of vacuum for each individual filtration funnel and with a provision for direct filtration into clean bottles. An example of a suitable soluble absorption filtration assembly is illustrated in Mitchell *et al*. (2000).
- Pre-soak each filter for at least 15 min in 10 % HCl. Rinse the filter thoroughly with purified water. Mount the filter on a filtration funnel and filter ~100 mL of purified water through it into a sample bottle. Shake the bottle, and discard the water, pouring it over the inside of the cap to rinse it. Cover the filtration funnel with aluminum foil until ready to filter the sample.
- Collect ~200 mL of seawater into a clean sample bottle. For the blanks, use purified water drawn directly from the purification unit into 2 clean sample bottles.
- Filter ~75 mL of the samples and 1 blank directly into clean bottles at low vacuum (<120 mm Hg). Do not allow filters to go dry during sample rinsing. Shake the bottles, and discard the water.
- Filter ~75 mL of the samples into bottles. For the blank, filter ~75 mL of purified water. When finished, cap the bottles and store them until they are to be measured in the spectrophotometer.
- If the samples will be measured within 4 hr, store them in the dark at room temperature.
- If the samples will be measured 4 hr to 24 hr later, refrigerate them in the dark.
- Longer storage is not recommended, because artifacts of undocumented magnitude are known to occur. Several researchers have reported results from measurements of frozen samples, but no systematic evaluation of possible artifacts resulting from freezing has yet been reported.
- Warm refrigerated samples to room temperature before beginning optical density measurements. If it is practical to do so, control the samples and the reference water to equal temperatures during the spectrophotometric measurements. Absorption by water is strongly temperature dependent at red and near infrared wavelengths (Pegau and Zaneveld 1993).
- Qorpak bottles can be re-used at sea. After spectrophotometric analysis is completed, thoroughly rinse each bottle and its cap three times with purified water, pour in 20 mL of 10 % HCl acid, and close the cap. Before the bottle is reused, shake it well, discard the 10 % HCl, rinse the bottle and cap copiously with purified water, and fill the bottle with purified water, to be used later to rinse a new sample filter. Purified water should be drawn directly from the pure water system.

Determination of Optical Density of Soluble Absorption Preparations

- If samples have been refrigerated, allow them to warm to room temperature.

- Allow the spectrophotometer to warm up for 30 min. Confirm that the optical windows of the spectrophotometer are clean. If necessary, clean them with purified water and ethanol, sequentially, and dry them thoroughly with lint-free laboratory tissues.
- Verify the instrument's spectral characteristics and precision as described in Section 4.3.
- Wash hands with soap and water to avoid contamination
- Between use, 10 cm quartz window spectrophotometer cuvettes should be stored with purified water. For analysis, discard the purified water in the cuvettes, rinse inside and outside of cuvettes twice with 10 % HCl, twice with ethanol, then rinse them inside and outside using copious volumes of purified water. After the cuvettes have been cleaned, use laboratory tissues to handle them. Avoid contacting the cuvettes with bare-hands, and do not contaminate their optical windows by touching them.
- Fill both cuvettes with purified water drawn directly from the water preparation system. Use of purified water stored in containers is not recommended. However, if freshly purified water is not available at sea, the carefully prepared standard water in combusted bottles can be used as a reference, but the investigator must document its degradation over time relative to air (see above).
- Carefully dry the cuvettes. Bulk dry with paper towels, but dry the quartz optical windows with lint-free laboratory wipes only (*e.g.* Kimwipes™).
- Inspect cuvettes carefully, especially along their optical paths, to ensure that they are clean. Make sure there are no bubbles, floating dust, or contaminants on the optical windows, or in suspension. Looking through the cuvette against a black background can usually identify any problems in the samples. Repeat cleaning and drying procedures as needed to obtain a clean sample.
- Run an air–to-air baseline reference spectrum for the spectrophotometer. Record the digital air baseline. This spectrum should be spectrally flat, with noise less than ± 0.0005 OD.
- Place the reference cuvette in spectrophotometer and scan $OD_{\mathrm{rwa}}(\lambda)$, the optical density of purified water relative to air. Remove the reference cuvette and repeat the measurement for the sample cuvette. Store both spectra noting which file is for the cuvette to be used as reference in subsequent analyses, and which is to be used for samples. See Figure 4.2 for spectra of $OD_{\mathrm{rwa}}(\lambda)$ determined during ACE-Asia.
- Compare the spectra of $OD_{\mathrm{rwa}}(\lambda)$ determined for the reference and sample cuvettes to each other, and with a digital library of previous reference water to air optical density spectra. Ensure that the two cuvettes are well matched optically, and that both conform to tolerance of pure water relative to air. Note anomalies and plan to make any needed corrections during data processing. If anomalies are associated with poor preparation of the cuvette, repeat the preparation and run new water-to-air baseline reference scans.
- Put both reference and sample cuvettes filled with purified reference water into the spectrophotometer for a double beam unit. For a single beam unit this will be done sequentially. Run a baseline correction for purified water. After the water-to-water baseline optical density measurement is complete, record the pure water baseline as a sample, $OD_{\mathrm{rww}}(\lambda)$. This spectrum should be spectrally flat, with magnitude less than ± 0.0005 OD. Save the digital baseline spectrum. Ensure the baseline is flat and stable over time and note any anomalies. It is common for the baseline to exhibit temperature-dependent artifacts 650-800 nm. These should be minimized if possible by ensuring the purified water in the sample and reference cuvette are at the same temperature.
- If the baseline reference spectrum $OD_{\mathrm{rww}}(\lambda)$ is not flat and stable during analysis according to specifications summarized in section 4.3, the precision of any estimate of soluble absorption may be seriously questioned. It is the investigator's responsibility to ensure satisfactory performance of the instruments and use of proper methods to ensure that the final result is reasonable. Significant deviation from the specifications in section 4.3 or improper consideration of sample preparation protocols may result in estimates of soluble absorption that are not meaningful given the small magnitude of this estimate in the visible spectral region of most interest for ocean color applications.

- Remove the sample cuvette and discard the liquid. Rinse the inside of the cuvette three times with ~5 mL to 10 mL of the next sample to be measured. A copious rinse is desired, but sample volume is often limited. Several vigorously shaken small sample rinses are recommended if the volume is extremely limited.
- Fill the sample cuvette with the purified water that has been filtered as though it were a sample and record the blank spectrum, $OD_{\mathrm{bs}}(\lambda)$, relative to the reference cuvette filled directly from the purified water source..
- Repeat the rinsing for each subsequent sample. The first sample rinse for seawater samples is most important to eliminate all purified water, especially for seawater samples due to refractive index differences between fresh and salt water. Fill the cuvette with the next water sample.
- Prior to running each sample, dry the exterior of the sample cuvette carefully, and inspect it, as described above, to ensure a clean sample.
- Replace the sample cuvette in the spectrophotometer, and measure the $OD_s(\lambda)$ spectrum relative to freshly purified water. Store the digital data and record all necessary information.

4.6 DATA PROCESSING AND ANALYSIS

The protocols in this section should be followed to compute particle and soluble material absorption coefficients from the spectrophotometric *OD* measurements described above. The following discussion assumes that all measured $OD(\lambda)$ spectra, whether for samples, or reference blanks, have been corrected for the instrument baseline spectrum, either automatically, or by post-measurement calculations appropriate to a particular spectrophotometer configuration (see above in Section 4.3, and specific reference spectrum measurement checks in the protocols of Sections 4.4 and 4.5).

Computations for absorption coefficients of particles concentrated on filters, and for materials dissolved in water, differ primarily in the determination of optical pathlength and in the treatment of reference blanks.

Soluble Absorption Coefficients

For soluble absorption, the calculations are directly proportional to the sample optical density relative to the pure water reference after correction for the pure water blank and specification of a null absorption

$$a_g(\lambda) = \frac{2.303}{l}\left[[OD_{\mathrm{s}}(\lambda) - OD_{\mathrm{bs}}(\lambda)] - OD_{\mathrm{null}}\right], \tag{4.3}$$

where l is the cuvette pathlength (usually 0.1 m), $OD_{\mathrm{s}}(\lambda)$ is the optical density of the filtrate sample relative to purified water, $OD_{\mathrm{bs}}(\lambda)$ is optical density of a purified water blank treated like a sample relative to purified water (see below), and OD_{null} is the apparent residual optical density at a long visible or near infrared wavelength where absorption by dissolved materials is assumed to be zero. Note that as long as the null wavelength region is the same for sample and blank, the sample and blank spectra can be set to zero at the null wavelength independently or after they are subtracted from each other, as indicated in Equation (4.3). Equation (4.3) assumes use of a spectrophotometer that automatically references the sample and blank optical density to freshly purified water. Most modern commercial single or double beam units will compute this optical density directly relative to the reference. The user must record both raw sample and blank optical densities relative to purified water, and assess the stability of the purified water $OD_{\mathrm{rww}}(\lambda)$ reference by routine determinations of the purified water relative to air (*e.g.* $OD_{\mathrm{rwa}}(\lambda)$; Figure 4.2) and also evaluate the sample preparation methods by determining the blanks routinely (*e.g.* daily when at sea; Figure 3B).

a. Filtered pure water blank spectra

There are generally small spectral effects of the filtration and preparation procedure that cause blanks prepared from purified water to have a higher $OD_{bs}(\lambda)$ at short wavelengths compared to the reference cuvette containing purified water drawn directly from the purification system. Examples of filtered blank spectra $OD_{bs}(\lambda)$ for ACE-Asia where Millipore Alpha-Q water was used as the purified water source in the reference cuvette are illustrated in Figures 4.3B and 4.3D (c.f. Mitchell *et al.* 2000). The $OD_{bs}(\lambda)$ spectrum should be determined, recorded and included with the data for each sample. It is recommended that the investigator carefully determine these blanks for each station, or at least once per day, during a field program, and evaluate the stability of this blank for quality control purposes. If the purified water system is performing well, and the preparation procedures are carefully implemented, the $OD_{bs}(\lambda)$ sample blank offsets will generally be very consistent (Figure 4.3B). In such cases, the recommended procedure is to average $OD_{bs}(\lambda)$ spectra over the entire cruise, and to then fit a smoothed exponential function over wavelength to the overall mean (the bold line in Figure 4.3B). A separate OD_{null} (see discussion below) should be determined for the averaged and smoothed $OD_{bs}(\lambda)$ spectrum before it is substituted in Equation (4.3). Because the signals are small, instrument noise is a large fraction of the signal, even for high quality spectrophotometers. Therefore subtraction of an individual blank spectrum, including its noise, is strongly discouraged as this effectively doubles the noise of an already noisy signal. Instead, it is recommended that a smoothed blank be determined from many individual blank spectra provided that the investigator can demonstrate, as in Figure 4.3B that there is consistency among the population of blank spectra that are determined. The procedure of determining blanks at least each day during routine sampling provides an important quality control on the sample preparation protocols. If the blank is found to deviate considerably from the norm, the investigator should immediately determine the cause of the discrepancy.

b. Null point corrections to soluble absorption spectra

The absorption spectrum of pure water varies strongly with temperature, especially in the wavelength region between 650 nm and 750 nm, but at other wavelengths as well (Pegau and Zaneveld, 1993). To avoid temperature related measurement artifacts, the sample and reference should be maintained at the same temperature, but in practice, this is often difficult to do. If strong temperature residuals are apparent in the spectra near 750 nm, one must inspect the data to determine an appropriate wavelength range to use as a null point. For the data in Figure 4.3, it appears that assuming a null point as the average from 590-600 nm is reasonable. This assumption may not be reasonable in turbid lake, bay and coastal waters, however, where large soluble absorption values may persist into the near IR. Selection of wavelengths for null correction must be evaluated carefully for each data set, following principles discussed at more length by Mitchell *et al*. (2000).

Particle Absorption Coefficients

To compute particle absorption $a_p(\lambda)$ in suspension from spectrophotometric $OD_{fp}(\lambda)$ measured with the particles concentrated on a GF/F filter, it is necessary to appropriately adjust the optical pathlength. This includes substituting the geometric optical pathlength of the particles in suspension, and a scaling factor, β, accounting for the increase in the optical measurement path by scattering within the filter sample. The geometric absorption pathlength l_s of the filtered material in suspension is given by

$$l_s = \frac{V_f}{A_f}, \tag{4.4}$$

where V_f is the volume of water filtered and A_f is the clearance area of the filter calculated from the diameter D_f of the part of each filter that contains the particles. D_f should be determined very carefully on numerous individual filters using AN accurate measurement tool like a caliper that is accurate to at least 0.1 mm.

Scattering of light within the GF/F filter increases the absorption pathlength. The absorption coefficient of filtered particles must be corrected for pathlength amplification and the equivalent absorption coefficient in m^{-1} in suspension is computed as

$$a_p(\lambda) = \frac{2.303 A_f}{\beta V_f}\left[[OD_{fp}(\lambda) - OD_{bf}(\lambda)] - OD_{null}\right], \quad (4.5)$$

where $OD_{fp}(\lambda)$ is the measured optical density of the sample filter, $OD_{bf}(\lambda)$ is the optical density of a fully hydrated blank filter, and OD_{null} is a null wavelength residual correction from the infrared where particle absorption is minimal. See also detailed discussion of null point selection in Mitchell *et al*. (2000)

a. Particle absorption blank spectra

If a spectrophotometer with automatic reference baseline correction is used, and the reference filter blank baseline is flat over the spectral range of interest, $OD_{bf}(\lambda)$ does not need to be subtracted. Spectra of $OD_{bf}(\lambda)$ must be determined, recorded and provided with the sample data. Properly prepared blanks generally have flat spectra relative to the reference baseline filters. If the $OD_{bf}(\lambda)$ is confirmed to be flat, then it is recommended that only a null absorbance is subtracted from the $OD_{fp}(\lambda)$ to compensate for baseline offsets. Subtraction of a spectrally flat baseline that varies only due to the instrument noise increases the noise of the result. If the instrument baseline cannot be maintained within the recommendations summarized in Section 4.3, the investigator should consider using a different instrument since the errors in the methods caused by using unstable instruments are difficult to control for.

b. Null point corrections to particle absorption spectra

To correct for residual offsets in the sample filter relative to the reference, and for scattering artifacts due to particle loading, it is assumed that a null absorption wavelength in the infrared can be identified. Historically, many investigators used 750 nm as the null absorption wavelength, but recent reports indicate that this wavelength is too short for some waters. It is recommended that the null wavelength be set at 800 nm (or longer), and that the investigator must examine the spectra to evaluate residual absorption structure near the null wavelength. Rather than use a single wavelength, a mean $OD_{fp}(\lambda)$ in a 10 nm interval (*e.g.* 790 nm to 800 nm) may be used as the null value to minimize the introduction of noise in the null correction procedure. Mitchell *et al.* (2000) discuss, at more length, factors affecting the choice of an appropriate wavelength for estimating OD_{null}. In Case 2 waters, the definition of the null absorption is more difficult and the investigator may consider the benefits of the transmission-reflectance estimates of particle absorption (Tassan and Ferrari, 1995a).

c. Pathlength amplification corrections

To correct for the pathlength increases due to multiple scattering in the filter, the prevalent current practice is to estimate β empirically through either a quadratic or power function that may be expressed in the form

$$\beta = \left[C_1 + C_2\left[OD_{fp}(\lambda) - OD_{null}(\lambda)\right]\right]^{-1}, \quad (4.6a)$$

or

$$\beta = C_0 + C_1\left[OD_{fp}(\lambda) - OD_{null}(\lambda)\right]^{C_2}, \quad (4.6b)$$

for quadratic equation or power function fits, respectively. C_0, C_1 and C_2 are coefficients of least squares regression fits of measured data. Recommended coefficients have been reported in the literature (Table 1). The investigator should either choose published coefficients consistent with the species composition, equipment and measurement conditions for a given data set (consider the discussion in Mitchell *et al*. 2000), or independently determine

pathlength amplification factors by comparing absorption in suspension and on filters following procedures described previously (Mitchell 1990, Mitchell *et al*., 2000).

d. De-pigmented Particle and Phytoplankton Absorption Coefficients

The de-pigmented particle absorption coefficients, $a_d(\lambda)$, may be calculated using Equation (4.5), by substituting. $OD_{fd}(\lambda)$ for $OD_{fp}(\lambda)$. At present it is recommended to use the same pathlength correction factor for the de-pigmented samples as for the particle absorption sample. The validity of this operational choice of β is difficult to assess, because the de-pigmented particles are created operationally from the treatment, and the relationships between their absorption on filters compared to suspensions may differ from those derived empirically for the original particles.

The spectral absorption coefficient for phytoplankton pigments can be computed as the difference between particulate and de-pigmented estimates:

$$a_\phi(\lambda) = a_p(\lambda) - a_d(\lambda). \tag{4.7}$$

4.7 DATA REPORTING

For purposes of data reporting and archiving, the absorption coefficients will be reported in m^{-1} and computed using the equations summarized above. Uncorrected optical density spectra for the filter samples, blank filter referenced to a blank filter, pure water referenced to air, pure water referenced to pure water and soluble absorption blank spectra must be recorded and provided so alternative algorithms could be applied to the original data. The pathlength amplification factor, a description of (or reference to) the method and the procedure for assignment of the null absorption, and any blank or spectral scattering corrections for the soluble absorption calculations must be reported.

4.9 PROTOCOL STATUS AND FUTURE DIRECTIONS

Absorption spectra for particles filtered on GF/F filters

Details of various issues related to this frequently used method for estimating particle absorption for filtered samples are not significantly changed since the summary of the NASA-sponsored Workshops found in Mitchell *et al*. (2000). It is important to address a few salient issues that are routinely asked by investigators interested in implementing the method. First, most modern dual-beam spectrophotometers that have a grating before the sample and illuminate the sample with spectrally resolved light have negligible differences (a few percent) in terms of determining the raw GF/F filter $OD_{fp}(\lambda)$ of the particles relative to a properly hydrated blank filter if the protocols are carefully followed. Thus, it is not essential to determine the pathlength amplification factor, β, for each different spectrophotometer that is used as long as the investigator makes an appropriate choice of instrumentation. However, some spectrophotometers have limited spectral range, limited dynamic range, more noise and inferior stability so the investigator should evaluate the unit to be used to ensure suitability by following the recommendations in section 4.3. Second, diode-array systems that illuminate with broad-band light and then disperse the post-sample light using a spectral photodiode array may have significantly different raw OD for the filtered sample. Example OD spectra estimated for a diatom culture for various systems used at the Scripps Workshop are shown in Figure 4.1 (see also details in Mitchell *et al*. 2000). Note the Hewlett-Packard spectral diode array system has a significantly higher OD than the other instruments. An empirical relation for this offset in the range 400-700 nm is reported in Mitchell *et al*. (2000) for that specific model. The Hewlett-Packard data is reported only for wavelengths greater than 400 nm because the instrument performs poorly at short wavelengths with the glass fiber filter method. If a user chooses such optical geometry for the determination of particle absorption they should carefully assess the potential issues illustrated in Figure 4.1. We recommend that the user compare several spectrophotometers for raw optical density of properly hydrated samples relative to blank filters and ensure the unit they use does not deviate from the typical result of most systems for which amplifications factors (β) have been determined (Table 4.1). Alternatively one must determine the pathlength amplification for the

instrument of choice, a laborious and unnecessary procedure if a spectrophotometer is selected that does not cause the bias illustrated in Figure 4.1.

Absorption spectra for particles transferred to glass slides

An alternative method, developed by Allali *et al*. (1995), to estimate absorption coefficients of cultures and seawater samples is to freeze transfer the particles to transparent microscope slides, following the protocols of Hewes and Holm-Hansen (1983). The investigator must have an integrating sphere or equivalent scattered transmission accessory to implement this method. This procedure produced results comparable to the GF/F filter method in comparisons reported by Mitchell *et al*. (2000), but sufficient uncertainties remain that the GF/F method continues to be recommended for the present.

Transmission-Reflectance (T-R) Method

Tassan and Ferrari (1995a) described a modification of the light-transmission method that corrects for backscattering. This technique combines light-transmission (T) and light-reflection (R) measurements, carried out using an integrating sphere attached to a dual-beam spectrophotometer. The data analysis is performed by a theoretical model that eliminates the effect of light backscattering by the particles. At the Scripps workshop, the global error of the T-R method was comparable to the error yielded by the simpler T method for monocultures. Subsequent modifications of the T-R experimental routine (Tassan and Ferrari, 1998; Ferrari and Tassan, 1999) yielded a significant reduction of the experimental error. Tassan and Ferrari (1995) reported that for case 1 waters that have negligible inorganic particle load, the amplification factor for GF/F filters determined with the T-R methods is similar to those determined by Mitchell (1990). The T-R method is particularly suited for applications to samples containing highly scattering mineral particles that are commonly found in Case 2 waters. Despite the more complicated procedure including an instrument with an integrating sphere, this method should be considered in special circumstances, and with further development may eventually supercede the presently recommended transmission protocol.

Absorption spectra for seawater filtered through membrane filters or cartridges

For most ocean regions, the optical density of dissolved organic material, relative to purified water in a typical 10 cm pathlength cuvette, is very small in the 400-600 nm region of most interest to ocean color satellite investigations. To ensure a common frame of reference for the global data collected by diverse investigators, we recommend $OD_{\mathrm{rwa}}(\lambda)$ spectra (250-850 nm) be determined relative to air for purified water directly introduced to properly cleaned quartz cuvettes. The purpose of such spectra is to obtain an independent reference of the quality of the purified water. $OD_{\mathrm{rwa}}(\lambda)$ spectra for the sample cuvette used during ACE-Asia are shown in Figure 4.2. $OD_{\mathrm{rwa}}(\lambda)$ should be determined daily for the sample and reference cuvettes used in analyses. The investigator should keep careful records of this data and assess any bias in final estimates that may be attributed to problems with the reference water. By plotting in the range of minimal absorption by water (250-600 nm; Figure 4.2A) one can assess whether or not the reference water on a ship has seriously degraded. Production of impure water by commercial systems is a relatively common problem on ships where the feed water may have serious contamination. If the purified water system fails at sea, the investigator should use the standard water prepared prior to the cruise as the reference. Spectra of $OD_{\mathrm{rwa}}(\lambda)$ of the bottled standard water should be determined before and after a cruise for each lot of bottled standards that are prepared. This precaution is important to assist in any corrections that might be required if standard water is used as a reference, or if the purified water system degrades over time during a cruise.

There are still relatively few spectra of soluble absorption determined fresh at sea using the revised protocols recommended here. Spectra of $OD_s(\lambda)$ and $OD_{\mathrm{bs}}(\lambda)$ collected during ACE-Asia are shown in Figure 4.3. Raw optical density, relative to Millipore Alpha-Q water are shown in 3A. We routinely find small positive offsets from 600-800 nm that we feel should be compensated by subtracting a null value. Figure 4.3B illustrates $OD_{\mathrm{bs}}(\lambda)$ during ACE-Asia prepared as recommended in section 4.5, but plotted at 10x smaller scale as Figure 4.3A. The recommended procedure is to subtract a cruise (or global) mean of this blank (solid line in Figure 4.3B) from the raw sample *OD* values, and then to adjust this difference to zero at a null reference [Equation (4.3)]. The smoothed

global blank was determined by taking the mean of all blanks for each cruise we have completed since 1998, subsequently taking the mean of all cruises and lastly fitting an exponential function to the global mean after setting a null point as the average from 590-600 nm. There can be small differences in blank spectra cruise to cruise, but we do not find this to be significant relative to the overall statistics of all cruises or the variance within a single cruse. For relatively weakly absorbing samples like open oceans observed during ACE-Asia, there is negligible apparent absorption > 600 nm and there is clear evidence in 3A of uncompensated temperature effects 650-800 nm. Therefore we chose to set the null value as the mean from 590-600 nm. However, if very strong soluble absorption is present, the temperature effects 650-800 nm will be less significant, and the absorption 590-600 nm may be important. The investigator should evaluate their data to determine the best null point and report that assessment. Figure 4.3C are optical density of spectra for a 10 cm cuvette after correcting for the null value and the blank spectrum The effort to carefully determine the purified water relative to air, and blanks during each cruise will allow different investigators to inter-compare their results better, and will ensure better quality control of data collected over time. We have also determined the time-dependent change of our standard water (data not shown), and when we use that as a reference due to the failure of our purified water system at sea, we subtract a different blank than the global fit shown in Figure 4.3B.

An alternate method for preparing samples for soluble absorption allows multiple use of Sterivex sealed filtration cartridges. Use of these cartridges has been described by D'Sa *et al*. (1999) who used the method to prepare samples delivered to a capillary light guide spectrophotometer for estimating absorption by soluble material. The procedure provides high sensitivity and can be adapted to continuous flow determinations. This new method may prove useful in various applications but has not been applied extensively at this time. Evaluation of the performance of the Sterivex cartridges for sample preparation, and of light guides for spectroscopy, warrant further research.

Constraints on the estimate of soluble and particle absorption

To constrain our water sample estimates of particle and soluble absorption we have compared them to spectral estimates of the diffuse attenuation coefficient for downwelling irradiance, $K_d(z,\lambda)$, determined using a free-fall radiometer during a Southern Ocean cruise (AMLR) and a western Pacific Ocean cruise (ACE-Asia). It is well known that accurate estimate of $K_d(z,\lambda)$ in the upper ocean is difficult. Problems include heave of the ship, foam, bubbles, shadow, tilt, sky conditions and other influences on this apparent optical property (see more detailed discussions in other chapters of these protocols). Waters *et al.* (1990) described advantages of free-fall systems and many investigators have adopted this procedure to minimize some of the problems cited above. In 2001 we deployed our Biospherical Instruments PRR 800 system at approximately 80 stations combined between our AMLR and ACE-Asia cruises. We consider this our highest quality radiometric data set because of the free-fall deployment, the spectral range from 312-710 nm and because we acquired 4-5 separate free-fall profiles at each station to improve the confidence in our final estimate. In Figure 4.4 we show estimates of the mean cosine for spectral downwelling irradiance, $\overline{\mu}_d(\lambda)$, of the upper ocean mixed layer (open symbols). Here we define $\overline{\mu}_d(\lambda)$ as the ratio $[a_w(\lambda)+a_p(\lambda)+a_g(\lambda)]/K_d$. For Figure 4.4, values for pure water are estimated from Pope and Fry (1997) for 380-700 nm, Quickenden and Irvin (1980) for 300-320 and a linear interpolation between those values for 320-380 nm as recommended by Fry (2000). If the individual components are accurate, this can be considered a reasonable estimate of the mean cosine near the ocean surface (see Mobley, 1994 for detailed discussion of the mean cosine). Theoretically the values of $\overline{\mu}_d(\lambda)$ should be less than 1.0 and for typical radiance distributions of the upper ocean, they should be in the range of 0.70-0.85 near the surface. For both AMLR and ACE-Asia all absorption data were determined fresh at sea with consistent methods between the two cruises. We found that in the region 500 nm to 650 nm there is little difference between the estimates of $\overline{\mu}_d(\lambda)$ for the Southern Ocean and the western Pacific. However, below 500 nm, the values for ACE-Asia are near 1.0 and below 400 nm they exceed 1.0. For AMLR, values approach 1.0 for wavelengths less than 350 nm.

The ratio of $a_g(\lambda)/a_t(\lambda)$ where $a_t = a_w + a_p + a_g$, is also plotted in Figure 4.4 (filled symbols). The trend clearly illustrates that the soluble component dominates at short wavelength. There are several hypotheses that should be considered to understand the overestimates of $\overline{\mu}_d(\lambda)$ below 400 nm. These could include underestimate of $K_d(z,\lambda)$ or overestimates of any of the absorption components. A combination of these factors may prevail.

The filter radiometer in the profiler has good out of band blocking, but the spectrum of surface irradiance is rapidly changing in the region <350 nm and this may cause a red shift in the effective band center of the channels, with an associated underestimate of $K_d(z,\lambda)$. There may be small particles or colloids that pass the 0.2 μm filters causing a spectrally dependent scattering error (Aas, 2000). The particle absorption we estimate is based on Mitchell (1990), which results in higher estimates compared to some other published methods (Table 1). Also, there has not been adequate attention paid to determination of the pathlength amplification factor for the region below 400 nm. It is also possible that the values for pure water absorption are too high. The very reasonable or slightly high (by about 10-15%) values for the mean cosine of downwelling irradiance shown in Figure 4.4 for 400-600 nm indicates that the absorption methods recommended here are rather robust compared to simple estimates of diffuse attenuation coefficients. Reynolds *et al*. (2001) and Stramska *et al*. (2000) have reported reasonable closure between estimates of absorption using these methods, radiometric observations and modeling.

We have used "pure water" absorption for our estimate of $a_w(\lambda)$, and salts should in fact be added, if important, in the comparison of absorption to diffuse attenuation in Figure 4.4. Our estimate of $a_g(\lambda)$ relative to purified water will include absorption by salts, if they are significant. Salts in seawater are significant absorbers at short wavelengths. Lenoble (1956; see also Shiffrin, 1988) reported values for pure salts dissolved in purified water that indicate absorption coefficients near 300 nm comparable to the sample optical density of filtered samples relative to purified water that we routinely determine at sea in this spectral region. This UV absorption (<320 nm), relative to purified water, is generally assumed to be caused by "colored dissolved organic matter" but this may be inaccurate at these short wavelengths. Therefore one must be very cautious interpreting the apparent optical density of seawater filtrates relative to purified water for wavelengths less than 320nm. We recommend that more careful research should be carried out on the methods for soluble absorption, which appears to have a potentially dominating influence on the overestimates of $\bar{\mu}_d(\lambda)$ less than 400 nm. In particular, the influence of scattering by small particles (organic or mineral) and the role of salt absorption must be more carefully assessed.

REFERENCES

Aas, E., 2000: Spectral slope of yellow substance: problems caused by small particles. Proceedings of Ocean Optics XV, Monaco, 16-20 October, 2000.

Allali, K., A. Bricaud, M. Babin, A. Morel, and P. Chang, 1995: A new method for measuring spectral absorption coefficients of marine particulates. *Limnology and Oceanography.* **40,** 1,526-1,523

Allali, K., A. Bricaud, and H. Claustre, 1997: Spatial variations in the chlorophyll-specific absorption coefficients of phytoplankton and photosynthetically active pigments in the Equatorial Pacific. *Journal of Geophysical Research.* **102,** 12,413-12,423

Blough, N.V., O.C. Zafiriou, and J. Bonilla, 1993: Optical absorption spectra of waters from the Orinoco River outflow: terrestrial input of colored organic matter to the Caribbean. *Journal of Geophysical Research.* **98,** 2,271-2,278

Bricaud, A., A. Morel, and L. Prieur, 1981: Absorption by dissolved organic matter of the sea (yellow substance) in the UV and visible domains. *Limnology and Oceanography.* **26,** 43-53

Bricaud, A., and D. Stramski, 1990: Spectral absorption coefficients of living phytoplankton and non-algal biogenous matter: A comparison between the Peru upwelling area and the Sargasso Sea. *Limnology and Oceanography.* **35,** 562-582

Butler, W.L., 1962: Absorption of light by turbid materials. *Journal of the Optical Society of America.* **52,** 292-299

Carder, K.L., S.K. Hawes, K.S. Baker, R.C. Smith, and R.G. Steward, 1989: Remote sensing algorithms for discriminating marine humus from chlorophyll. *Limnology and Oceanography.* **30**(2), 286-298

Carder, K.L., R.G. Steward, G.R. Harvey, and P.B. Ortner, 1989: Marine humic and fulvic acids: Their effects on remote sensing of ocean chlorophyll. *Limnology and Oceanography.* **34,** 68-81

Chavez, F.P., K.R. Buck, R.R. Bidigare, D.M. Karl, D. Hebel, M. Latasa, L. Campbell, and J. Newton, 1995: On the chlorophyll *a* retention properties of glass-fiber GF/F filters. *Limnology and Oceanography.* **40(2),** 428-433

Cleveland, J.S., and A.D. Weidemann, 1993: Quantifying absorption by aquatic particles: A multiple scattering correction for glass-fiber filters. *Limnology and Oceanography.* **38,** 1321-1327

D'Sa, E.J., R.G. Steward, A. Vodacek, N.V. Blough, and D. Phinney, 1999: Determining optical absorption of colored dissolved organic matter in seawater with a liquid capillary waveguide. *Limnology and Oceanography.* **44,** 1,142-1,148

Duntley, S.Q., 1942: The optical properties of diffusing materials. *Journal of the Optical Society of America.* **32,** 61-70

Ferrari, G.M., and S. Tassan, 1996: Use of the 0.22 μm Millipore membrane for light-transmission measurements of aquatic particles. *Journal of Plankton Research.* **18,** 1,261-1,267

Ferrari, G.M, 1999: A method for removal of light absorption by phytoplankton pigments using chemical oxidation. *Journal of Phycology.* **35,** 1,090-1,098

Fry, E.S., 2000: Visible and near-ultraviolet absorption spectrum of liquid water: comments. *Applied Optics.* **39,** 2,743-2,744

Hewes, C.D., and O. Holm-Hansen, 1983: A method for recovering nanoplankton from filters for identification with the microscope: The filter-transfer-freeze (FTF) technique. *Limnology and Oceanography.* **28,** 389-394

Hoge, F.E., A. Vodacek, and N.V. Blough, 1993: Inherent optical properties of the ocean: retrieval of the absorption coefficient of chromophoric dissolved organic matter from fluorescence measurements. *Limnology and Oceanography.* **38,** 1394-1402

JGOFS, 1991: JGOFS Core Measurements Protocol. *JGOFS Report #6, Scientific Committee on Oceanic Research.* 40

Kahru, M., and B.G. Mitchell, 1998: Spectral reflectance and absorption of a massive red tide off Southern California. *Journal of Geophysical Research.* **103,** 21,601-21,609

Kalle, K., 1938: Zum problem der meerwasserfarbe. *Ann.Hydr.u.martim.Meterol.* **66,** 1.S.55-

Kiefer, D.A., R.J. Olson, and W.H. Wilson, 1979: Reflectance spectroscopy of marine phytoplankton. Part 1. Optical properties as related to age and growth rate. *Limnology and Oceanography.* **24,** 664-672

Kiefer, D.A., and J.B. SooHoo, 1982: Spectral absorption by marine particles of coastal waters of Baja California. *Limnology and Oceanography.* **27,** 492-499

Kishino, M., N. Okami, M. Takahashi, and S. Ichimura, 1986: Light utilization efficiency and quantum yield of phytoplankton in a thermally stratified sea. *Limnology and Oceanography.* **31,** 557-566

Kishino, M., N. Takahashi, N. Okami, and S. Ichimura, 1985: Estimation of the spectral absorption coefficients of phytoplankton in the sea. *Bulletin of Marine Science.* **37,** 634-642

Kou, L., D. Labrie and P. Chylek, 1993: Refractive indices of water and ice in the 0.65 to 2.5 μm spectral range, *Appl. Opt.*, **32:** 3531-3540.

Lenoble, J., 1956: L'absorption du rayonment ultraviolet par les ions presents dans la Mer. *Revue d'Optique.* **35** (10), 526-531

Mitchell, B.G. and D. A. Kiefer, 1988a: Chlorophyll *a* specific absorption and fluorescence excitation spectra for light-limited phytoplankton. *Deep-Sea Research I.* **35,** 639-663

Mitchell, B.G. and D. A. Kiefer, 1988b: Variability in pigment specific particulate fluorescence and absorption spectra in the northeastern Pacific Ocean. *Deep-Sea Research I.* **35,** 665-689

Mitchell, B.G., A. Bricaud, and others, 2000: Determination of spectral absorption coefficients of particles, dissolved material and phytoplankton for discrete water samples, In: Fargion, G.S. and J.L. Mueller, [Eds.] *Ocean Optics Protocols for Satellite Ocean Color Sensor Validation, Revision 2.* NASA/TM-2000-209966, NASA Goddard Space Flight Center, Greenbelt, MD. Chapter 12, pp125-153.

Mitchell, B.G. 1990: Algorithms for determining the absorption coefficient of aquatic particulates using the quantitative filter technique (QFT).*Ocean Optics X.* 137-148

Mitchell, B.G., M. Kahru, and P.J. Flatau, 1998: Estimation of spectral values for the mean cosine of the upper ocean. SPIE, Ocean Optics XIV. **CD-ROM**.

Mitchell, B.G., and D.A. Kiefer 1984: Determination of absorption and fluorescence excitation spectra for phytoplankton. *Marine phytoplankton and productivity.* **8,** 157-169

Moore, L.R., R. Goericke, and S.W. Chisholm, 1995: Comparative physiology of *Synechococcus* and *Prochlorococcus*: influence of light and temperature on growth, pigments, fluorescence and absorptive properties. *Marine Ecology Progress Series.* **116,** 259-275

Nelson, N.B., D.A. Siegel, and A.F. Michaels, 1998: Seasonal dynamics of colored dissolved material in the Sargasso Sea. *Deep-Sea Research.* **45,** 931-957

Pegau, W.S., and J.R.V. Zaneveld, 1993: Temperature-dependent absorption of water in the red and near infrared portions of the spectrum. *Limnology and Oceanography.* **38,** 188-192

Pope, R.M., and E.S. Fry, 1997: Absorption Spectrum (380-700 nm) of Pure Water: II. Integrating Cavity Measurements. *Applied Optics.* **36,** 8,710-8,723

Preisendorfer, R.W., 1976: Hydrologic optics 1. Introduction 2. Foundations 3. Solutions 4. Imbeddings 5. Properties 6. Surfaces 1450

Quickenden, T. I. and J. A. Irvin, 1980: The ultraviolet absorption spectrum of liquid water. *Journal of Chemical Physics*, **72**, 4,416-4,428

Reynolds, R. A., D. Stramski, and B. G. Mitchell, 2001: A chlorophyll-dependent semianalytical reflectance model derived from field measurements of absorption and backscattering coefficients within the Southern Ocean. *Journal of Geophysical Research,* **106(C4)**, 7,125-7,138.

Roesler, C.S., 1998: Theoretical and experimental approaches to improve the accuracy of particulate absorption coefficients derived from the quantitative filter technique. *Limnology and Oceanography.* **43,** 1,649-1,660

Shibata, K., 1958: Spectrophotometry of intact biological materials. Absolute and relative measurments of their transmission, reflection and absorption spectra. *Journal of Biochemistry.* **45,** 599-623

Shifrin, K.S., 1988*: Physical Optics of Ocean Water*. New York, American Institute of Physics, 285

Sogandares, F.M. and E. S. Fry. 1997: Absorption spectrum (340-640 nm) of pure water. I. Photothermal measurements. *Appl. Opt*. **36**: 8699-8709.

Sosik, H.M., 1999: Storage of marine particulate samples for light-absorption measurements. *Limnology and Oceanography.* **44,** 1,139-1,141

Sosik, H.M., and B. G. Mitchell, 1991: Absorption, fluorescence and quantum yield for growth in nitrogen limited *Dunaliella tertiolecta*. *Limnology and Oceanography.* **36,** 910-921

Sosik, H.M. and B. G. Mitchell, 1995: Light absorption by phytoplankton, photosynthetic pigments, and detritus in the California Current System. *Deep-Sea Research I.* **42,** 1,717-1,748

Stramska, M., D. Stramski, B. G. Mitchell and C. D. Mobley, 2000: Estimation of the absorption and backscattering coefficients from in-water radiometric measurements. *Limnology and Oceanography*, **45(3**): 628-641.

Stramski, D., 1990: Artifacts in measuring absorption spectra of phytoplankton collected on a filter. *Limnology and Oceanography.* **35,** 1,804-1,809

Tassan, S. and G.M. Ferrari, 1995a: An alternative approach to absorption measurements of aquatic particles retained on filters. *Limnology and Oceanography.* **40,** 1,358-1,368

Tassan, S., 1995b: Proposal for the measurement of backward and total scattering by mineral particles suspended in water. *Applied Optics.* **34,** 8,345-8,353

Tassan, S., 1998: Measurement of the light absorption by aquatic particulates retained on filters: determination of the optical pathlength amplification by the "Transmittance-Reflectance" method. *Journal of Plankton Research.* **20,** 1,699-1,709

Tassan, S., G.M. Ferrari, A. Bricaud, and M. Babin, 2000: Variability of the amplification factor of light absorption by filter-retained aquatic particles in the coastal environment. *Journal of Plankton Research.* **22,** 659-668

Vodacek, A., N.V. Blough, M.D. DeGrandpre, E.T. Peltzer, and R.K. Nelson, 1996: Seasonal variation of CDOM and DOC in the Middle Atlantic Bight: Terrestrial inputs and photooxidation. *Limnology and Oceanography.* **42,** 674-686

Waters, K. J., R. C. Smith and M. R. Lewis, 1990: Avoiding ship-induced light-field perturbation in the determination of oceanic optical properties. *Oceanography*. November: 18-21

Yentsch, C.S., 1957: A non-extractive method for the quantitative estimation of chlorophyll in algal cultures. *Nature.* **179,** 1302-1304

Yentsch, C.S., 1962: Measurement of visible light absorption by particulate matter in the ocean. *Limnology and Oceanography,* **7,** 207-217

Table 4. 1. Published coefficients for determining pathlength amplification effects. The suspension optical density, OD_{sp}, computed for a GF/F filter with $OD_{fp} = 0.2$ is provided for comparison.

Quadratic Functions	Particle Type	C_0	C_1	C_2	OD_{sp} (0.2)
Mitchell (1990)	Mixed Cultures	--	0.392	0.655	0.105
Cleveland & Weidemann (1993)	Mixed Cultures	--	0.378	0.523	0.097
Moore *et al*. (1995)	Prochlorococcus marinus	--	0.291	0.051	0.060
Moore *et al*. (1995)	Thalassiosira weissflogii	--	0.299	0.746	0.090
Moore *et al*. (1995)	Synechococcus WH8103	--	0.304	0.450	0.080
Tassan & Ferrari (1995)	Scenedesmus obliqus	--	0.406	0.519	0.102
Nelson *et al*. (1998)	Dunaliella tertiolecta	--	0.437	0.022	0.088
Nelson *et al*. (1998)	Phaeodactylum tricornutum	--	0.294	0.587	0.082
Nelson *et al*. (1998)	Synechococcus WH7803	--	0.277	0.000	0.055
Power Functions					
Mitchell and Kiefer (1988a)	Dunaliella tertiolecta	1.3	0.540	-0.467	0.082
Bricaud and Stramski (1990)	Field samples; D. tertiolecta Cultures of Mitchell & Kiefer (1988a)	0.0	1.630	-0.220	0.086
Kahru and Mitchell (1998)	Mitchell (1990) data	0.0	1.220	-0.254	0.109
Constant					
Roesler (1998)	Assume $\beta = 2.0$	--	--	--	0.100

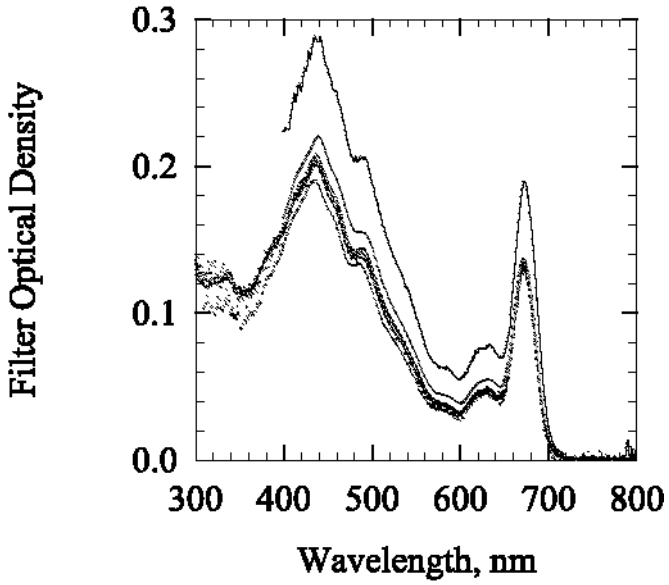

Figure 4.1: Optical density for various spectrophotometers for a diatom culture filtered onto GF/F filters. The average from 790-800 nm was used for a null value and the same volume was used for all samples. The data from the Hewlett Packard diode array system is higher than the other spectrophotometers as discussed in detail in Mitchell *et al*. (2000). Below 400 nm, the Hewlett Packard unit was too noisy for the glass fiber filter method.

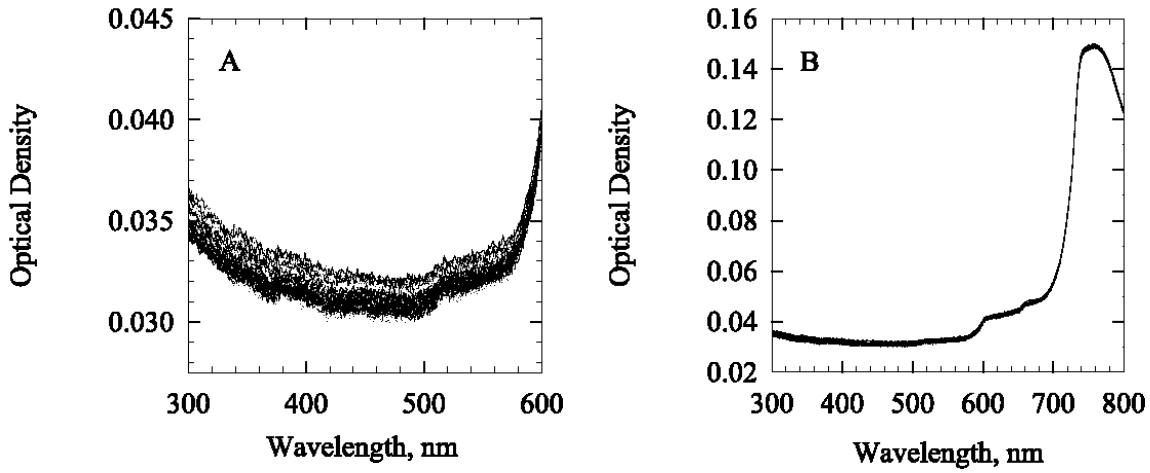

Figure 4.2: Optical density for fresh Millipore Alpha-Q water in the sample cuvette referenced to air in a dual beam spectrophotometer, $OD_{\mathrm{rwa}}(\lambda)$, determined during the ACE-Asia experiment. **A)**. $OD_{\mathrm{rwa}}(\lambda)$ plotted for the spectral range 300 nm to 600 nm. **B)**. Plotted for the spectral range 300 nm to 800 nm.

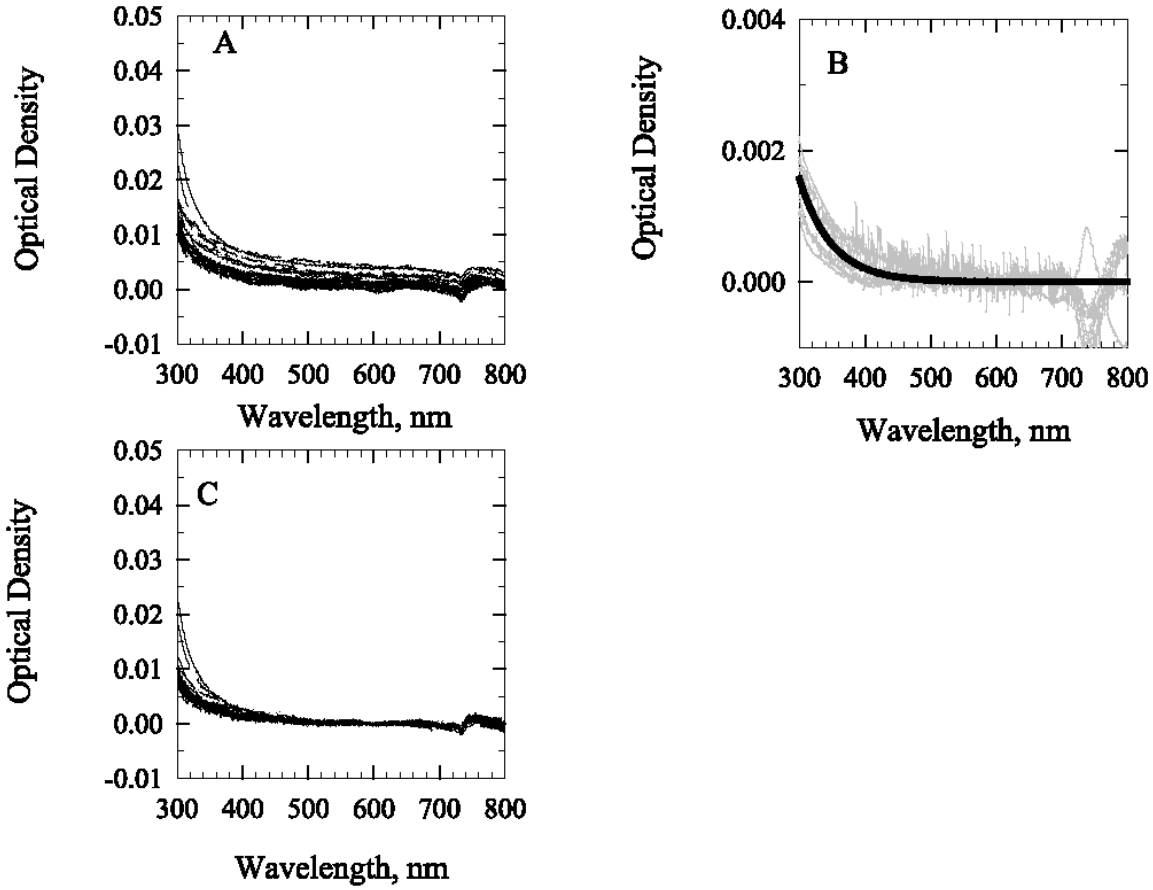

Figure 4.3: Typical results for soluble absorption determined during the ACE-Asia cruise (March – April 2001) in the western Pacific according to the protocols recommended here. **A)**. Raw optical density, $OD_s(\lambda)$, for samples relative to Millipore Alpha-Q water. **B)**. Blank optical density spectra, $OD_{bs}(\lambda)$ (after null offset, gray) compared to a global value (solid line). The global blank is determined by fitting an exponential function to the mean blank for more than 15 cruises from 1998-2001 where the mean for each cruise was determined as the mean of all individual blanks for each cruise. A fitted curve to a cruise or global mean for $OD_{bs}(\lambda)$ is recommended for correction of the soluble sample blank because individual spectra (gray) have significant instrument noise. Note the scale for 3B is approximately 10x smaller than the scale in 3A. **C)**. Estimates of sample optical density spectra after subtraction of the null value (average of raw values 590-600nm) and after subtraction of a global blank according to Equation (4.3). Temperature effects are evident 650-800 nm in the individual spectra.

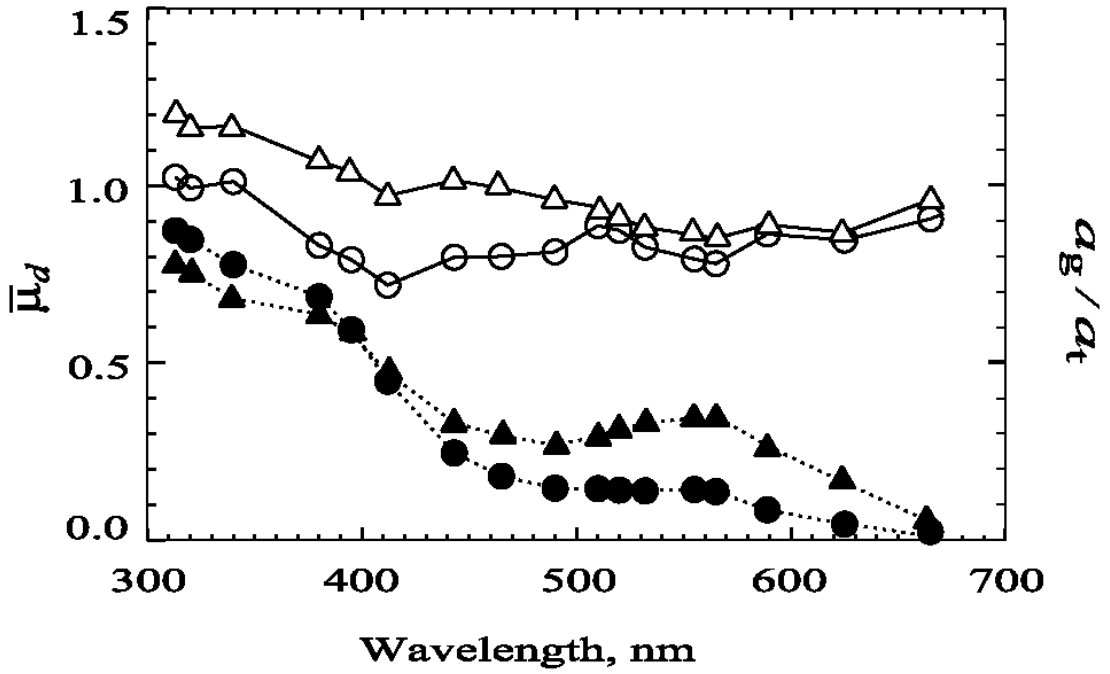

Figure 4.4: Median values for $\bar{\mu}_d(\lambda)$, the mean cosine for downwelling irradiance (open symbols, see text for definition) determined for the upper mixed layer. Values are plotted at each wavelength of the PRR 800 reflectance radiometer deployed during 2001 cruises to the Southern Ocean (AMLR) and the Western Pacific (ACE-Asia). The ratio of $a_g(\lambda)/a_t(\lambda)$ for the same data set are shown in solid symbols and plotted to the same scale. For both sets of spectra, AMLR data are circles and ACE-Asia data are triangles.

Chapter 5

Volume Scattering Function and Backscattering Coefficients: Instruments, Characterization, Field Measurements and Data Analysis Protocols

J. Ronald V. Zaneveld[1], Scott Pegau[1] and James L. Mueller[2]

[1]*College of Oceanographic and Atmospheric Sciences, Oregon State University, Corvallis*
[2]*Center for Hydro-Optics and Remote Sensing, San Diego State University, California*

5.1 INTRODUCTION

The volume scattering function (VSF) $\beta(\lambda,\psi)$ [$sr^{-1}m^{-1}$] and the volume absorption coefficient $a(\lambda)$ [m^{-1}] provide the most fundamental description of a medium's inherent optical properties (IOP), as all other IOP can be derived from them. In particular, the volume scattering coefficient $b(\lambda)$ and volume backscattering coefficient $b_b(\lambda)$ may be derived by integrating $\beta(\lambda,\psi)$ over the unit sphere and backward hemisphere, respectively. In terms of determining the "complete" IOP from *in situ* measurements, a useful combination is $a(\lambda)$, the beam attenuation coefficient $c(\lambda)$, and the volume scattering phase function $\tilde{\beta}(\lambda,\psi)=\dfrac{\beta(\lambda,\psi)}{c(\lambda)-a(\lambda)}$. The reader is referred to Vol. I, Chapter 2 (Sect. 2.4) and to Chapter 1 of the present volume for further details regarding these definitions and relationships.

Knowledge of the VSF is a critical prerequisite to accurate radiative transfer modeling of remote sensing reflectance and water-leaving radiance. In Vol. III, Chapter 4 (and references cited there), it is shown that irradiance reflectance $R(\lambda)$ is approximately proportional to the ratio of the backscattering to absorption coefficients, and that upwelled radiance just beneath the sea surface is proportional to $R(\lambda)$, so that

$$L_u\left(0^-,\lambda,\theta,\phi\right)=E_d\left(0^-,\lambda\right)\frac{f}{Q}\frac{b_b(\lambda)}{a(\lambda)}.$$

This relationship is completely general and exact, but it does not express a linear proportionality to the IOP ratio, because the factors *f* and *Q* are not simply coefficients. .They are functions, $f\left[\lambda,(\theta_o,\tau_a,W),a(\lambda),\beta(\lambda,\Psi)\right]$ and $Q\left[(\lambda,\theta',\phi),(\theta_o,\tau_a,W),a(\lambda),\beta(\lambda,\Psi)\right]$, that account for the bidirectional nature of the ocean's reflectance; this bidirectionality may be traced directly to the shape of the VSF. Bidirectionality of remote sensing reflectance, as it arises from the VSF, is shown more explicitly in the formulation by Zaneveld (1982).

Equation (1.18) could be used directly as a basis for measuring the VSF if an instrument's source and detector were well collimated, and there were no flux losses, or FOV distortions, associated with an its optical elements. Some general angle scattering meters (Petzold 1972; Lee *et al*. 2003) are designed with a well-enough collimated beam and very small detector acceptance angle, so that equation (1.18) may be applied directly. In terms of equation (1.19), this is equivalent to assuming that the scattering response weighting function $W(\lambda,\psi,\varphi;c)$ is narrow enough to set it to unity. The General Angle Scattering Meter (GASM), built at the Scripps Institution of Oceanography's Visibility Laboratory (Petzold 1972), consists of a lamp focused into a cylindrical beam, and a narrow field of view detector mounted to swing in an arc to view the beam at many off-axis scattering angles between approximately 10^o and 170^o. Petzold (1972) reported VSF's measured for selected natural waters using the

(GASM). This reference has been widely used to describe shapes of $\tilde{\beta}(\lambda,\psi)$ in natural waters. Mobley *et al*. (2001) compared measured and modeled nadir-viewing remote sensing reflectances, using measured $c(\lambda)$ and $a(\lambda)$ with $\tilde{\beta}(\lambda,\psi)$ of different assumed shapes, including that of Petzold (1972), and the VSF measured using a general angle scattering meter of a new design (Lee *et al*., 2003); best agreement was achieved using the measured VSF. Their results showed that large systematic offsets can result if one arbitrarily assumes a scattering phase function having an incorrect backward scattering fraction. The results of Mobley *et al*. (2001) also indicated that nadir-viewing radiance reflectance is less sensitive to the detailed shape of the forward scattering lobe of $\tilde{\beta}(\lambda,\psi)$. Details of scattering at intermediate forward angles might, however, be more important for off-nadir viewing geometry (Vol. III, Ch. 4).

At present, commercially available VSF sensors[12] are designed with detector beam-spread and detector acceptance angles ranging from 10^{o} to 20^{o} Full-Width Half-Maximum (FWHM). These instruments measure the VSF, weighted as in (1.19), at one (or a few) scattering angle(s) and are typically used to determine the backscattering coefficient using the methods described below in Sect. 5.4. Although these methods depend on assumptions concerning $\tilde{\beta}(\lambda,\psi)$, determinations of $b_b(\lambda)$ from VSF profile measurements with these instruments, when combined with absorption and beam attenuation coefficients, radiometric profiles and pigment concentration measurements, have provide useful information about relationships between IOP, AOP and optically important material constituents of the water column (*e.g.* Stramska *et al*. 2000).

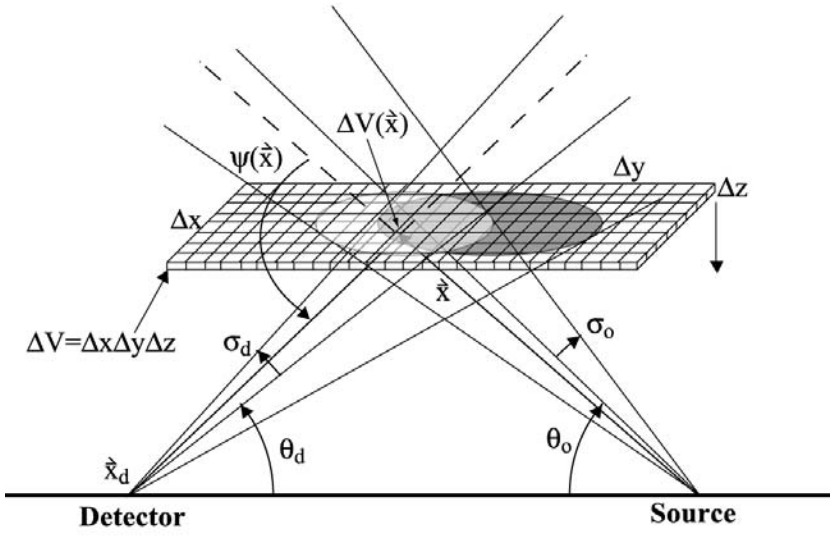

Fig. 5.1: Schematic illustration of a VSF sensor geometry used for numerical integration over the volume intersected by a source beam and detector FOV of incremental elements of the scattered radiant flux received by the detector.

[12] Certain commercial equipment, instruments, or materials are identified in this chapter to foster understanding. Such identification does not imply recommendation, or endorsement, by the National Aeronautics and Space Administration, nor does it imply that the materials or equipment identified are necessarily the best available for the purpose.

An example of a generalized source and detector arrangement to measure the VSF $\beta(\lambda,\psi)$ at a scattering angle $\psi > \frac{\pi}{2}$ is illustrated schematically in Fig. 5.1. To determine a calibration factor relating the detector response to flux scattered from the source beam into the field of view (FOV) of the detector, we must determine the sensor's response weighting function $W(\lambda,\psi,\varphi;c)$ [equation (1.19)], either explicitly, or implicitly. The explicit approach to this problem is to determine $W(\lambda,\psi,\varphi;c)$ from geometry and first principles, and then calibrate the instrument's response signals in a medium having a known VSF $\beta(\lambda,\psi)$; the detailed steps in this approach are described below in Sect. 5.2. The implicit approach (Maffione and Dana 1997) is to insert a plaque of known near-Lambertian reflectance in the position of the horizontal *xy*-plane, at distance *z* from the source-detector axis, illustrated Fig. 5.1, and record the instrument's responses as the plaque is moved vertically in small increments through the volume defined by the intersection of the source beam and detector FOV; this approach is briefly outlined in Sect. 5.3 below, but the reader is referred to Maffione and Dana (1997) for the detailed derivation and method of implementation.

For brevity, we will henceforth omit the explicit wavelength dependence of variables.

5.2 CHARACTERIZATION AND CALIBRATION OF A VSF SENSOR FROM ITS GEOMETRY AND RESPONSE TO SCATTERING BY POLYSTYRENE BEADS

Geometric Determination of W(ψ)

Figure 5.1 illustrates a source located at the origin $\vec{\mathbf{x}}_o = (0,0,0)$ and a detector located on the y-axis at position $\vec{\mathbf{x}}_d = (0, y_d, 0)$. As illustrated, the source beam and detector FOV are assumed to be cones with divergence angles σ_o and σ_d, respectively. At a distance z above the xy plane, a horizontal plane is shown passing through the the source beam (a nearly transparent, light-shaded ellipse) and detector FOV (a dark shaded ellipse); the intersection of the source beam and detector FOV is the intermediate gray-shaded area. The plane is divided into elemental volume elements $\Delta V = \Delta x \Delta y \Delta z$, and a particular volume element is denoted $\Delta V(\vec{\mathbf{x}})$.

The radiant flux Φ_o emitted by the source is assumed to be evenly distributed over the solid angle Ω_o, so by definition, the source radiant intensity is, by definition $I_o = \left(\frac{\Phi_o}{\Omega_o}\right)$. The flux transmitted in direction $\hat{\boldsymbol{\varepsilon}}(\vec{\mathbf{x}}) = \frac{1}{|\vec{\mathbf{x}}|}\vec{\mathbf{x}}$, where the vector length $|\vec{\mathbf{x}}| = \sqrt{\vec{\mathbf{x}} \bullet \vec{\mathbf{x}}}$, from the source to the elemental volume $\Delta V(\vec{\mathbf{x}})$ is

$$\Delta\Phi_o\left[\Delta V(\vec{\mathbf{x}});c\right] = I_o \Delta\Omega_o\left[\Delta V(\vec{\mathbf{x}})\right]\exp\left(-c|\vec{\mathbf{x}}|\right) = \Phi_o \frac{\Delta\Omega_o\left[\Delta V(\vec{\mathbf{x}})\right]}{\Omega_o}\exp\left(-c|\vec{\mathbf{x}}|\right), \tag{5.1}$$

where $\Delta\Omega_o\left[\Delta V(\vec{x})\right] = \frac{\Delta x \Delta y \left|\hat{\boldsymbol{\varepsilon}}(\vec{\mathbf{x}}) \bullet \hat{\mathbf{n}}\right|}{\vec{\mathbf{x}} \bullet \vec{\mathbf{x}}}$ is the solid angle subtended at the source by the horizontal elemental area $\Delta x \Delta y$ at position $\vec{\mathbf{x}}$, and $\hat{\mathbf{n}}$ is the unit normal to the *xy*-plane (Fig. 5.1). Thus, the irradiance incident on $\Delta V(\vec{\mathbf{x}})$ is

$$E_o(\vec{\mathbf{x}};c) = \frac{\Phi_o}{\Delta x \Delta y}\left|\hat{\boldsymbol{\varepsilon}}(\vec{\mathbf{x}}) \bullet \hat{\mathbf{n}}\right| \frac{\Delta\Omega_o\left[\Delta V(\vec{\mathbf{x}})\right]}{\Omega_o}\exp\left(-c|\vec{\mathbf{x}}|\right). \tag{5.2}$$

The radiant flux intensity scattered from $\Delta V(\vec{\mathbf{x}})$ in direction $\hat{\boldsymbol{\varepsilon}}(\vec{\mathbf{x}}_d - \vec{\mathbf{x}})$ toward the detector at $\vec{\mathbf{x}}_d$ is

$$I_S\left[\psi(\vec{\mathbf{x}})\right] = \beta\left[\psi(\vec{\mathbf{x}})\right] E_o(\vec{\mathbf{x}}) \Delta V, \tag{5.3}$$

where the scattering angle $\psi(\vec{\mathbf{x}})$ for the incremental volume element is

$$\cos\left[\psi\left(\vec{\mathbf{x}}\right)\right]=\hat{\boldsymbol{\varepsilon}}\left(\vec{\mathbf{x}}\right)\bullet\hat{\boldsymbol{\varepsilon}}\left(\vec{\mathbf{x}}_{\mathrm{d}}-\vec{\mathbf{x}}\right). \tag{5.4}$$

Combining (5.2) and (5.3), and multiplying by the flux transmittance over the pathlength $\left|\left(\vec{\mathbf{x}}_{\mathrm{d}}-\vec{\mathbf{x}}\right)\right|$ leads to

$$\frac{\Delta\Phi_{\mathrm{d}}\left[\Delta V\left(\vec{x}\right);c\right]}{\Phi_{\mathrm{o}}}=\beta\left[\psi\left(\vec{\mathbf{x}}\right)\right]\frac{\Delta V}{\Delta x\Delta y}\left|\hat{\boldsymbol{\varepsilon}}\left(\vec{\mathbf{x}}\right)\bullet\hat{\mathbf{n}}\right|\frac{\Delta\Omega_{\mathrm{o}}\left[\Delta V\left(\vec{\mathbf{x}}\right)\right]\Delta\Omega_{\mathrm{d}}\left[\Delta V\left(\vec{\mathbf{x}}\right)\right]}{\Omega_{\mathrm{o}}}\exp\left[-c\left(\left|\vec{\mathbf{x}}\right|+\left|\left(\vec{\mathbf{x}}_{\mathrm{d}}-\vec{\mathbf{x}}\right)\right|\right)\right], \tag{5.5}$$

where the solid angle subtended by the area ΔxΔy at the detector is $\Delta\Omega_{\mathrm{d}}\left[\Delta V\left(\vec{x}\right)\right]=\frac{\Delta x\Delta y\left|\hat{\boldsymbol{\varepsilon}}\left(\vec{\mathbf{x}}_{\mathrm{d}}-\vec{\mathbf{x}}\right)\bullet\hat{\mathbf{n}}\right|}{\left(\vec{\mathbf{x}}_{\mathrm{d}}-\vec{\mathbf{x}}\right)\bullet\left(\vec{\mathbf{x}}_{\mathrm{d}}-\vec{\mathbf{x}}\right)}$. With reference to (1.18) through (1.20), we may now write

$$\frac{\Delta\Phi_{\mathrm{d}}\left[\Delta V\left(\vec{x}\right);c\right]}{\Phi_{\mathrm{o}}}=\beta\left[\psi\left(\vec{\mathbf{x}}\right)\right]W\left(\vec{\mathbf{x}};c\right), \tag{5.6}$$

and by subsitution we obtain the incremental weighting function for each volume element $\Delta V\left(\vec{\mathbf{x}}\right)$ as

$$W\left(\vec{\mathbf{x}};c\right)=\frac{\Delta V}{\Delta x\Delta y}\left|\hat{\boldsymbol{\varepsilon}}\left(\vec{\mathbf{x}}\right)\bullet\hat{\mathbf{n}}\right|\frac{\Delta\Omega_{\mathrm{o}}\left[\Delta V\left(\vec{\mathbf{x}}\right)\right]\Delta\Omega_{\mathrm{d}}\left[\Delta V\left(\vec{\mathbf{x}}\right)\right]}{\Omega_{\mathrm{o}}}\exp\left[-c\left(\left|\vec{\mathbf{x}}\right|+\left|\left(\vec{\mathbf{x}}_{\mathrm{d}}-\vec{\mathbf{x}}\right)\right|\right)\right]. \tag{5.7}$$

To obtain the desired weighting function $W\left(\psi;c\right)$ for each scattering angle ψ it is necessary to sum the weights for all volume elements at which the scattering angle falls within a discrete angular interval of ψ , *i.e.*

$$W\left(\psi;c\right)=\sum_{x}\sum_{y}\sum_{z}W\left(\vec{\mathbf{x}};c\right)\delta\left[\psi,\psi\left(\vec{\mathbf{x}}\right),\Delta\psi\right] \tag{5.8}$$

where

$$\delta\left[\psi,\psi\left(\vec{\mathbf{x}}\right),\Delta\psi\right]=\begin{cases}1; & \psi-\frac{\Delta\psi}{2}<\psi\left(\vec{\mathbf{x}}\right)\le\psi+\frac{\Delta\psi}{2}\\ 0; & \text{Otherwise}\end{cases}. \tag{5.9}$$

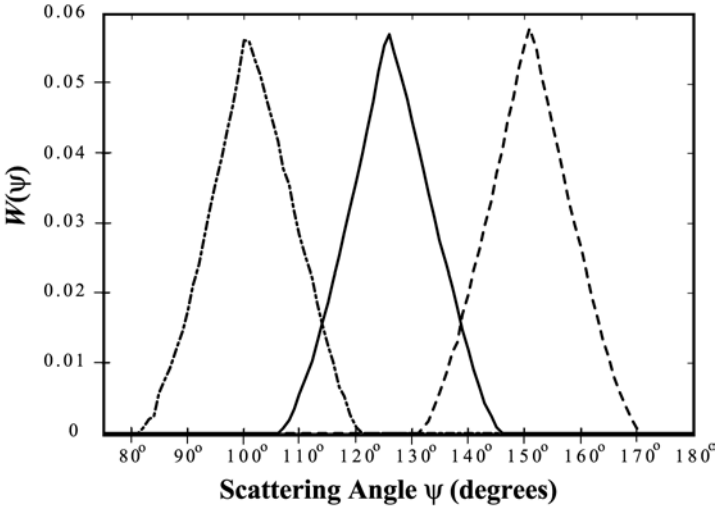

Figure 5.2: Examples of weighting functions $W\left(\psi\right)$ calculated for VSF measurements by source-detector pairs aligned at nominal scattering angles $\left(\bar{\psi}_1,\bar{\psi}_2,\bar{\psi}_3\right)=\left(100°,125°,150°\right)$ (Figs. 5.1 and 1.4).

Once the weighting functions are computed for all scattering angles ψ falling within the beam and detector FOV intersection volume, they are normalized such that

$$\sum_{\psi} W(\psi;c) = 1. \tag{5.10}$$

As an example, the weighting functions calculated for the WET Labs VSF-3 are illustrated in Fig. 5.2 for nominal scattering angles $(\bar{\psi}_1, \bar{\psi}_2, \bar{\psi}_3) = (100°, 125°, 150°)$. These particular, triangular source functions were derived assuming that both the source beam and detector FOV are conical about the respective centerlines illustrated in Fig. 5.1.

Generalized Weighting Functions for Arbitrary Source Beam and Detector FOV Geometries

In the above development of equations (5.1) through (5.7), it was assumed that the flux emitted by the source was uniformly distributed over a conical beam with its axis directed in direction

$$\hat{\boldsymbol{\varepsilon}}_o = \begin{bmatrix} \sin\left(\frac{\pi}{2} + \theta_o\right) \\ 0 \\ \cos\left(\frac{\pi}{2} + \theta_o\right) \end{bmatrix},$$

and that the detector flux responsivity was also uniformly distributed over a conical FOV having its axis aligned in direction

$$\hat{\boldsymbol{\varepsilon}}_d = \begin{bmatrix} -\sin\left(\frac{\pi}{2} + \theta_d\right) \\ 0 \\ \cos\left(\frac{\pi}{2} + \theta_d\right) \end{bmatrix}.$$

We may generalize the vector solid angle associated with the source beam as $\bar{\boldsymbol{\Omega}}_o$, which represents the angular solid angle domain, measured relative to $\hat{\boldsymbol{\varepsilon}}_o$, over which flux emitted by the source is non-zero. Similarly, $\bar{\boldsymbol{\Omega}}_d$ is the solid angle domain relative to $\hat{\boldsymbol{\varepsilon}}_d$ over which the detector's responsivity is non-zero. There are no restrictions on either the patterns of angular limits associated with $\bar{\boldsymbol{\Omega}}_o$ and $\bar{\boldsymbol{\Omega}}_d$, or on the relative distributions of flux within $\bar{\boldsymbol{\Omega}}_o$, or of flux responsivity within $\bar{\boldsymbol{\Omega}}_d$.

Real sources generally emit flux in a somewhat irregular beam pattern that typically peaks in the vicinity of $\hat{\boldsymbol{\varepsilon}}_o$, may be relatively flat for much of its FWHM beam width, and then tends to fall sharply near the edges of the beam and gradually decay beyond the nominal FWHM limits. Detector angular responsivity FOV patterns generally exhibit similar geometric characteristics relative to $\hat{\boldsymbol{\varepsilon}}_d$.

The flux variations within the source beam may be expressed as a normalized relative flux distribution function $h_o\left[\hat{\boldsymbol{\varepsilon}} \in \bar{\boldsymbol{\Omega}}_o\right]$ that takes non-zero values only in directions included in the solid angle beam pattern. Similarly, the angular response function of the the detector may be written $h_d\left[\hat{\boldsymbol{\varepsilon}} \in \bar{\boldsymbol{\Omega}}_d\right]$. To generalize the weighting functions to account for arbitrary source beam and detector FOV geometries, and relate the phase function to incremental detector responses $\Delta D_d\left[\Delta V(\bar{\mathbf{x}}); c\right]$:

1. Multiply the right-hand-sides of equations (5.1) and (5.2) by $h_o\left[\hat{\boldsymbol{\varepsilon}}(\bar{\mathbf{x}}) \in \bar{\boldsymbol{\Omega}}_o\right]$, and carry this factor through subsequent substitutions.

2. Substitute using the relationship $\Delta D_d\left[\Delta V(\bar{\mathbf{x}});c\right] = h_d\left[-\hat{\boldsymbol{\varepsilon}}(\bar{\mathbf{x}}_d - \bar{\mathbf{x}}) \in \bar{\boldsymbol{\Omega}}_d\right]\Delta\Phi_d\left[\Delta V(\bar{\mathbf{x}});c\right]$ on the left-hand-side of (5.7) to relate $\beta\left[\psi(\bar{\mathbf{x}})\right]$ to the incremental detector response.

3. Absorb the source flux and detector responsivity distributions into the weighting function $W(\bar{\mathbf{x}};c)$ by multiplying the right-hand-side of (5.7) by the product $h_o\left[\hat{\boldsymbol{\varepsilon}}(\bar{\mathbf{x}}) \in \bar{\boldsymbol{\Omega}}_o\right]h_d\left[-\hat{\boldsymbol{\varepsilon}}(\bar{\mathbf{x}}_d - \bar{\mathbf{x}}) \in \bar{\boldsymbol{\Omega}}_d\right]$.

The numerical implementation of the general form of (5.7) is straightforward. The more difficult aspect of obtaining generalized weighting functions is the experimental determination of the functions $h_o\left[\hat{\boldsymbol{\varepsilon}} \in \bar{\boldsymbol{\Omega}}_o\right]$ and $h_d\left[\hat{\boldsymbol{\varepsilon}} \in \bar{\boldsymbol{\Omega}}_d\right]$.

The detector FOV responsivity distribution function may be measured by mounting the detector in a rotating stage, with its entrance aperture centered on the intersection of the axis of rotation and the optical axis of a stable collimated source. The stage is rotated in small angular increments, and the detector response is recorded at each angle to measure the relative variations in response in one plane containing $\hat{\boldsymbol{\varepsilon}}_d$. The instrument is then rotated in increments about $\hat{\boldsymbol{\varepsilon}}_d$ and the process is repeated to map the distribution of responses in a sequence of planes adequate to resolve the full function $h_d\left[\hat{\boldsymbol{\varepsilon}} \in \bar{\boldsymbol{\Omega}}_d\right]$. This is essentially the same procedure used to characterize the angular FOV of field radiometers (Vol. II, Ch. 3).

The inverse of the above setup may be used to map the flux distribution of the source beam. The instrument is mounted with the source aligned with the optical and rotation axes, and a narrow FOV detector is substituted for the collimated source. The stage is rotated through a suitable angular range to map out flux variations in a plane through $\hat{\boldsymbol{\varepsilon}}_o$, and the instrument is rotated about $\hat{\boldsymbol{\varepsilon}}_o$ and the process repeated to measure flux distributions in a sequence of planes. If the temporal stability of flux output by the source is in question, a second detector may be mounted to monitor the source output from a fixed off-axis direction relative to $\hat{\boldsymbol{\varepsilon}}_o$, *i.e.* by mounting it on an extension to the rotational stage.

Whether one must go to the trouble to determine the beam and FOV weighting functions more accurately than can be modeled from simple geometric elements of the optical design depends on the shape of the VSF in the region to be measured. The detailed behaviour of the outer edges of the two distribution functions are not important factors in determing the weighting functions for measurements of the VSF of pure water, or of a particulate VSF at scattering angles near, or greater than, 90^o (Figs. 1.2 and 1.3). Therefore, relatively simple approximations to $h_o\left[\hat{\boldsymbol{\varepsilon}} \in \bar{\boldsymbol{\Omega}}_o\right]$ and $h_d\left[\hat{\boldsymbol{\varepsilon}} \in \bar{\boldsymbol{\Omega}}_d\right]$ should be completely adequate for the commercial backscattering instruments mentioned above. Conversely, the angular breadth and details of the beam and FOV distribution functions both become increasingly more critical when one wishes to measure the VSF at decreasing angles in the forward direction.

Dependence of the Weighting Functions on the Beam Attenuation Coefficient c

The effect of the beam attenuation coefficient on the weighting function $W(\bar{\mathbf{x}};c)$ for each volume element is explicitly represented in (5.7) by the transmittance over the combined pathlength from the source to the volume element at $\bar{\mathbf{x}}$ and from there to the source location. The transmittance term is integrated into each angular weighting function $W(\psi;c)$ determined using (5.8). Strictly speaking, near-forward scattered light still enters $\Delta V(\bar{\mathbf{x}})$ and can be scattered to the detector (see also the discussion of transmissometer acceptance angles in Chapter 2), but we will neglect this complication in the present discussion. The ratios of integrated weighting functions $\dfrac{\int W(\psi;c)\sin\psi d\psi}{\int W(\psi;c=0)\sin\psi d\psi}$ are compared against increasing beam attenuation coefficient c for the three ECO-VSF weighting functions illustrated in Fig. 5.2. These functions are clearly log-linear, and should we choose to represent the weighting function exclusively using $W(\psi;c=0)$, it would be a simple matter to adjust the results for c dependence. This dependence may either be applied as a correction to the weighting function, or by a

transmittance function of the form $\bar{\beta}_p(\lambda,\bar{\psi};c)=\bar{\beta}_p(\lambda,\bar{\psi})\exp\left[cr_{eff}(\bar{\psi})\right]$, where $\bar{\beta}_p(\lambda,\bar{\psi})$ is the measured VSF using $W(\psi;c=0)$ (see below) and $r_{eff}(\bar{\psi})$ is an effective net pathlength for the particular scattering angle measurement.

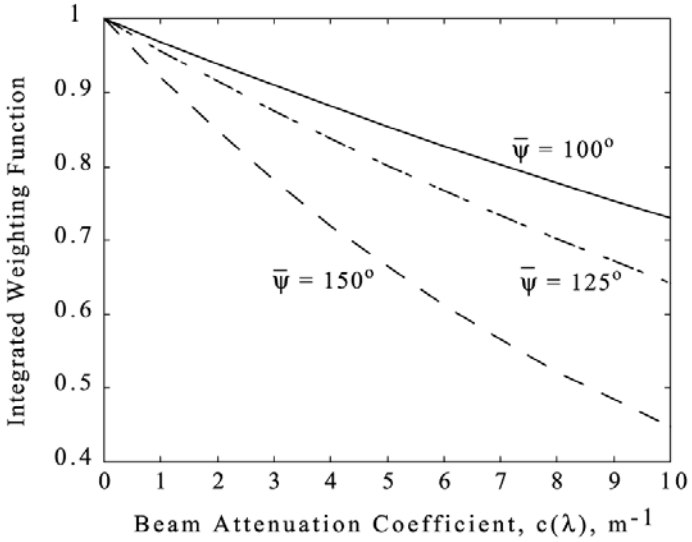

Fig. 5.3: Dependence of the integrated weighting functions $\int W(\psi;c)\sin\psi d\psi$ on the beam attenuation coefficient for the 3 ECO-VSF weighting functions of Fig. 5.2.

Calibration with Polystyrene Spheres

In this approach, a sample of polystyrene microsphere beads must be obtained and prepared for use in the calibration procedure. The following procedures are recommended:

1. Assume the bead diameters D_p in the sample are distributed as a Gaussian probability density function (pdf) $p(D_p)$ with the mean $\bar{D}_p$ and standard deviation S_D provided by the manufacturer; normalize the pdf to unit area.

   a. It is good practice to occasionally verify the reported mean diameter and standard deviation using a Coulter Counter, or other particle size counting device, for randomly selected samples received from a manufacturer.

2. Calculate the refractive index of the polystyrene spheres relative to pure water

$$n_p(\lambda)=\frac{n_p^{air}(\lambda)}{n_w(\lambda)}, \tag{5.11}$$

where the particle refractive index relative to air is determined according to a relationship provided by the manufacturer, *e.g.* from Duke Scientific as

$$n_p^{air}(\lambda)=1.5663+0.00785\lambda^{-2}+0.000334\lambda^{-4},\ \lambda \text{ in } \mu m, \tag{5.12}$$

and the refractive index of water relative to air is (Austin and Halikas 1976)

$$n_w(\lambda)=1.325147+\frac{6.6096}{\lambda-137.1924},\ \lambda \text{ in nm}. \tag{5.13}$$

Note carefully the different wavelength units in the empirical equations (5.12) and (5.13).

3. Calculate the particle scattering phase function for each diameter D_p, in 500 equally spaced intervals spanning ± 3 standard deviations about the mean diameter (*i.e.* $\Delta D_p = \frac{6S_D}{500}$), using a Mie (1908) scattering model code (*e.g.* Bohren and Huffman 1983; other coding implementations are also available at various web sites). The Mie scattering intensity functions should be calculated at angle intervals $\Delta\psi$ matching those at which the weighting functions $W(\psi;c)$ were resolved [equations (5.8) and (5.9)]. It is important that the selected angle increment adequately resolves variations in $\tilde{\beta}_{ps}(\lambda,\psi;D_p)$ for the narrow size distributions typically used in this application; an interval $\Delta\psi \le 0.5°$ is recommended.

4. Determine the phase function for the sample polydispersion by numerical quadrature of the convolution integral

$$\tilde{\beta}_{ps}(\lambda,\psi) = \int \tilde{\beta}_{ps}(\lambda,\psi;D_p)p(D_p)dD_p = \sum_{n=-250}^{250} w_n \tilde{\beta}_{ps}(\lambda,\psi;\bar{D}_p + n\Delta D_p)\, p(\bar{D}_p + n\Delta D_p)\Delta D_p \qquad (5.14)$$

where w_n are the weighting coefficients of the selected numerical quadrature algorithm (*e.g.* the composite Simpson formula).

5. To obtain the weighted phase function to be measured by the sensor, divide both sides of (1.19) by $b(\lambda)$ and numerically approximate the integral equation as

$$\bar{\tilde{\beta}}_{ps}(\lambda,\bar{\psi}) = \sum_{n=-\frac{N_{\Delta\psi}}{2}}^{\frac{N_{\Delta\psi}}{2}} w_n \tilde{\beta}_{ps}(\lambda,\bar{\psi}+n\Delta\psi)W(\bar{\psi}+n\Delta\psi;c)\sin\psi\Delta\psi\,, \qquad (5.15)$$

where again w_n are the quadrature weighting coefficients.

6. Measure and record the instrument's dark offset response $V_{dark}(\bar{\psi})$ by pointing the source and detector at a black velvet cloth, at a distance of approximately 2 m in a completely dark room.

7. Prepare a volume of filtered optically pure water, using the procedures described in Chapter 3.

8. Using an ac-9, calibrate it using the freshly prepared pure water (Chapters 2 and 3).

9. Immerse the VSF sensor in the pure water volume and record its response $V_w(\bar{\psi}) - V_{dark}(\bar{\psi})$.

10. Add a sufficient amount of the polystyrene microsphere bead sample to increase the instrument's response to approximately the maximum level desired for the calibration run.

    a. Label this bead concentration as C0 and record the VSF sensor response $V_{C0}(\bar{\psi})$.

    b. Measure $a_{C0}(\lambda)$ and $c_{C0}(\lambda)$, relative to the pure water calibration offsets, using the ac-9 for bead concentration C0. Determine $b_{ps}^{C0}(\lambda) = c_{C0}(\lambda) - a_{C0}(\lambda)$, including scattering and temperature corrections to the ac-9 measurements (Chapter 3).

11. Add pure water to dilute the sequence to bead concentration C1 and record the VSF response signal $V_{C1}(\bar{\psi})$, and repeat this step several times to obtain N+1 VSF response signal $V_{C0}(\bar{\psi}),\ldots,V_{CN}(\bar{\psi})$ corresponding to N+1 bead concentrations. It is not necessary to determine either the absolute, or relative bead concentrations, so dilution volumes of pure water need not be measured. At each dilution concentration Cn, repeat steps 10a and 10b.

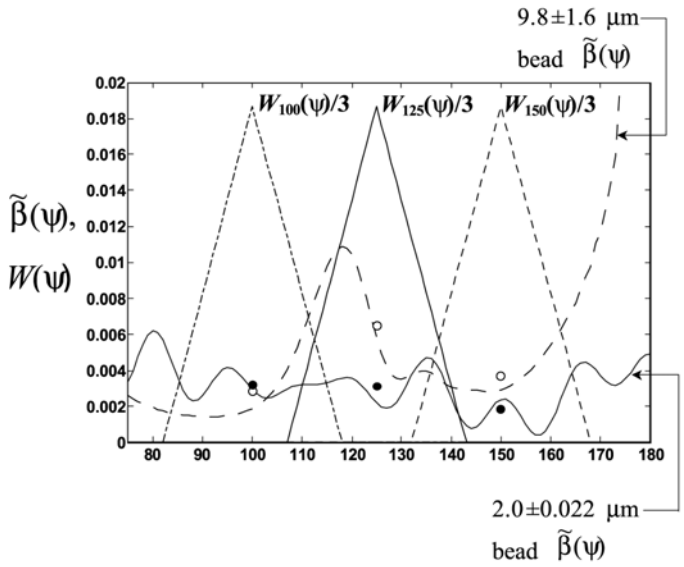

Figure 5.4: Examples of phase functions $\tilde{\beta}_{ps}(\lambda,\psi)$ calculated using Mie theory for polydispersions of polystyrene microsphere beads having mean diameters of 2 μm (solid line) and 9.8 μm (dashed line), and in both cases relatively small standard deviations. The open and closed circles show the corresponding weighted phase functions $\overline{\tilde{\beta}}_{ps}(\lambda,\overline{\psi})$ calculated by convolving each phase function with the ECO-VSF weighting functions $W(\psi)$ illustrated in Fig. 5.2.

The response calibration factor for a given bead concentration C0 to CN is determined as

$$F_{Cn}(\overline{\psi}) = \frac{b_{ps}^{Cn}(\lambda)\overline{\tilde{\beta}}_{ps}(\lambda,\overline{\psi})}{V_{Cn}(\overline{\psi}) - V_{w}(\overline{\psi}) - V_{dark}(\overline{\psi})} \tag{5.16}$$

where the polystrene sphere phase function $\overline{\tilde{\beta}}_{ps}(\lambda,\overline{\psi})$ is determined from (5.15). If necessary, the coefficient for each Cn is adjusted for dependence on the beam attenuation coefficient, and the sample is averaged to obtain the linear calibration coefficient $F(\overline{\psi})$. Given VSF measurements $V_m(\overline{\psi})$ in an unknown natural water mass, the weighted VSF for particles is calculated as

$$\overline{\beta}_p(\lambda,\overline{\psi}) = F(\overline{\psi})\left[V_m(\overline{\psi}) - V_w(\overline{\psi}) - V_{dark}(\overline{\psi})\right]. \tag{5.17}$$

5.3 CHARACTERIZATION and CALIBRATION OF A VSF SENSOR USING A REFLECTING PLAQUE

Maffione and Dana (1997) approach the calibration of a VSF sensor by inserting a horizontal plaque of assumed Lambertian reflectance $\frac{\rho}{\pi}$ into the position of the xy-plane illustrated in Fig. 5.1. Substituting this reflectance for the VSF in (5.6) and integrating over x and y yields the equation

$$\frac{\Phi_{d\rho}[\Delta z;c]}{\Phi_o} = \frac{\rho}{\pi}\int_x\int_y \left|\hat{\boldsymbol{\varepsilon}}(\hat{\mathbf{x}}_d - \hat{\mathbf{x}})\bullet\hat{\mathbf{n}}\right| W(\vec{\mathbf{x}};c)\,dxdy = \frac{\rho}{\pi}W_\rho(z;c), \tag{5.18}$$

representing the total flux reflected from the plaque into the FOV of the detector. If the plaque is moved continuously over z the integral of (5.18) yields the total relative flux reflected from the plaque to the detector from the volume intersection of the source beam and detector FOV as

$$\frac{\Phi_{d\rho}[c]}{\Phi_o} = \frac{\rho}{\pi}\int_z W_\rho(z;c)\,dz\,. \tag{5.19}$$

A similar integration of (5.1) yields

$$\frac{\Phi_{d\beta}[c]}{\Phi_o} = \int_z\int_x\int_y \beta\left(\psi(\bar{\mathbf{x}})\right)W(\bar{\mathbf{x}};c)dxdydz = \beta\left(\psi^*\right)\int_z W(z;c)\,dz \tag{5.20}$$

where the angle ψ^* is selected so that the equality holds; the mean value theorem assures that this must be true for at least one scattering angle. Taking the ratio of (5.10) and (5.20) and solving for $\beta(\psi^*)$ yields the result

$$\beta\left(\psi^*\right) = \frac{\rho}{\pi}\frac{\Phi_{d\beta}[c]}{\Phi_{d\rho}[c]}\frac{\int_z W_\rho(z;c)\,dz}{\int_z W(z;c)\,dz}\,. \tag{5.21}$$

We refer the reader to Maffione and Dana (1997) for the derivation of the unknown terms in (5.21) from the plaque integral and differential measurements, and defer further comparative analysis and description of this method and the explicit approach of Section 5.2 for a future revision to this chapter.

5.4 METHODS FOR THE DETERMINATION OF THE BACKSCATTERING COEFFICIENT FROM VSF MEASUREMENTS AT ONE OR MORE SCATTERING ANGLES

If the complete VSF is measured at fine angular resolution using a general angle scattering meter, then it is straightforward to integrate it over the backward hemisphere to determine $b_b(\lambda)$ directly.

Determination of $b_b(\lambda)$ from VSF Measurements at Three or More Angles

The approach used to determine $b_b(\lambda)$ from measurements of $\bar{\beta}(\lambda,\psi_i,\varphi)$; at $i = 1,2,\ldots,N$ angles, *e.g.* using a WET Labs VSF-3, is to fit a polynomial to the N+1 values $2\pi\bar{\beta}(\lambda,\psi_i,\varphi)\sin\psi_i$ derived from the N measurements and the endpoint $2\pi\beta(\lambda,\pi,\bullet)\sin\pi \equiv 0$ and integrate it from $\frac{\pi}{2}$ to π (following Beardsley and Zaneveld 1969).

Determination of $b_b(\lambda)$ from VSF Measurements at Only One Angle

Oishi (1990) used Mie scattering calculations and VSF observations to determine $\beta^n(\lambda,\psi)$ and $b_b^n(\lambda)$ for polydispersions of spheres having different size distributions similar to those observed for marine hydrosols. He invoked the mean value theorem to observe, from the definition of $b_b(\lambda)$, that for each n$^{\underline{th}}$ polydispersion phase function $\tilde{\beta}^n(\lambda,\psi)$ there must be at least one angle ψ_n^* for which

$$b_b^n(\lambda) = 2\pi\beta^n\left(\lambda,\Psi_n^*\right)\int_{\frac{\pi}{2}}^{\pi}\sin\Psi d\Psi = 2\pi\beta^n\left(\lambda,\Psi_n^*\right).^{13} \tag{5.22}$$

Oishi (1990) then futher observed that for a selected common reference angle ψ^*, he could determine an approximate linear estimate of the backscattering coefficient for each polydispersion as

[13] Recalling that $\beta(\lambda,\psi) = b(\lambda)\tilde{\beta}(\lambda,\psi)$ [Vol. I, Ch. 2, Sect. 2.4].

$$\hat{b}_b^n(\lambda) \approx 2\pi\chi(\Psi^*)\beta^n(\lambda,\Psi^*), \tag{5.23}$$

where the coefficient $\chi(\Psi^*)$ is selected to minimize the uncertainty

$$U(\Psi^*) = \sqrt{\frac{\sum_{n=1}^{N}\left[b_b^n(\lambda) - \hat{b}_b^n(\lambda)\right]^2}{N}}. \tag{5.24}$$

By varying ψ^*, Oishi found that the minimum overall uncertainty for the ensemble of N size distributions occurred at $\psi^* = 120°$, with $\chi(120°) = 1.14$.

Boss and Pegau (2001) separated the VSF and backscattering coefficient as

$$\begin{aligned} &\beta(\lambda,\Psi) = \beta_w(\lambda,\Psi) + \beta_p(\lambda,\Psi) \text{ and} \\ &b(\lambda) = b_w(\lambda) + b_b(\lambda), \end{aligned} \tag{5.25}$$

where the subscripts "p" and "w" designate contributions due to particles and water, respectively. The scaling factor $\chi(\Psi^*)$ is correspondingly partitioned as

$$\chi(\Psi^*) = \chi_p(\Psi^*)\frac{\beta_p(\lambda,\Psi^*)}{\beta(\lambda,\Psi^*)} + \chi_w(\Psi^*)\frac{\beta_w(\lambda,\Psi^*)}{\beta(\lambda,\Psi^*)}. \tag{5.26}$$

Analyses similar to those of Oishi (1990) and Maffione and Dana (1997), but in this partitioned framework, led Boss and Pegau (2001) to conclude that $\chi(\Psi^*) = \chi_p(\Psi^*) = \chi_w(\Psi^*) \cong 1.1$ only when $\Psi^* = 117° \pm 3°$, consistent with the results of Oishi (1990). For measurements at other scattering angles, they recommend modifying Equation (4.6) to correct for the water scattering contribution as

$$\hat{b}_b(\lambda) = 2\pi\chi_p(\Psi^*)\left[\beta(\lambda,\Psi^*) - \beta_w(\lambda,\Psi^*)\right] + b_{bw}(\lambda). \tag{5.27}$$

They provide equations for estimating $\beta_w(\lambda,\Psi)$ and $b_w(\lambda)$, based on the theoretical equations and experimental results of Morel (1974), and tabulate estimates of $\chi_p(\Psi^*)$ in the range $90° \le \Psi^* \le 170°$.

REFERENCES

Beardsley, G.F. and J.R.V. Zaneveld, 1969: Theoretical dependence of the near-asymptotic apparent optical properties of sea water. *J. Opt. Soc. Amer*. 59: 373-377.

Bohren, C.F., and D.R. Huffman, 1983: *Absorption and Scattering of Light by Small Particles*, Wiley, New York, 530pp

Boss, E. and W.S. Pegau, 2001: Relationship of light scattering at an angle in the backward direction to the backscattering coefficient. *Appl. Opt.,* **40:** 5503-5507.

Mie, G., 1908: Beitrage zur Optic truber Medien, speziell kolloidalen Metallosungen, *Ann. Phys*., **25:** 377-442.

Maffione, R.A. and D.R. Dana, 1997: Instruments and methods for measuring the backward-scattering coefficient of ocean waters. *Appl. Opt*. **36**: 6057-6067.

Mobley, C.D., L.K. Sundman, and E. Boss, 2002. Phase function effects on oceanic light fields. *Appl. Opt.*, **41**(6): 1035-1050.

Oishi, T., 1990. Significant relation between the backward scattering coefficient of sea water and the scatterance at 120 degrees. *Appl. Opt.*, *29(31)*: 4658-4665.

Petzold, T.J., 1972. Volume scattering functions for selected ocean waters. Contract No. N62269-71-C-0676, UCSD, SIO Ref. 72-78.

Stramska, M., D. Stramski, B.G. Mitchell and C.D. Mobley. 2000: Estimation of the absorption and backscattering coefficients from in-water radiometric measurements. *Limnol. Oceanogr*., **45**: 628-641.

Zaneveld, J.R.V., 1982: Remotely sensed reflectance and is dependence on vertical structure: a theoretical derivation. *Appl. Opt*., **21(22):** 4146-4150.